DISSERTATION

submitted to the
Combined Faculty of Natural Sciences and Mathematics
of the Ruperto Carola University Heidelberg, Germany
for the degree of
Doctor of Natural Sciences

Presented by

Benjamin Lau, Diploma

born in Reinbek (Germany)

Oral examination: …….

Transition of the 90S Pre-Ribosome into the Primordial pre-40S Subunit involving the RNA Exosome, Utp24 Endonuclease and Dhr1 Helicase

Referees: Prof. Dr. Ed Hurt

Prof Dr. Michael Brunner

Statement of Contributions and Licenses

I conducted this PhD thesis under the supervision of Prof. Dr. Ed Hurt at the Biochemistry Institute Heidelberg of the Ruperto Carola University Heidelberg. I herewith declare that I worked on my Thesis independently and under supervision, and that all sources and aids are indicated throughout the thesis.

During the course of my thesis, I collaborated with several coworkers. Their contribution, indicated in the appropriate sections, is the following:

(i) Lab of Prof. Dr. Roland Beckmann
Cryo-EM analysis, calculation of 3D models and building molecular models of the Noc4-Dhr1, Dhr1-Dim1 and Csl4-Dim1 samples: Jingdong Cheng, Otto Berningshausen

(ii) Lab of Prof. Dr. Ed Hurt, Biochemistry Center Heidelberg
Northern Blot analysis of Noc4-Dhr1 samples fractionated on sucrose gradients and final flag eluates of different precipitations: Dr. Giuseppe La Venuta

(iii) Dr. Dirk Flemming, Biochemistry Center Heidelberg
negative-stain EM analysis of Dhr1-Dim1 and Csl4-Dim1 samples

This thesis contains Figures, which were either created by myself or adapted from publications as indicated. The following journals kindly permitted reuse of the listed Figures under the indicated licenses:

License No.	Date	Publisher	Journal	Reference	Figure taken
5152980623046	20.09.2021	Elsevier	Trends in Biochemical Science	(Klinge et al., 2012)	1
1148772-1	19.09.2021	Annual Reviews, Inc.	Annual Review of Biochemistry	(Bassler & Hurt, 2018)	1, S1
5153061353157	20.09.2021	Elsevier	Molecular Cell	(Osheim et al., 2004)	2
open access article		Wiley	WIREs RNA	(Turowski and Tollervey, 2015)	1
5152620234880	19.09.2021	Springer	Nature Reviews Molecular Cell Biology	(Klinge & Woolford, 2018)	2
open access article		Public Library of Science	Plos Biology	(Sardana et al., 2015)	1
5153070566377	20.09.2021	Springer	Nature Reviews Molecular Cell Biology	(Kilchert et al., 2016)	1
5153070844155	20.09.2021	Elsevier	Cell	(Thoms et al, 2015)	5

Parts of this thesis were published in the articles:

(1) “Thermophile 90S Pre-ribosome Structures Reveal the Reverse Order of Co-transcriptional 18S rRNA Subdomain Integration” Jingdong Cheng*, Jochen Baßler*, Paulina Fischer*, Benjamin Lau, Nikola Kellner, Ruth Kunze, Sabine Griesel, Martina Kallas, Otto Berninghausen, Daniela Strauss, Roland Beckmann, Ed Hurt. Molecular Cell 2019. doi: 10.1016/j.molcel.2019.06.032. As author I retain the right to include the Figures in my thesis without explicit permission or license.

(2) “90 S pre-ribosome transformation into the primordial 40 S subunit” Benjamin Lau*, Jingdong Cheng*, Giuseppe La Venuta, Michael Ameismeier, Otto Berningshausen, Ed Hurt, Roland Beckmann. Science 2020. doi: 10.1126/science.abb4119 * Co-First Authorship. As author I retain the right to include the Figures in my thesis without explicit permission or license.

(3) “Structure of the maturing 90 S pre-ribosome in association with the RNA exosome.” Benjamin Lau*, Jingdong Cheng*, Dirk Flemming, Giuseppe La Venuta, Otto Berninghausen, Roland Beckmann, Ed Hurt. Molecular Cell 2021. doi: 10.1016/j.molcel.2020.11.009 * Co-First Authorship. As author I retain the right to include the Figures in my thesis without explicit permission or license.

Thank you!!!

Prof. Dr. Ed Hurt – Thank you for giving me the opportunity to work in your lab and patiently supervising me and my research. Over the time of my PhD I learned a lot about science and how it is implemented. Thank you, Ed for giving me such a strong support, I enjoyed the manifold fruitful scientific discussions over the past years. One thing I learned from you, is that there is no science without a pocket full of creativity, building on this you showed me how to chase our ideas and hypotheses. I am glad, that you provided me with a surrounding which offered everything which is needed for state-of-the-art research and therefor prepared me for whatever will follow.

Prof. Dr. Michael Brunner – thank you for taking the time and making the effort to be my second evaluator of my doctoral thesis.

Dr. Mandy Jeske – thank you for making the effort to be my TAC member and being part of my oral examination as my 3rd examiner.

Dr. Jirka Peschek – thank you for making the effort in taking part in my oral examination as my 4th examiner.

I want to thank all the members of the Hurt lab, especially our amazing technicians (Sabine, Ruth, Selene, Martina) and Andrea you are the backbone of our lab. I want to thank Giuseppe for purifying hundreds of liters of yeast culture together with me and for collaborating in an interesting project. A big thank you to Paulina, for your ideas and your amazing support with my thesis.

A special thank you goes to Roland Beckmann and Jingdong Cheng, your cryo-EM structures boosted my projects in so many ways. Working together with Jingdong was always a pleasure and I enjoyed that you were always open for my ideas.

This one goes out to the ones I love, my family and friends you supported me in so many ways, gave me confidence, faith … and so much more. For the ones I lost and can't go this far, you still give me inspiration, Dad!

Summary

Ribosomes, which are the molecular machines that synthesize the proteins of the cell, consist of ribosomal RNA (rRNA) and ribosomal proteins. To produce these ribosomes, a large precursor rRNA molecule (pre-rRNA) is transcribed by RNA-polymerase I, which in yeast is processed to form the three mature rRNAs (18S, 25S and 5.8S rRNA) accompanied by concomitant incorporation of 79 ribosomal proteins. This complicated process of ribosome assembly and maturation is driven by numerous (~200) and highly conserved assembly factors (AFs). A number of AFs are enzymes such as helicases or exo- and endonucleases, which play a vital role in remodeling and processing of the pre-rRNA, thereby allowing distinct and often irreversible transitions in the long cascade of pre-ribosome assembly.

In my PhD thesis, I have investigated the 90S-to-pre-40S ribosome transition by biochemical, genetic and structural approaches, with the goal to gain mechanistic insight into this process. One important initial observation was the sequential AF shedding of the 90S pre-ribosome after cleavage of 5'-ETS at site A_1, which challenged our common view of an *en bloc* release of the 5'-ETS particle. Subsequently, I followed the mechanism of Utp24 endonuclease driven pre-RNA cleavage at site A_1 between the 5'-ETS and 18S rRNA, which turned out to be prerequisite for the 90S-to-pre-40S transition. Moreover, I was able to isolate a 90S-exosome super-complex, revealing how the nuclear RNA exosome is docked via its co-factor Mtr4 helicase to the 90S pre-ribosome at the base of the 5'-ETS helices H9-9' that were already dislodged in the 90S-exosome super-particle. This finding suggested that Mtr4 channels the free 3'-end of 5'-ETS at site A_0 into the exosome for RNA degradation, thereby acting as a key driver in following 90S-to-pre-40S transition. The last transition intermediate observed in the series of discovered pre-ribosomal particles was shown to be the primordial pre-40S, which however was still decorated with a few 90S factors. One such factor was the RNA helicase Dhr1, which was seen to be directly positioned at its U3 snoRNA substrate to unwind the final hybrid between U3 and the 5'-end of the 18S rRNA. Taken together, these findings from my PhD study revealed key steps of the 90S-to-pre-40S transition, both biochemically and structurally, thereby shining light on the mechanism of pre-rRNA processing and its coupling to remodeling during eukaryotic ribosome biogenesis.

Zusammenfassung

Ribosomen, die molekularen Maschinen verantwortlich für die Biosynthese von Proteinen in der Zelle, sind aufgebaut aus ribosomaler RNA (rRNA) und ribosomalen Proteinen. Um Ribosomen herzustellen, wird zuerst ein großes Vorläufer-rRNA-Molekül (prä-rRNA) durch die RNA-Polymerase I transkribiert. Dieses wird in Hefe zu drei reifen rRNA Molekülen (18S, 25S und 5.8S rRNA) prozessiert bei gleichzeitig ablaufender Inkorporation von 79 ribosomalen Proteinen. Dieser komplexe Prozess der Ribosomenreifung wird von zahlreichen (~200), stark konservierten Assemblierungs-Faktoren (AFs) gefördert. Einige der AFs sind Enzyme wie Helikasen oder Exo- und Endonukleasen, welche eine wichtige Rolle bei der Restrukturierung und dem Prozessieren der prä-rRNA spielen und dadurch spezifische und oft irreversible Reifungen in der Ribosomenbiogenese erlauben.

In meiner Doktorarbeit habe ich den 90S-zu-prä-40S Übergang erforscht mit biochemischen, genetischen und strukturellen Ansätzen, um Erkenntnisse über den mechanistischen Ablauf dieser Prozesse zu gewinnen. Eine wichtige anfängliche Beobachtung war die aufeinander folgende Ablösen von AFs vom 90S Prä-Ribosom nachdem die 5'ETS an der A1 Stelle geschnitten wurde, was unserer allgemeinen Annahme eines en bloc Freisetzung des 5'ETS Partikels widersprach. Anschließend verfolgte ich den Mechanismus des durch Utp24 geförderten Schnitts der prä-rRNA an der A1 Stelle zwischen der 5'ETS und der 18S rRNA, der sich als Voraussetzung für den 90S-zu-prä-40S herausstellte. Außerdem konnte ich einen 90S-Exosom Super-Komplex isolieren und zeigen wie das RNA Exosom und das 90S Prä-Ribosom mit seinem Kofaktor Mtr4 über bereits dislozierte Helices H9-9' der 5'ETS andockt. Dies legt nahe, dass Mtr4 maßgeblich am 90S-zu-prä-40S Übergang beteiligt ist, indem es das freie 3' Ende der 5'ETS an der A0 Seite in das Exosom zur Degradation führt. Der letzte Übergangspartikel in der Serie entspricht einem primordialem prä-40S, das noch ein paar 90S AFs trägt, darunter die RNA Helikase Dhr1, die direkt an ihrem Substrat, der U3 snoRNA, positioniert ist, um den letzten U3-18S rRNA hybrid zu entwinden. Zusammengefasst zeigen die Ergebnisse meiner Doktorarbeit entscheidende biochemische und strukturelle Schritte des 90S-zu-prä-40S Übergangs. Dadurch konnte zeigen, wie prä-rRNA Prozessierung mit Remodellierungen während der eukaryotischen Ribosomenbiogenese zusammenhängen.

Table of contents

1. Introduction

1.1 The eukaryotic ribosome is a macromolecular ribozyme translating genetic information into proteins

The eukaryotic ribosome is a macromolecular RNA-protein complex and highly conserved across the three kingdoms of life. The function of ribosomes within the cell is the *de novo* synthesis of polypeptide chains. Proteins have manifold functions within the cell, such as catalyzing biochemical reactions in the form of enzymes, regulating cellular processes as signaling proteins, transporting cargos across cell membranes and giving structure to complexes or even structure to compartments of the whole cell. The discovery of the ribosome occurred in 1955 by George Palade, who described them as dense round particles in the cytoplasm of mammalian cells by electron-microscopy (EM) (Palade, 1955). The great importance of proteins for diverse cellular functions made the ribosome one of the most studied macromolecular complex of all times with regard to their structure, protein composition, mechanism of protein production, biogenesis and evolutionary diversity.

In all living cells mature ribosomes are built from two subunits, the large ribosomal subunit (LSU) and the small ribosomal subunit (SSU) (Klinge et al., 2012; Schuwirth et al., 2005). Both subunits are RNA-protein complexes consisting of ribosomal RNA (rRNA) and ribosomal proteins (r-proteins) (Figure 1.1). Since the mechanism of protein synthesis in every cell is highly conserved, the overall design of a ribosome is highly similar, too. Genetic studies revealed that the r-proteins of distant eukaryotes like *Homo sapiens*, *Drosophila melanogaster*, *Caenorhabiditis elegans* and *Saccharomyces cerevisiae* (*S. cerevisiae* further referred to as yeast) show a noteworthy homology of 63% (Jenner et al., 2012; Yoshihama et al., 2002). Even though ribosomes are highly conserved, the prokaryotic ribosome varies in size and composition from its eukaryotic counterpart. The eukaryotic ribosome has expansion segments (ES) in the rRNA and additional as well as extended r-proteins. The 2.5 MDa size of the prokaryotic ribosome from *Escherichia coli* (*E. coli*) increases to 3.3 MDa in *S. cerevisiae* and 4.4 MDa in human cells.

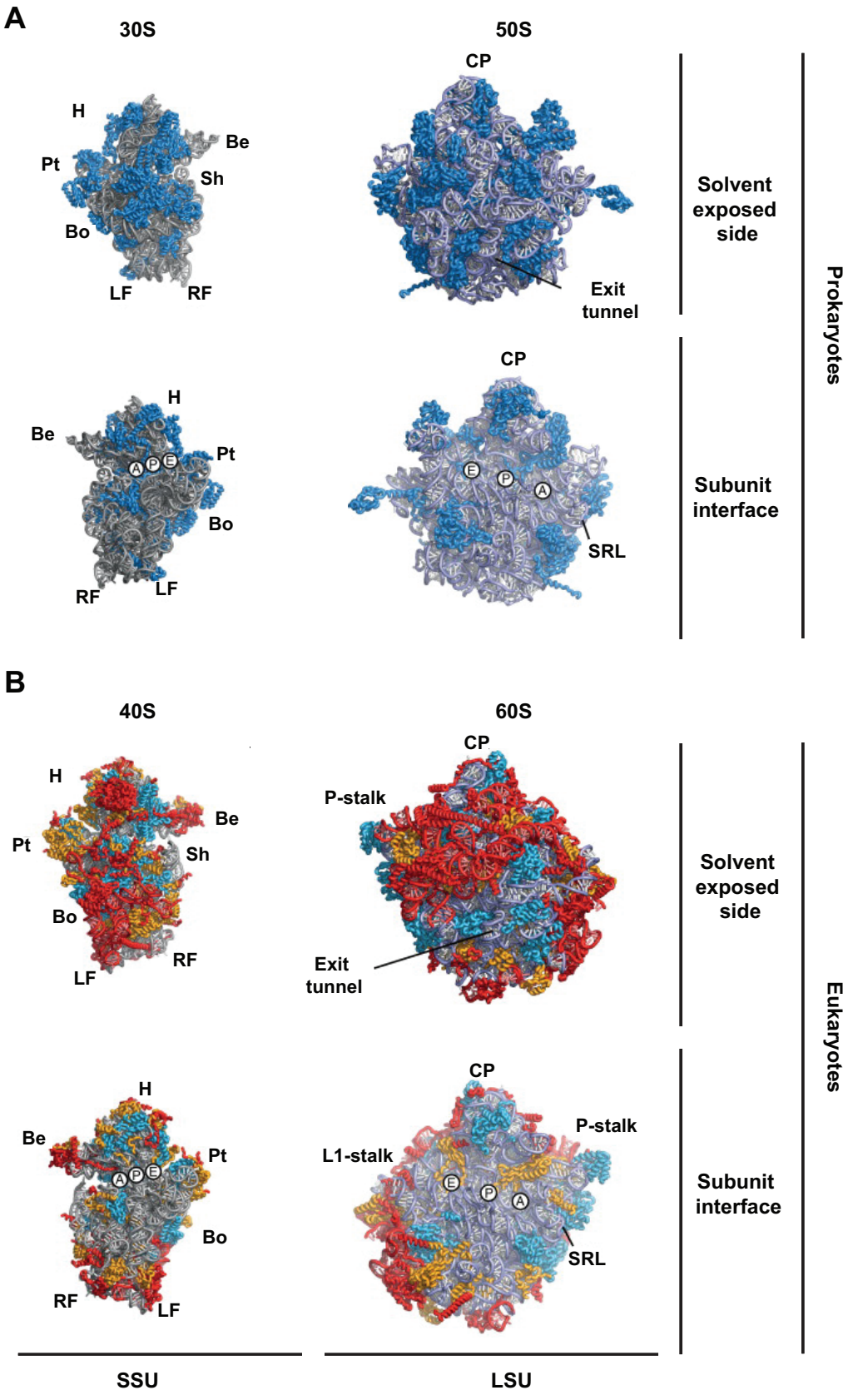

Figure 1.1 Structural comparison of prokaryotic and eukaryotic ribosomal subunits. (A) and (B): The SSU and LSU are shown as a structural model depicting the solvent exposed and the subunit interface site. (A) Prokaryotic ribosomal subunits from *T. thermophilus*. Prokaryotic r-proteins are

colored in dark blue (B) Eukaryotic ribosomal subunits from *T. thermophila*. Universally conserved r-proteins are colored in light blue, r-proteins found in archaea and eukaryotes are colored in orange and eukaryotic specific r-proteins are depicted in red. rRNA is colored in gray. Important structural features are labeled on each subunit (H: head, Be: beak, Pt: platform, Sh: shoulder, Bo: body, LF: left foot, RF: right foot, A: aminoacyl site, P: peptidyl site, E: exit site, SRL: sarcin-ricin loop, CP: central protuberance). Figure adapted from (Klinge et al., 2012).

This increase in size likely reflects the higher order of organisms and their increased complexity regarding translation regulation (Ben-Shem et al., 2010; Cate et al., 1999; Jenner et al., 2012; Khatter et al., 2015). The prokaryotic 70S ribosome (S, for Svedberg unit) consists of a 30S SSU and 50S LSU. It is 30-40% smaller than the eukaryotic 80S ribosome, which is formed by the 40S SSU and 60S LSU. The prokaryotic ribosome of *E. coli* has an SSU containing 21 r-proteins and the 16S rRNA, whereas 36 r-proteins together with the 5S and 23S rRNA form the LSU. The eukaryotic ribosome in yeast, which is the model organism used in this work, has a 40S SSU containing 33 r-proteins and the 18S rRNA, while the LSU is built of 46 r-proteins together with three rRNA molecules (5S, 5.8S and 25S). The four rRNA molecules give both subunits their three-dimensional structure and shape. Most of the r-proteins have a globular domain and are frequently located on the ribosomes' surface complementing the rRNA's fold. They sometimes have long tail domains, which penetrate into the rRNA core or meander along the rRNAs surface. One common feature of r-proteins is the high content of basic amino acids. Their positive charge counterparts the negatively charged character of the rRNA phosphate backbone and therefore reduces the repulsive force in the three-dimensional structure of the ribosome (Lecompte et al., 2002; Melnikov et al., 2012). In comparison to prokaryotes, most additional eukaryotic r-proteins associate with expansion segments (ES) of the rRNA molecules or the surface of the ribosomal subunits. In contrast, the functional sites of translation, such as the subunit interface or the exit tunnel, are conserved (Melnikov et al., 2012; Yusupova and Yusupov, 2017). Both small and large subunit have characteristic three dimensional structures (Figure 1.1). The SSU has specific structural landmarks, the head region with beak, platform, shoulder and foot (left and right), whereas the LSU structural features are the acidic stalk, central protuberance and L1 stalk.

Translating the information of a messenger RNA (mRNA) into a polypeptide chain and finally into a protein means for the ribosome that it will decode the nucleotide-sequence into a sequence of amino acids (AA) connected by peptide bonds. To accomplish this task, the ribosome is channeling the mRNA between its two subunits, where three distinct binding sites interact with transfer RNAs (tRNAs), which carry specific amino acids. The aminoacyl-tRNA is recruited to the A-site via its complementary anticodon, which binds to the codon in the mRNA molecule. At the P-site, a peptide bond is formed between the tRNA carrying the previously formed polypeptide chain and the newly recruited amino acid in the A-site. The deacetylated tRNA molecule from the P-site is transferred to the E-site before being dissociated from the ribosome (Ben-Shem et al., 2010). This catalytic process is mediated by the 28S/25S rRNA of the 60S subunit and consequently, ribosomes can also be called ribozymes. The translation process involving every actively translating ribosome can be divided into three phases: initiation, elongation and termination. Evolutionary, this process arose from a highly conserved minimal RNA core, which consists of the peptidyl transferase center (PTC) and the decoding center. As the complexity of living organisms increased over the course of evolution, this minimal RNA core was expanded on its surface with additional RNA segments and r-proteins. An important feature of this expansion was the creation of the nascent polypeptide exit tunnel (NPET), a major characteristic in the interior of the 60S subunit, which serves as a tunnel for the emergence of newly synthesized growing polypeptide chain (Ben-Shem et al., 2010; Schmeing and Ramakrishnan, 2009; Wilson et al., 2020).

1.2 Ribosome biogenesis provides the cell with ribosomes

The assembly of ribosomes is one of the most challenging and energy exhausting processes within a cell. For example, in the rapidly dividing organism yeast, 90% of its transcripts and over 25% of its translation products are consumed for the biogenesis of ribosomes. Yeast can assemble approximately 2 000 ribosomes per minute and accordingly the cell must produce 160 000 r-proteins and 14 Mb of precursor rRNA (pre-RNA) to fulfill this remarkable task (Turowski and Tollervey, 2015; Warner, 1999). In *E. coli,* during exponential growth around half of the cells' dry-mass is ascribed to ribosome content, which demonstrates the outstanding role ribosomes and especially

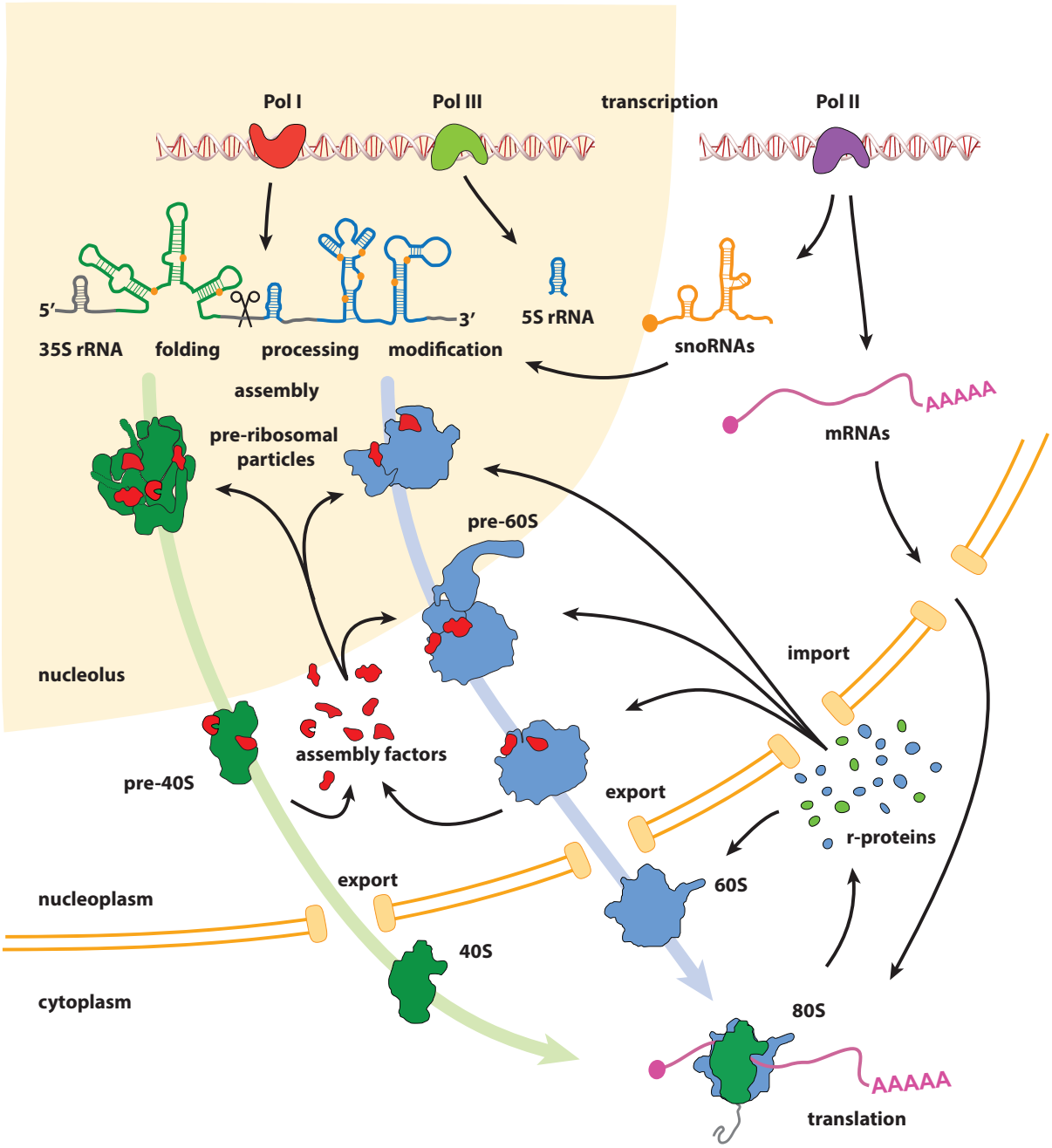

Figure 1.2 Dynamic model of ribosome biogenesis in eukaryotes. Ribosome biogenesis starts in the nucleolus with the transcription of rRNAs by Pol I (35S rRNA) and Pol III (5S rRNA), while Pol II transcribes snoRNAs and mRNAs, which are translated into assembly factors and r-proteins. Pre-rRNA molecules undergo extensive modification, processing, folding and they associate with different assembly factors while they mature as they move across the nucleus, from the different compartments of the nucleolus to the nucleoplasm. In the cytoplasm, final maturation steps take place before mature 40S and 60S subunits can engage actively in protein production. Taken from (Bassler and Hurt, 2018).

their biogenesis plays for fast growing cells like *E. coli*, yeast and even cancer cells (Dennis et al., 2004). Nearly every process in the cell is depending on proteins and consequently the large macromolecular structure of a ribosome must be made with

high accuracy. Mistakes in translation can lead to proteins with altered properties such as proteins with loss of function. The production of ribosomes needs to integrate two seemingly opposite requirements. On the one hand it has to be very accurate and on the other hand it needs to be fast to fulfil the high demand for proteins that the cells need for cell function and cell division. The process of ribosome biogenesis includes transcription and trimming of pre-rRNA, chemical modification of rRNA as well as folding, recruitment of r-proteins and ribosome assembly factors (AFs) involved in subunit maturation (Figure 1.2). The successful completion of the diverse assembly processes leads to the export of the ribosomal subunits from the nucleus into the cytoplasm (Albert et al., 2019; Gallagher et al., 2004; Lebaron et al., 2012; Meskauskas et al., 2003; Phipps et al., 2011; Warner, 1999). The amount of actively translating ribosomes and therefore the synthesis of ribosomes is adjusted to the needs of every cell. It depends on the proliferation rate as well as the intra- and extracellular environment, including nutrients and stress factors. To react to the changing circumstances accordingly, the production of ribosomes must be tightly regulated and controlled. An imbalance in ribosome biogenesis can lead to dramatic or even lethal consequences for the cell or the whole organism. Such disorders caused by alterations in the function or structure of ribosomal components are described as ribosomopathies in human cells and are a research field that is rapidly growing and of general interest. The various diseases can have its origin in diverse factors contributing to ribosome biogenesis. For example, mutations affecting RNA polymerase I (POL I) lead to reduced transcription levels of pre-RNA molecules. This can affect downstream biogenesis steps such as pre-RNA processing, ribosome assembly and correct steady state levels of actively translating ribosomes. Additionally, it will have detrimental feedback on the activity of POL II and POL III (Laferte et al., 2006; Schneider et al., 2007). One of the most studied ribosomopathies is called Diamond-Blackfan anemia. It can be caused by over 220 different mutations identified predominantly in r-proteins (Rps19, Rps24, Rps17, Rps7, Rps10, Rps26, Rpl5, Rpl11, Rpl35A), with 25% of patients having Diamond-Blackfan anemia carrying a mutation in the gene encoding Rps19. Patients not only have anaemia, but they often have organ abnormalities and are growth retarded (Boria et al., 2010). Another ribosomopathy is X-linked dyskeratosis congenita (DKCX), which is caused by mutations in the gene *DKC1.* This gene encodes the protein Dyskerin, a pseudouridine

synthase responsible for the modification of noncoding RNA. Its mutation leads to a loss of pseudouridines in mature rRNA (Thumati et al., 2013).

1.3 Hierarchical processing steps of pre-rRNA are key events in ribosome biogenesis

The synthesis of eukaryotic ribosomes starts in the nucleolus. The nucleolus is a membrane free compartment in the nucleus accommodating clustered tandem repeats of rDNA, which contribute significantly to the nucleus' structure. Transcription of rDNA genes takes place at the border of the dense fibrillar compartment (DFC) and the fibrillar center (FC), subdividing the nucleolus into two major regions. The nascent pre-rRNA molecules start to be assembled and processed with r-proteins, ribosome assembly factors and snoRNA's in the DFC (Correll et al., 2019; Thiry and Lafontaine, 2005). Upon further maturation progresses, the pre-rRNA reaches the third region of the nucleolus, the granular compartment (GR), which is filled with many pre-ribosomal particles. Folding and maturation of pre-rRNA continues during translocation in the nucleoplasm and final maturation steps and quality control occur in the cytoplasm (Cheutin et al., 2002; Raska et al., 2006). The mature rRNA species of both SSU and LSU have a characteristic 3D fold which shapes the 3D structure of the ribosome. Ribosome maturation needs to ensure that the pre-rRNA reaches its characteristic 3D structures, which are essential for the rRNAs catalytic function. The 18S and 25S rRNAs are divided into subdomains, which can be depicted in a 2D model of helices (Figure 1.2A).

Ribosome biogenesis is initiated with the transcription of a long precursor rRNA by Pol I, which contains two external transcribed spacers (5'-ETS and 3'-ETS) and two internal transcribed spacers (ITS1 and ITS2) (Figure 1.3). These spacer sequences are flanking and separating the three mature rRNA molecules (18S, 5.8S, 25S/28S) and are removed in a hierarchical manner by specific endo- and exonucleases during pre-ribosome maturation. The pre-rRNA and mature RNA molecules differ between species. In yeast, the rDNA is transcribed by Pol I as the 35S pre-rRNA (approx. 6900 nt) in a timeframe of around 170 seconds at optimal conditions (approx. 40nt/second). The 35S pre-rRNA can be processed either co-transcriptionally or post-transcriptionally, creating the 18S rRNA, which is part of the SSU, as well as the 5.8S and 25S rRNA, which are part of the LSU. The ITS2 is separating the 5.8S and

25S rRNA, whereas the ITS1 is dividing the rRNA destined for the SSU from the rRNA destined for the LSU. The endo- and exonucleolytic processing of the long pre-rRNA is still not fully understood in all details regarding succession of cleavage steps and the enzymes involved. The exact order of pre-rRNA can vary between species, even though they share common cleavage sites (Kos and Tollervey, 2010; Tomecki et al., 2017). In yeast, only half of the rDNA repeats are active (approximately 150) and therefore, accessible for Pol I, whereas the other half remains inactive. This ratio can be quickly modulated and is therefore an efficient way to react to changing environmental conditions or stress levels (Conconi et al., 1989; Dammann et al., 1993; Toussaint et al., 2005). Another way to regulate the activity of Pol I is the step of transcription initiation or elongation. The Pol I initiation-complex in association with the rDNA gene promoter recruits Pol I, which was previously activated by its initiation factor Rrn3 (Moss et al., 2007).

The 5S rRNA is transcribed by Pol III separately. This mature rRNA molecule associates with the LSU and is transcribed at loci separating the repeats of 35S rRNA genes on the chromosome. The short 5S rRNA (132 nt) is only processed at the 3'-end by the exonucleases of the RNase D family (Rex1, Rex2 and Rex3), which remove the last 12 nucleotides that serve as the termination signal for Pol III (Lee and Nazar, 1997; van Hoof et al., 2000).

The synthesis rate of 35S rRNA is kinetically coupled to rates of rRNA folding and processing and thus a balanced process, which can also serve as maturation checkpoint, as one example is the formation of the central pseudoknot (CPK) for the biogenesis of the small subunit (Choudhury et al., 2019; Sardana et al., 2015; Schneider et al., 2007). The removal of spacer sequences (ETS and ITS) of the 35S pre- rRNA does not only release the three mature 18S, 5.8S and 25S rRNA molecules, but the spacer sequence can also contribute with their secondary and tertiary structure to prevent premature folding or misfolding (Hughes, 1996; van Nues et al., 1995). A cleavage in the ITS1 spacer is necessary to separate the pre-18S rRNA from the pre-5.8S rRNA molecule, at the same time also separating the SSU from the LSU maturation pathway. The removal of the two ETS sequences is performed in a different way. The 3' end of 35S rRNA is endo-nucleolytically cut by the enzyme Rnt1, a member of the RNase III family. Rnt1 is localized in sub-nucleolar dots in the nucleolus, where the 35S rRNA, the first detectable pre-rRNA, can be identified. It is suggested that Rnt1 is removing the 3'-ETS co-transcriptionally since the

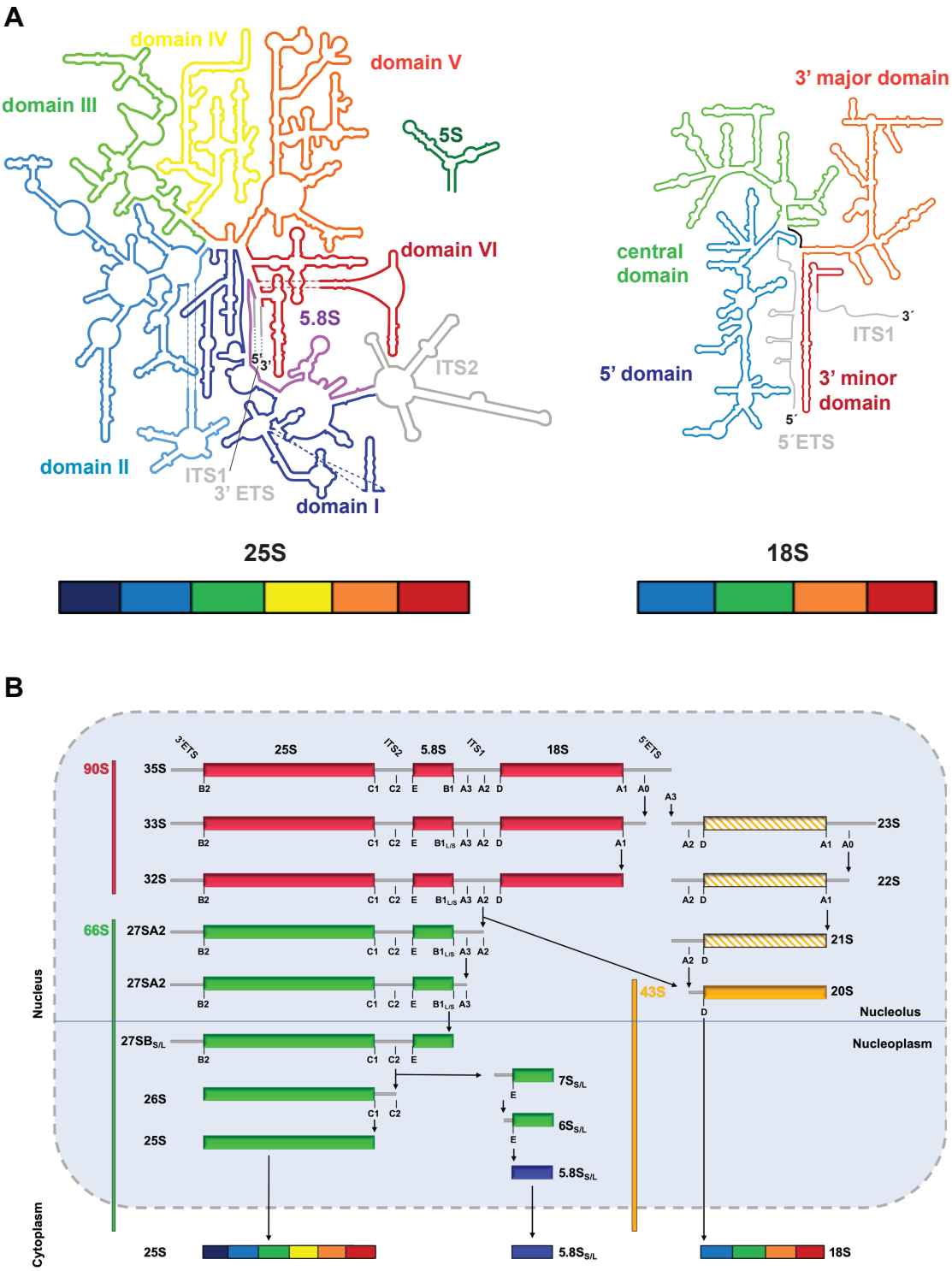

Figure 1.3 Mature rRNA is organized in specific subdomains as a result of hierarchical RNA processing. (A) 2D model of secondary structure of mature 25S, 5.8S, 5S and 18S rRNA. Subdomains of each species are indicated in different colors. Left panel: the six rRNA domains (dark blue: domain I, light blue: domain II, green: domain III, yellow: domain IV, orange: domain V, red: domain IV) of the large subunit 25S rRNA, the 5.8S (purple) and the 5S rRNA (green). Right panel: the four rRNA domains (blue: 5'domain, green: central domain, orange: 3'major domain, red: 3'minor domain) of the small

subunit 18S rRNA. (B) Schematic drawing of a single rDNA repeat transcribed by Pol I to yield the 35S pre-rRNA transcript, indicating the cleavage sites and processing pathways to produce mature 25S, 5.8S and 18S rRNA molecules. Figure (A) is adapted from (Bassler and Hurt, 2018).

accumulation of Rnt1 in dots-shaped structures co-localizes with the site of rDNA transcription (Henras et al., 2004).

The 5'-ETS is cut at two distinct sites. First, the A_0 cleavage site is processed and subsequently the downstream cleavage site A_1, which removes the reminder 5'-ETS from the 18S pre-rRNA. Processing at the A_0 and A_1 site results in the 33S rRNA and 32S rRNA, respectively (Beltrame et al., 1994). No processing enzyme has been identified yet for the first cleavage reaction of the nascent pre-rRNA at the A_0 site in the 5'-ETS. In contrast, it has been shown that Utp24 can efficiently cleave pre-rRNA at site A_1 and possibly at site A_2 in yeast and human cells (Tomecki et al., 2015; Wells et al., 2016a). The cleavage at site A_2 separates the SSU from the LSU moiety and generates the SSU 20S pre-rRNA and the LSU $27SA_2$ or $27SA_3$ pre-rRNA, depending on whether the cleavage in ITS1 occurs at site A_2 or A_3, respectively (Houseley et al., 2006; Lygerou et al., 1996; Mitchell et al., 1996). The 20S pre-rRNA is finally processed in the cytosol at site D by endonuclease Nob1, creating the mature 18S rRNA (Fatica et al., 2003; Vanrobays et al., 2001).

In yeast, the ITS1 cleavage at site A_3 is performed by the RNase MRP complex. If A_3 processing occurs prior to 5'-ETS processing, the 23S pre-rRNA is generated. Processing at cleavage site A_3 is proposed to target the 23S pre-rRNA to TRAMP (Trf4/Air2/Mtr4p Polyadenylation complex) complex, which belongs to the RNA surveillance machinery (Houseley et al., 2006; Houseley and Tollervey, 2008; Lygerou et al., 1996). An alternative explanation for A_3-cleavage is that cells under starvation distress prefer processing at site A_3 to create a 23S pre-rRNA as storage intermediate awaiting more favourable growth conditions (Kos-Braun and Kos, 2017). Furthermore, the 23S precursor rRNA has been identified as fully functional post-transcriptional processing intermediate capable to develop into mature 18S rRNA, although still under pre-60S mutant conditions (Talkish et al., 2016).

In higher eukaryotes like in plants or human cells, rRNA processing of ITS1 is mediated by cleavage at site A_2 (site 2a in human) and A_3 (site 2 in human) (Preti et al., 2013; Zakrzewska-Placzek et al., 2010). However, in contrast to the yeast system,

higher eukaryotes show a preference for cleavage at site A_3, while cleavage at site A_2 is the minor rRNA processing pathway (Sloan et al., 2013).

For the LSU ribosome biogenesis, the ITS rRNA processing is more complex and occurs in multiple steps, since both the ITS1 and ITS2 must be released. The $27SA_2$ pre-rRNA carrying a remainder of ITS1 can be processed in two mutually exclusive pathways. The major ITS1 processing pathway (85%) is mediated by the RNase MRP complex, cleaving ITS1 at site A_3 and thus generating the $27SB_S$ species (Schmitt and Clayton, 1993). The remaining ITS1 nucleotides are further processed by nuclear exonuclease Rat1 together with its co-factor Rai1 (Henry et al., 1994) or in a similar processing pathway by exonuclease Rrp17 (Oeffinger et al., 2009). Both exonucleases stop at site $B1_S$, creating the $27SB_S$ pre-rRNA species. The minor $27SA_2$ rRNA processing pathway (15%) cleaves at site $B1_L$, directly removing the remainder ITS1 by a yet still unknown RNA endonuclease resulting in a $27SB_L$ pre-rRNA molecule (Tomecki et al., 2017; Woolford and Baserga, 2013). Both 27SB rRNA species are substrates for the endonuclease Las1 and polynucleotide kinase Grc3 performing cleavage at site C_2 in ITS2. They generate the corresponding $7SB_S$ and $7SB_L$ forms, together with a 25.5S pre-rRNA molecule, which is processed to mature 25S rRNA by exonuclease Rat1 (Gasse et al., 2015; Pillon et al., 2017; Schillewaert et al., 2012). Both 7S rRNA molecules are successively processed in the nucleus by the RNA exosome releasing a $6S_S$ or $6S_L$ pre-rRNA intermediate. The remaining 30 nt long rRNA extension located in the RNA exosome tunnel is being processed by the exosome associated exonuclease Rrp6 (Lygerou et al., 1996). After export into the cytoplasm, the 6S pre-rRNA undergoes final maturation by cytoplasmic exonucleases Rex1, Rex2, Rex3 and Ngl2, generating the mature 5.8S rRNA (Faber et al., 2002; Fromm et al., 2017).

1.4 Ribosome assembly factors together with assembling ribosomal proteins drive the various ribosome maturation steps

The long ongoing research in the field of ribosome biogenesis uncovered over the past 20 years more than 200 eukaryotic assembly factors, which participate in the maturation pathways of the SSU and LSU. They were identified with genetic and biochemical approaches and to date, ribosome biogenesis is best understood in the model organism yeast (Fromont-Racine et al., 2003; Woolford and Baserga, 2013).

The first pre-ribosomal particles were identified in the 1970 by radiolabeling and sucrose-gradient analysis of HELA and yeast cells. The different isolated pre-ribosomes were determined by their sedimentation coefficients in Svedberg (S), thus leading to the nomenclature of the first discovered species: 90S, 43S/pre-40S and 66S/pre-60S particles (Kumar and Warner, 1972; Trapman et al., 1975; Udem and Warner, 1972). Affinity purified pre-ribosomal particles could be analyzed by cryo-EM, which had a strong impact in the ribosome biogenesis research field, giving detailed structural information of pre-ribosomes and specific maturation intermediates. The biochemical approach of tandem-affinity purification (TAP) of assembly factors was successfully applied to isolate distinct pre-ribosomal maturation intermediates, which could be further analyzed by various methods such as mass-spectrometry, northern blot or cryo-EM (Kressler et al., 2010). Many AFs display a broad variety of enzymatic functions (RNA helicases, methyltransferases, acetyltransferases, nucleases, kinases, phosphatases, AAA-type ATPases and GTPases). However, there are a number of AFs with no enzymatic function but still carrying out important roles during maturation of pre-ribosomes. These proteins serve as chaperones or act as placeholders in shielding and scaffolding the maturing pre-ribosome. Many of these AFs share motifs, which include classical RNA-binding motifs like RRM, KH, GAR, Brix, dsRBD, S1 and Zinc finger domains or protein binding domains like WD40, HEAT/ARM, HAT and TPR, respectively (Henras et al., 2015). Moreover, assembly factors can be organized in modules by protein-protein interaction or protein-rRNA interaction (Kressler et al., 2010). Even though a good number of the AFs are located within the structure of the pre-ribosome and contain conserved protein motifs, their detailed function within the complex RNA-protein network of the pre-ribosome remains still unknown.

Most of the highly conserved ribosomal proteins are essential for the function of ribosomes. In yeast, many ribosomal proteins have two copies (A/B) which arose from whole genome duplication. Hence, a single knockout is still viable, but a double knockout dead. Out of the 79 r-proteins, only 15 are nonessential and none of the 79 r-proteins have an enzymatic function, giving all of them a structural role. At high Mg^{2+} concentrations and in the absence of r-proteins the rRNA can rapidly fold in secondary and tertiary structures very similar to those of the mature ribosomal subunits. Nevertheless, without the guidance of r-proteins, the complex pathway of rRNA folding can lead easily to unstable or kinetically trapped structures (Woodson, 2011).

Moreover, the pre-rRNA is folded and complexed with r-proteins in a hierarchical manner, a principle that is evolutionary conserved from prokaryotes to eukaryotes (Woodson, 2008).

1.5 As the pre-rRNA emerges, the 90S pre-ribosome is co-transcriptionally assembled

The 90S pre-ribosome is an approximately 5 MDa huge macromolecular complex located in the nucleolus. This pre-ribosomal particle was first identified by sucrose centrifugation as huge protein assembly containing the 35S pre-rRNA in yeast (45S pre-rRNA in human) (Tamaoki, 1966; Trapman et al., 1975). Around the same time (1969), the 35S pre-rRNA could be observed by electron microscopy in *Xenopus laevis*, revealing a dense knob like structure at the 5'-end of nascent pre-rRNA transcripts called terminal knobs. These structures could be validated in several other eukaryotes. They depict the emerging pre-rRNA molecules as protruding from the rDNA strand in a tree like structure decorated with the dense balls at the pre-rRNA's 5'-ends (Figure 1.4 A). This visualization gave the electron microscopy pictures its name: "Christmas trees" (Granneman and Baserga, 2004; Miller and Beatty, 1969; Mougey et al., 1993). The terminal knobs correspond to assembly intermediates of pre-rRNA complexed with AFs (Figure 1.4 B). The recruitment of AFs to the newly transcribed pre-rRNA already initiates compaction of the terminal knobs as transcription proceeds. The first biochemically accessible pre-ribosome is the 90S particle, also termed SSU. Besides containing the r-proteins and AFs for maturation of the 40S subunit, the 90S pre-ribosome consists of several small snoRNAs and the large U3 snoRNP (Grandi et al., 2002). Noteworthy, pre-60S biogenesis factors are mainly absent from the 90S particle, even though the 35S rRNA carries both the SSU and LSU rRNA species. Depletion of most of the 90S AFs results in an impairment of pre-40S maturation but has only minor effects on the pre-60S pathway (Bernstein et al., 2004). The 90S pre-ribosome has a special place in ribosome biogenesis because with cleavage of the 35S pre-cursor rRNA at site A_2 (alternatively at A_3 or B_1), maturation of the SSU and LSU follows independent pathways. The two different maturation routes also share a unique set of r-proteins (RpS for SSU and RpL for LSU) and AFs, with very few shared AFs (Rrp5, Has1, Prp43, Pol5) (Braun et al., 2020; Emery et al., 2004; Lebaron et al., 2013).

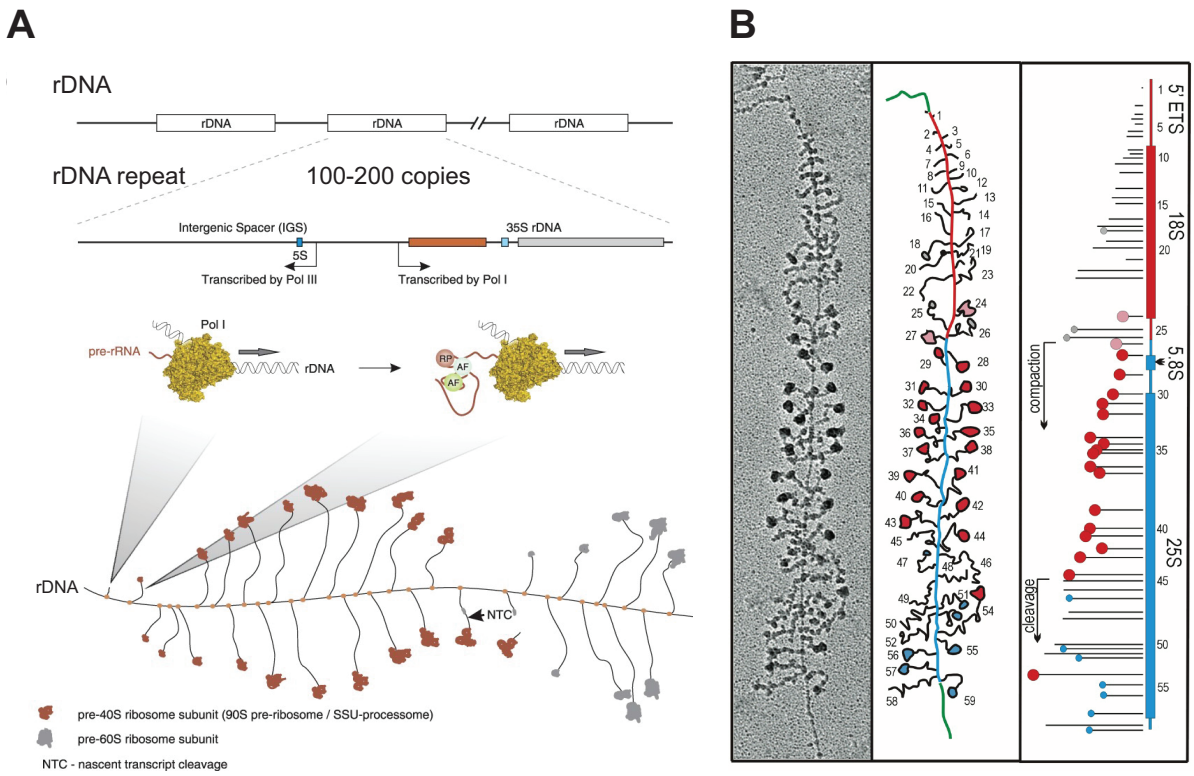

Figure 1.4 Co-transcriptional visualization of emerging pre-ribosomes as terminal knobs on rDNA repeats with the chromatin spread technique. (A) Structure of the rDNA locus and schematic visualization of rDNA transcription and co-transcriptional association of the nascent pre-rRNA with AFs. Figure taken from (Turowski and Tollervey, 2015). (B) Miller Spreads with the characteristic “terminal blobs” corresponding to the very first, pre-ribosomal assembly intermediates as well as a schematic interpretation of the EM graphs. Figure taken from (Osheim et al., 2004).

Because of the lack of 60S AFs and r-proteins, an alternative nomenclature for this particle was chosen at the time of discovery, the small subunit processome (SSU) (Bernstein et al., 2004; Dragon et al., 2002). However, this term does not fully describe this intermediate, because the real processing machinery, the RNA exosome, is still not incorporated (see later).

Pol I transcribes the 35S pre-rRNA in 5’-3’ direction, and thus the 5’-ETS is the first pre-RNA segment to emerge. Consequently, 90S AFs are being recruited to the pre-RNA in a hierarchical manner following the direction of transcription (Figure 1.5). Depletion studies showed that the UTP-A module is the first to be recruited to the nascent 35S pre-rRNA, serving as a major hub for the recruitment of other AFs, some of which are organized in modules (e.g., UTP-B, UTP-C and Mpp10), as well as for the recruitment of snoRNPs (Bernstein et al., 2004; Grandi et al., 2002; Krogan et al., 2004; Lee and Baserga, 1999; Perez-Fernandez et al., 2011). On the other hand,

depletion of many 90S AFs results in accumulation of 35S pre-rRNA and indicates a defect in pre-rRNA processing. In contrast, depletion of factors belonging to the UTP-A module force inhibition of pre-rRNA transcription altogether. Therefore, the UTP-A module is sometimes referred to as transcriptional UTP module (tUTP) (Gallagher et al., 2004; Granneman and Baserga, 2005). Besides being the first module, which assembles with the nascent pre-rRNA, UTP-A is also the largest module containing seven AFs (Utp4, Utp5, Utp9, Utp10, Utp15 and Utp17). It forms a large compact protein-protein network, mainly connected within the 90S pre-ribosome via binding interfaces to the U3 snoRNP and 5'-ETS (Osheim et al., 2004; Perez-Fernandez et al., 2007; Pöll et al., 2014). The UTP-B module, the second largest, is composed of 6 AFs (Pwp2, Utp6, Utp12, Utp13, Utp18 and Utp21) and has a more extended structure compared to the UTP-A module. It is thought to have a more scaffolding function for the 90S particle. The 5'-ETS rRNA is predominantly its rRNA binding interface. Both the UTP-A and UTP-B modules have no AFs with enzymatic activity and most factors predominantly consist of WD40 domains (ß-propeller) combined with α-helical domains (Hunziker et al., 2016; Kornprobst et al., 2016; Pöll et al., 2014; Zhang et al., 2016). A central and important RNA structure of the 90S, beside the rRNA, is the essential U3 snoRNP consisting of the U3 snoRNA and its core factors Nop1, Nop56, Nop58, Snu13 and Rrp9. Historically, many of the 90S factors are termed U three proteins (Utp), since they co-purified with the U3 snoRNA (Dragon et al., 2002; Grandi et al., 2002). The U3 snoRNP, the UTP-A and UTP-B module are thought to be a nucleation core for the evolving 90S particle. These three modules are the protein-scaffold of the early 90S particle, combining protein-protein and protein-RNA interactions. Together with the 5'-ETS, they serve as a platform for the recruitment of many other AFs and modules, finally generating the biochemically stable 90S pre-ribosome, which was also suitable for detailed cryo-EM analysis (Barandun et al., 2018; Champion et al., 2008; Kornprobst et al., 2016; Zhang et al., 2016).

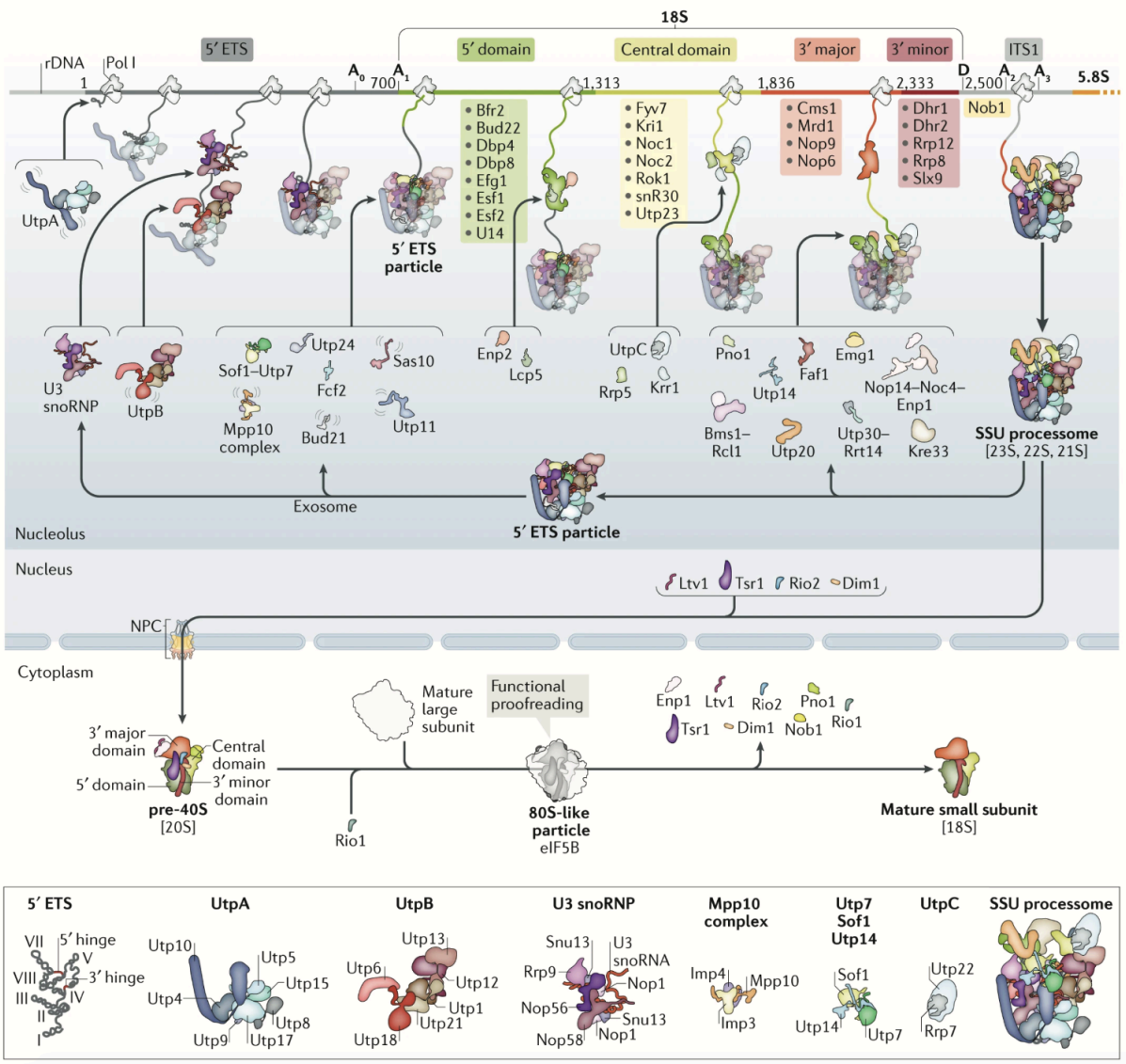

Figure 1.5 The 90S pre-ribosome is co-transcriptionally assembled with a set of AFs and modules that associate with the emerging pre-rRNA. Dynamic model of the co-transcriptional association of various AFs and modules with the emerging pre-rRNA, maturation of the resulting 90S intermediate and export of pre-40S subunits. NPC: nuclear pore complex, Pol I: RNA polymerase I, snoRNP: small nucleolar ribonucleoprotein. Figure taken from (Klinge and Woolford, 2018).

The U3 snoRNP plays a pivotal role in 18S pre-rRNA folding and processing (Hughes and Ares, 1991) and belongs to the class of C/D box snoRNPs, which catalyse a 2'-*O(H)*-ribose methylation to its RNA substrate. Thereby a hydrophobic group is introduced into the ribose, which helps strengthening RNA-protein interactions by weakening the RNAs hydrophilic character (Decatur et al., 2007). The U3 C/D box snoRNA, concentrated in the nucleolus and associated with pre-ribosomes, is highly conserved among all eukaryotes and was the first of its class to be identified (1968) (Hodnett and Busch, 1968; Weinberg and Penman, 1968). Early studies, before

structural cryo-EM data were available, demonstrated the interconnectivity of the U3 snoRNA within the 90S pre-ribosome. RNA cross-linking analysis showed base pairing of U3 to the 5'-ETS (5' hinge and 3' hinge) and 18S rRNA (box A and box A'). Noteworthy, the U3 snoRNA forms a hetero-duplex with the pre-18S rRNA sequence at a strategic position (Figure 1.6). Thereby, it prevents formation of the central 18S rRNA pseudoknot (CPK), a key feature in the mature 40S ribosomal subunit (Beltrame and Tollervey, 1992; Granneman et al., 2009; Hughes and Ares, 1991; Hughes, 1996). The biogenesis factor Imp3, serving as an RNA chaperone protein, partially unfolds the U3 snoRNA and therefore promotes hetero-duplex formation with the 18S rRNA (Shah et al., 2013). The release of the U3 snoRNA and initiation of the self-folding process of the central 18S rRNA pseudoknot is an important maturation step in 40S ribosome biogenesis and speculated to be facilitated by RNA helicase Dhr1 (Colley et al., 2000; Zhu et al., 2016).

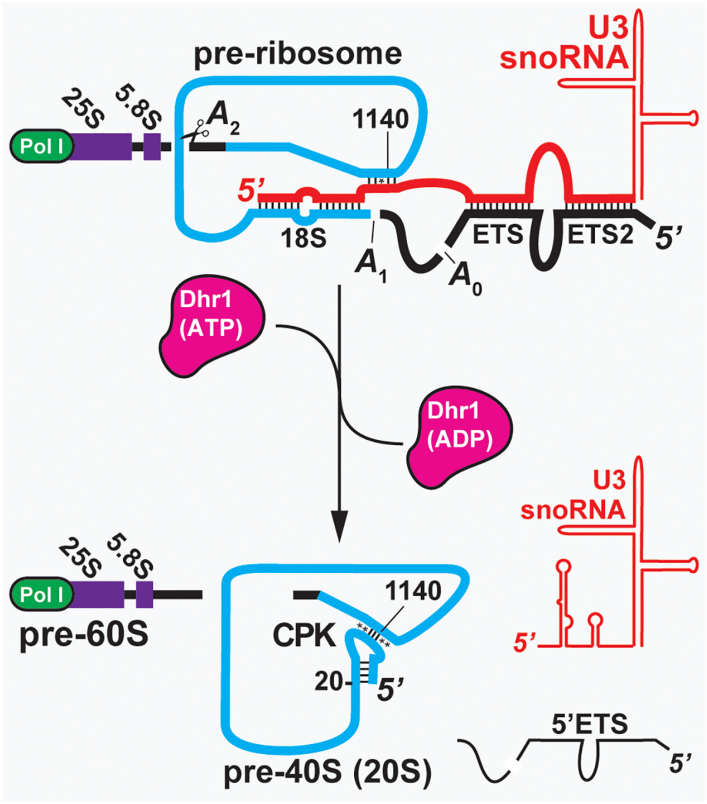

Figure 1.6 Formation of the central pseudoknot in the 18S pre-rRNA is prevented by heteroduplex formation with the U3 snoRNA. Upper panel: U3 snoRNA (red) base pairs co-transcriptionally with the 5'-ETS (black) as well as with the pre-18S rRNA (blue). Lower panel: Upon pre-rRNA processing at A_0, A_1, and A_2, ATP hydrolysis by Dhr1 releases the U3 snoRNA, which enables CPK formation in the pre-40S subunit. Figure taken from (Sardana et al., 2015).

The Mpp10 module (Mpp10, Imp3 and Imp4) does not exhibit a known enzymatic function and hence may mainly serve a structural role in the 90S particle. Imp4 is a member of the Brix family (biogenesis of ribosomes in *Xenopus*). Brix domain containing proteins share RNA and protein binding sites, which are supposed to function as a structural hub for protein and RNA interactions. In the case of Imp4, the Brix domain mediates binding to the U3 snoRNA and to a small helical element of Mpp10. Furthermore, the Mpp10 module is described as an essential component for U3::18S hetero-duplex formation and stabilization, as described in the previous chapter (Dunbar et al., 1997; Granneman et al., 2003; Sa-Moura et al., 2017; Wormsley et al., 2001). Moreover, the Mpp10 module is connected via Sas10/Utp3 to the UTP-B module, pointing to the interconnectivity of this rather small protein-complex within the 90S particle (Charette and Baserga, 2010).

The AFs Rcl1 and Bms1 form a heterodimer, which is recruited early to the 90S pre-ribosome. Rcl1 has been speculated to be the endonuclease performing cleavage at site A_2 within ITS1, which separates the pre-rRNAs of the large and small subunit biogenesis pathway. However, Rcl1 does not contain a typical nuclease domain fold (Gelperin et al., 2001; Horn et al., 2011; Karbstein et al., 2005). There is more data, from human and yeast cells, supporting the view that another endonuclease, Utp24, performs cleavage at site A_2, since Utp24 has a PIN domain typically found in many endonucleases (Bleichert et al., 2006; Sharma and Tollervey, 1999; Wells et al., 2016a). The assembly factor Bms1 is the only known GTPase acting within the 90S/SSU biogenesis pathway. Rcl1 binds to Bms1 in the presence of GTP to form a heterodimer, whereas GTP hydrolysis is thought to promote Rcl1 release from the pre-ribosome (Karbstein and Doudna, 2006; Karbstein et al., 2005). The importance of this enzymatic activity for 90S and 40S biogenesis has not been clarified in detail so far.

Another conspicuous module of the 90S is the Kre33 module, which consists of the assembly factors Bfr2, Lcp5, WD40 domain containing protein Enp2 and the nucleolar RNA acetyltransferase Kre33, which is assembled on the 90S as a homodimer. The human homolog of Kre33 (NAT10) is associated with the Hutchinson-Gilford progeria syndrome (Larrieu et al., 2018; Sleiman and Dragon, 2019). The Kre33 module assembles with the 5' domain of pre-18S rRNA (Bammert et al., 2016; Bassler et al., 2017; Sleiman and Dragon, 2019).

The UTP-C module of the 90S particle contains Utp22, Rrp7 and the CK2 kinase (Cka1, Cka2, Ckb1 and Ckb2 complex). Utp22 has structural similarity to tRNA nucleotidyltransferase but shares no catalytic activity. The UTP-C module is associated to the 90S particle through Rrp7 via its flexible carboxy-terminus, which is binding to ES6 of the 18 rRNA (Lin et al., 2013). Several studies support the idea that the CK2 kinase complex phosphorylates r-proteins and/or AFs and thus potentially has a role in the regulation of ribosome biogenesis (Phipps et al., 2011; Wojda et al., 2002). Noteworthy, the UTP-C module has been identified to associate with transcription factor Ifh1 and promotor associated protein Fhl1. Together, they form the so called CURI complex, which can control expression of r-protein genes (Albert et al., 2016; Rudra et al., 2007; Rudra et al., 2005). In addition, the TORC1 kinase (target of rapamycin 1) leads to dissociation of Ifh1 from promotor sequences when inactivated and thus causes silencing of r-protein gene expression. These two pathways, both linked to the UTP-C complex, show the fine balanced regulation of r-protein gene expression with levels of free r-proteins in the cell and the needs of ribosome biogenesis based on available nutrients (Albert et al., 2019).

To date, the exact function of most 90S AFs remains unknown, besides those carrying an enzymatic domain and thus defined through their enzymatic activity. Many of the AFs have WD40 (beta-propeller) and HEAT repeat domains like UTP-A and UTP-B module members, suggesting that protein-protein and protein-RNA interactions sites give those AFs a scaffolding function in the 90S pre-ribosomal structure (Phipps et al., 2011). Noteworthy, with the comprehensive structural information gained in recent years by cryo-EM analysis, some AFs could be located within the 90S particle. One example is Rrp5, a protein with dual function because it is essential for the maturation of both ribosomal subunits. It contains 12 S1 RNA binding domains and 7 TPR motifs, which mediate protein-protein interactions. Rrp5 is thought to be required for the initiation of the pre-60S pathway by bridging the pre-18S and pre-5.8S rRNA molecules within the 35S pre-rRNA (Lebaron et al., 2013). Some parts of Rrp5 could be located at the periphery of the 90S particle, binding close to the UTP-C module. The endonuclease Utp24, which is supposed to be responsible for rRNA cleavage at site A_1 and A_2, could be pinpointed to the central part of 90S particles in cryo-EM models of pre-ribosomes where A_1 cleavage has not occurred yet. It is seen in proximity to its putative rRNA substrate (Helix H1) for cleavage at site A_1 but still too far to reach it (approx. 35Å) (Cheng et al., 2017; Kornprobst et al., 2016).

Even though ribosome biogenesis has profited immensely from recent advances in cryo-EM technology, major parts of the 90S particle remained unresolved. For example, the ES3, ES6 and ITS1 pre-rRNA and associated proteins could not be visualized by cryo-EM due to the flexibility of rRNA segments and assembled proteins. Moreover, cryo-EM coupled with tandem-affinity purification is presenting only snapshots of pre-ribosomal particles in ribosome biogenesis (referred to in this work as states). It is likely that these techniques favour thermodynamically stable particles and states with a certain longevity as opposed to the high dynamic of individual events in ribosome biogenesis. One such transient event is the function of AFs with enzymatic activities. For example, at least 10 RNA helicases have been proposed to associate with the 90S particle (Dbp4, Dbp8, Has1, Utp25, Dhr1, Dhr2, Prp43, Fal1, Rrp3 and Rok1). They are thought to participate in ribosome biogenesis by unwinding RNA duplex structures while simultaneously consuming energy (ATP). However, none of them could be visualized on pre-ribosomes by cryo-EM or any other technique with the exception of Has1 assembled on pre-60S particles (Phipps et al., 2011)(Plus QUELLE Has1!). The RNA helicase Dhr1 in association with its activation-factor Utp14 is supposed to unwind the U3 snoRNA::18S rRNA duplex and therefore release the U3 snoRNA, finally allowing the formation of the 18S rRNA CPK (Granneman et al., 2009; Sardana et al., 2015; Zhu et al., 2016). With cryo-EM it was possible to visualize parts of Utp14. However, the location of Dhr1 on the 90S particle could not be identified prior to my PhD studies (Cheng et al., 2017).

1.6 Biogenesis of the pre-40S particle

The eukaryotic small subunit emerges from the 90S pre-ribosome in a process which is still largely unknown. It already contains several RpS proteins and some assembly factors, which are needed for later maturation of the pre-40S subunit. The factors associating with both pre-ribosomal intermediates, the 90S and pre-40S particle, are Pno1, Slx9, Noc4, Nop14, Enp1 and Rrp12 (Schafer et al., 2003). Notably, these AFs are already associated with rather early pre-40S biogenesis intermediates. Others, like Slx9 and Rrp12, are thought to play a role in the export of the SSU form the nucleus into the cytoplasm, and thus contribute to later events in the pre-40S biogenesis pathway (Fischer et al., 2015; Moriggi et al., 2014). The emergence of pre-40S particles from the 90S pre-ribosome requires a dramatic loss of 90S protein

modules and assembly factors, as well as RNA molecules like the U3 snoRNA, 5'-ETS and parts of ITS1. One major step to achieve this goal is thought to be the cleavage at site A_1, which releases the 5'-ETS from the pre-18S rRNA. It was assumed that the vast majority of AFs (UTP-A, UTP-B, U3 snoRNP, Mpp10 and single AFs) dissociate with the so called 5'-ETS particle as one moiety from the pre-18S remainder (Kornprobst et al., 2016). The emerging, first pre-40S particle, which contains the 20S rRNA, should then recruit a set of specific RpS proteins and later AFs (e.g., Tsr1, Dim1, Rio1, Rio2, Hrr25, Ltv1 and Nob1), which are required for the next steps in SSU maturation (Schafer et al., 2003). It is worth mentioning that in contrast to the 90S particle, the pre-18S rRNA molecule of the pre-40S particle already shares the typical structural features of a mature 40S subunit (body, platform, shoulder, and head domains) (Campbell and Karbstein, 2011; Karbstein, 2011; Schäfer et al., 2006; Schäfer et al., 2003; Strunk et al., 2011). Most of the processing of the SSU takes place at the head, platform, and shoulder regions of the particle, whereas the body region is close to a mature conformation. The formation of the beak structure, which is part of head region, is mainly triggered by the three proteins RpS3, Enp1 and Ltv1 (Schäfer et al., 2006). When Enp1 and Ltv1 are assembled to the pre-40S particle, a formation of the beak structure is prevented, which will finally form upon assembly of RpS3, RpS10, RpS12, RpS20 and RpS31. In a first step the phosphorylation of the three proteins RpS3, Enp1 and Ltv1 by kinase Hrr25 will lead to their dissociation. In a second step, RpS3 is dephosphorylated and can immediately reassemble to the pre-40S particle and thereby initiate the formation of the beak structure (Ghalei et al., 2015; Johnson et al., 2017; Schäfer et al., 2006). The position of Pno1 at the platform of the pre-40S particle is preventing a premature assembly of RpS26. The assembly factors Tsr1, Dim1 and Rio2 are located at the intersubunit side of the pre-40S particle and thus prevent association of translation factors eIF1 and eIF1A as well as association of mature 60S subunits to an immature pre-40S subunit (Lebaron et al., 2012; McCaughan et al., 2016; Strunk et al., 2011; Strunk et al., 2012). Noteworthy, the AF Tsr1 has a strong structural similarity to translational GTPases of the EF-Tu family (e.g., SelB and eIF5B). However, it lacks the enzymatic motif and can thus be seen as a placeholder, blocking the binding site of eIF5B. This GTPase plays a role in translation initiation and recruitment of 60S subunit in the cytosol (McCaughan et al., 2016). The endonuclease Nob1 is performing the final cytoplasmic processing of the pre-18S rRNA by cleaving the 20S rRNA at site D (Fatica et al., 2004; Granneman et

al., 2005; Lamanna and Karbstein, 2009). Notably, assembly factor Pno1 is masking cleavage site D of the pre-18S rRNA. Pno1 has first to dissociate or relocate to allow for D site processing and therefore it prevents premature endonucleolytic activity of Nob1 on pre-40S particle (Turowski et al., 2014). The ATPase Rio1 has the ability to displace Pno1, allowing Nob1 to perform cleavage at site D, and in a later biogenesis step to release Dim1 and Nob1 (Ameismeier et al., 2020; Parker et al., 2019).

1.7 Biogenesis of the pre-60S particle

Maturation of the large ribosomal subunit was always assumed and also seen to be independent of the pre-40S maturation, although it requires a successful transcription of pre-18S rRNA with flanking 5'-ETS and ITS1. The SSU and LSU biogenesis pathways are uncoupled upon cleavage at site A_2. Impairment of cleavage in ITS1 (A_2, A_3 and B_1) will also affect SSU biogenesis, whereas later defects in maturation do not affect biogenesis of the other ribosomal subunit (Axt et al., 2014; Gallagher et al., 2004; Kos and Tollervey, 2010; Osheim et al., 2004). The LSU maturation pathway shows complex and comprehensive remodeling and processing of the LSU scaffold. It has been shown that the pre-60S particle follows a hierarchical maturation route and can be divided in three major phases. Beginning with the formation of the solvent side interface, the construction of the exit tunnel follows and eventually the subunit interface is assembled (Gamalinda et al., 2014; Nissan et al., 2002).

More than 75 AFs are being recruited to pre-60S particle during maturation. Some are associated very transiently (e.g., Dbp3, Drg1, and Lsg1), whereas others stay associated with the pre-60S particles for most of the LSU biogenesis pathway (e.g., Nop7, Nog1 and Tif6). The maturation of the LSU is a highly energy-consuming process because many enzymes such as RNA helicases, AAA-type ATPases and GTPases are involved. Most of the AFs are found on early pre-ribosomes already and remain associated during maturation. The complexity of the pre-ribosome is decreased as a consequence of correct folding and the replacement of assembly factors by r-proteins (de la Cruz et al., 2015; Harnpicharnchai et al., 2001; Kressler et al., 2008; Nerurkar et al., 2015).

One of the first isolated intermediates of the LSU pathway is a 27S rRNA molecule containing particle associated with approximately 30 AFs (e.g., Ssf1, Mak5 and Has1) and several RpL proteins (Kressler et al., 2010). One of the earliest major

maturation events of the nucleolar pre-60S particle is the incorporation of the 5S rRNA in topologically twisted orientation. The 5S rRNA is assembled as 5S RNP together with Rpl5 and Rpl11 and the two factors Rpf2 and Rrs1 (Zhang et al., 2007). Another early event is the recruitment of the Noc2-Noc3 module and the assembly of Rix7, an AAA-type ATPase, which triggers the dissociation of the factor Nsa1 at a later stage. The Ytm1-Erb1-Nop7 complex plays an important role in $27SA_3$ to $27SB_S$ pre-rRNA conversion, supposedly by formation of a scaffold in nascent ribosomes and thus organizing certain regions of the pre-ribosome necessary for pre-rRNA processing (Granneman et al., 2011; Kressler et al., 2008; Miles et al., 2005; Milkereit et al., 2001; Tang et al., 2008). Similarly, to the early steps of the 90S biogenesis pathway, it has to be considered for early pre-60S particles that many maturation steps remain elusive probably due to heterogeneity and a short life span of intermediates.

The processing of ITS2 depends on cleavage at site C_2 and is catalyzed by Las1-Grc3-Rat1-Rai1 complex in a highly coordinated fashion. The endonuclease Las1 performs cleavage at site C_2 and subsequently, Grc3 phosphorylates the resulting 26S rRNA molecule. This allows exonuclease Rat1, together with Rai1, to directly process the remainder rRNA to a 25S molecule (Gasse et al., 2015). The remaining ITS2 moiety, being part of 7S rRNA, is further processed by the nuclear RNA exosome in association with RNA helicase Mtr4. The exosome is being recruited to the so called “foot structure” of pre-60S particles by the assembly factor Nop53. Bound to the pre-60S intermediate, the exosome is processing the 7S to a 5.8S rRNA molecule, thereby releasing the foot structure from pre-60S particles (Barrio-Garcia et al., 2016; Schuller et al., 2018; Thoms et al., 2015; Wu et al., 2017). Another major event taking place at this stage in ribosome biogenesis is the 180° rotation of the 5S RNP. The recruitment of the ATP-dependent Rix1-Rea1 machinery is a prerequisite for this rotation. Structural remodeling of rRNA helices together with the 5S RNP rotation finally results in the successful construction of the central protuberance (CP) (Barrio-Garcia et al., 2016; Wu et al., 2016).

Upon ATP hydrolysis, the AAA-type ATPase Rea1 triggers a cascade of rearrangements within the pre-60S particle, as well as a release of assembly factors Rsa4, but also at an earlier step release of the Ytm1-Erb1-Nop7 and the Rix1 complexes (Bassler et al., 2010; Kater et al., 2017; Thoms et al., 2016; Ulbrich et al., 2009). These ATP-consuming processes drive further maturation of the pre-60S particle. Noteworthy, some assembly factors act also as check-point proteins

remaining on the pre-60S particle until a correct remodeling step has occured. One such example is the GTPase Nug2, which is a placeholder for the pre-60S export factor Nmd3. The recruitment of Nmd3 needs the dissociation of Nug2, which on the other hand has been stimulated by the ATPase activity of Rea1. Together, this causes maturation of the central protuberance on pre-60S particles. Moreover, this checkpoint ensures a correct maturation of the yet immature particle before being exported from the nucleus into the cytoplasm (Matsuo et al., 2014). Due to the relative complexity of the pre-60S particles, there is a sophisticated quality control ensuring that only correctly assembled intermediates leave the nucleus. Several proteins are involved, including export adaptors Arx1 and Nmd3, as well as export receptor module Mex67-Mtr2, which is supposed to guide the large pre-60S subunit through the nuclear pore (Bradatsch et al., 2007; Bradatsch et al., 2012; Ho et al., 2000; Nerurkar et al., 2015; Yao et al., 2007).

Once exported into the cytoplasm, the pre-60S particle accomplishes the final maturation steps. The release of assembly factors is another checkpoint of pre-60S maturation. The AAA-type ATPase Drg1 mediates the release of shuttling factors Nog1 and Rlp24 in the cytoplasm. It is assumed that Drg1 does actively strip off these factors upon ATP hydrolysis (Kappel et al., 2012; Pertschy et al., 2007). Functionally similar, the GTPases Lsg1 and Ria1 together with Rei1 are necessary for the release of shuttling factors Nmd3, Arx1 and Tif6 from cytosolic pre-60S particles (Hedges et al., 2005; Hung and Johnson, 2006; Kressler et al., 2010; Ma et al., 2017; Malyutin et al., 2017). Finally, the mature 60S and 40S subunits can assemble, after a long and comprehensive biogenesis to form the 80S ribosome, ready to engage in translation.

1.8 The RNA exosome – a processing and degradation machinery involved in ribosome biogenesis

The eukaryotic RNA exosome is a conserved RNA degrading machinery involved in RNA quality-control, turnover and processing with the capability to completely degrade or precisely trim the RNA substrates. It is found both in the nucleus and in the cytoplasm (Chlebowski et al., 2013; Zinder and Lima, 2017). The exosome was discovered first in yeast but soon afterward a human counterpart was found (Allmang et al., 1999; Mitchell et al., 1997), which was shown to be related to many human disorders caused by genetic abnormalities (Morton et al., 2018; Reis et al., 2013). Both

the human and the yeast exosomes share nine catalytically inactive subunits (Exo-9), which form a barrel-like structure. It consists of a six-subunit ring (Rrp41, Rrp42, Rrp43, Rrp45, Rrp46 and Mtr3) and three cap proteins (Rrp4, Rrp40 and Csl4), which represent the exosome core. A tenth catalytic subunit, the 3'-5' exo- endonuclease Rrp44 (Dis3) associates with the base of the nine-subunit barrel-like structure to form the Exo-10, which is the active RNA processing core of both the nuclear and cytoplasmic exosome (Dziembowski et al., 2007; Makino et al., 2013) (Figure 1.7 A). The Exo-10 contains a long RNA binding tunnel with the entry at the exosome cap, channeling the RNA substrate through the exosome barrel where at the base the exonuclease Rrp44 is finally degrading the RNA (Makino et al., 2015; Schuller et al., 2018).

From yeast to higher eukaryotes, the nuclear exosome has four distinct co-factors. The exoribonuclease Rrp6 together with Rrp47 bind to the exosome cap and shuttle the Exo-10 into the nucleus (Gonzales-Zubiate et al., 2017). The Rrp6-Rrp47 dimer together with the third nuclear cofactor Mpp6 are recruiting the 3'-5' RNA helicase Mtr4 to the nuclear exosome (Lingaraju et al., 2019; Wasmuth et al., 2017). The Mtr4 helicase can unwind RNA duplex structures and therefore channel the RNA substrate to the exosome core. Furthermore, it can remodel or release ribonucleoproteins tethered to the RNA (Johnson and Jackson, 2013; Weick et al., 2018).

Moreover, the nuclear exosome is directly involved in processing of ribosomal RNA precursors of both the small and the large ribosomal subunit (Kornprobst et al., 2016; Schuller et al., 2018; Thoms et al., 2015). In case of pre-60S maturation, the RNA exosome is remodeling the particle and trimming its substrate rRNA to a precise point, before dissociating again. First, the exosome is recruited together with its RNA helicase co-factor Mtr4 at a specific maturation stage to the pre-60S ribosome via the adaptor protein Nop53. The recruitment is mediated by the so-called arch-interacting motif (AIM) of Nop53, which binds to the "arch" domain of Mtr4 (Figure 1.7 B) (Falk et al., 2017; Lingaraju et al., 2019; Thoms et al., 2015). Once Mtr4 helicase has bound the 3'-end of its 7S rRNA substrate, the RNA is pulled upon ATP hydrolysis by Mtr4 through the exosome core, where the 7S rRNA is trimmed by exonuclease Rrp44 to a precursor 5.8S rRNA, carrying a 30 nt 3' extension, which remains in the exosome tunnel.

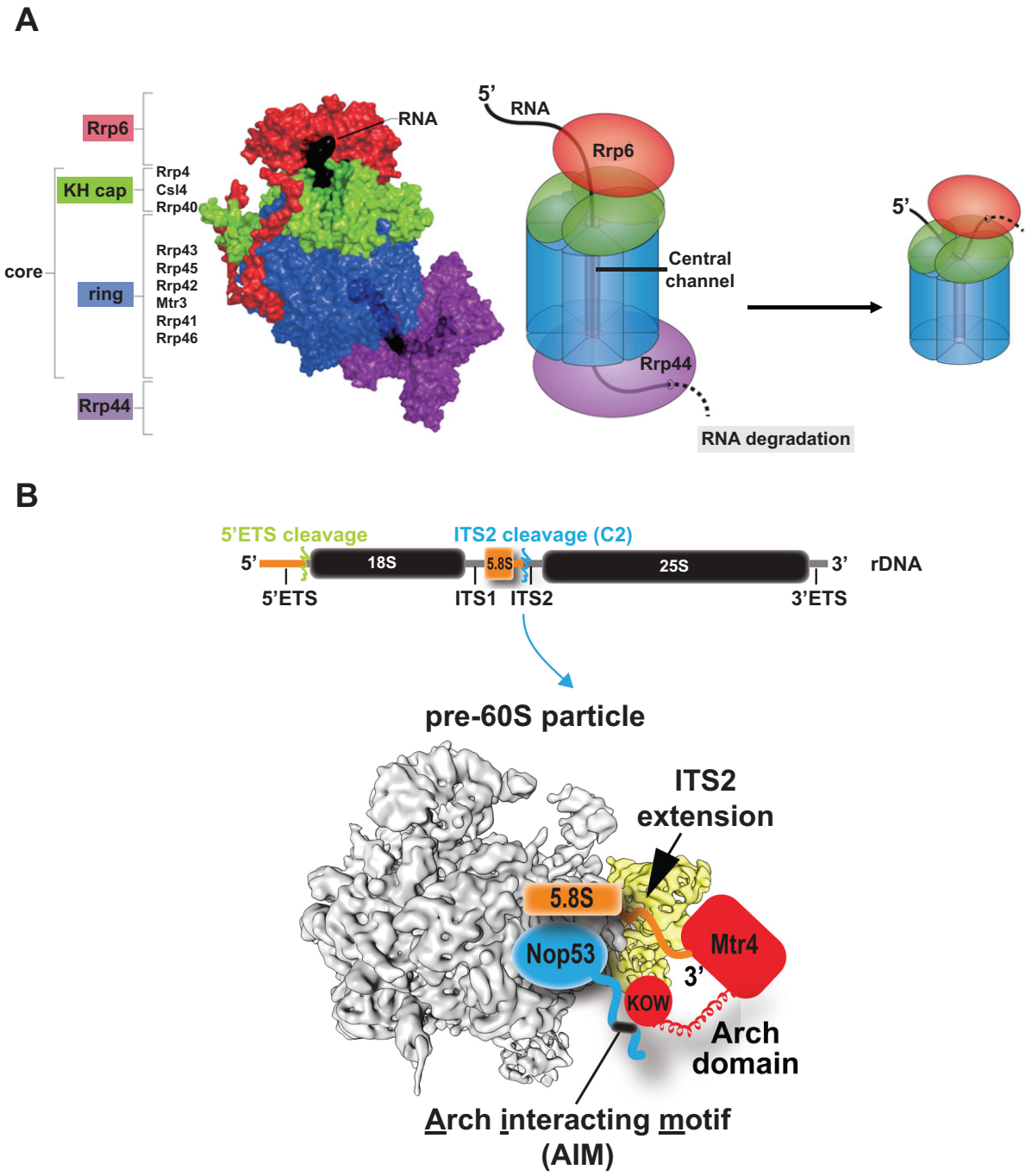

Figure 1.7 Structure of the nuclear exosome and its involvement in pre-60S ribosome maturation. (A) Left: density model of the yeast core exosome (green: cap and blue: PH-ring (barrel)) in association with Rrp44/Dis3 (purple), Rrp6 (red) and channeled RNA (black). Right: Schematic model of the exosome channeling the substrate RNA in 5'>3' direction for degradation by Rrp44/Dis3 or for degradation of 30 nt remainder RNA molecule by Rrp6. Figure adapted from (Kilchert et al., 2016). (B) Schematic model of the AIM motif of Nop53 interacting with the arch domain of Mtr4. Nop53 recruits the exosome to pre-60S particles and is guiding ITS2 extension into exosome tunnel for degradation. Figure adapted from (Thoms et al., 2015).

Subsequently, this 30 nt remainder is processed by the nuclear exosome subunit Rrp6 exonuclease to a 6S rRNA species (5.8S with a 6-8 nt 3' extension) (Briggs et al., 1998). This precise trimming of the 7S rRNA can be mediated by a decisive interplay of ribosomal proteins and AFs (e.g., Nop53, Nop7) with the exosome. Moreover, besides the RNA trimming, the exosome is remodeling the so called "foot structure" (parts of ITS2, Nop7, Nop15, Nop53, Rlp7 and Cic1) of the pre-60S particle, which is eventually leading to its dissociation ((Fromm et al., 2017; Schuller et al., 2018).

Taken together the exosome is an efficient RNA degrading and processing machinery and, when tethered to the pre-60 ribosome, can besides precisely trimming of the 7S rRNA also efficiently remodel the pre-60S particle and therefore play an important role in large subunit maturation. Noteworthy, the 90S pre-ribosome AF Utp18 is carrying an AIM motif, which was shown to bind to Mtr4 *in vitro*. Therefore, it is speculated that Mtr4 together with the exosome is degrading the 5'-ETS rRNA of the 90S pre-ribosome after it was released from particle (Kornprobst et al., 2016; Thoms et al., 2015).

1.9 Aims of the PhD study

At the beginning of my PhD study, the 90S pre-ribosome (also called SSU processome) has been for the first time structurally characterized by cryo-EM, revealing about 50 AFs decorating or even sometimes deeply penetrating into the core structure of the 90S particle. A number of 90S AFs were known to be organized in subcomplexes, but for many of them little was known whether they exist in biochemically stable modules. One of these factors was Noc4, which together with Nop14 was known to form a subcomplex. However, I wanted to explore whether Noc4 biochemically interacts with further 90S factors. Therefore, I performed a yeast 2-hybrid assay to find new interactors, with the plan to validate them by *in vitro* reconstitution. This finally revealed a new module of the 90S, the Noc4-Nop14-Emg1-Enp1-Rrp12 complex, composed of factors that are present in both the 90S and pre-40S particles.

After reconstitution of the Noc4 module, I wanted to learn more about the 90S-to-pre-40S transition in the ribosome biogenesis pathway, which finally gives rise to a first pre-40S particle upon dismantling of the huge 90S pre-ribosome. For that, I considered to isolate pre-ribosomal intermediates specifically covering this so far poorly understood biogenesis step. To reach this goal, I sought to use the split-tag affinity-purification technique with Noc4 as a broad 90S bait and as a second bait the RNA helicase Dhr1, known to dismantle the U3 snoRNP, which is a key module of the 90S pre-ribosome. By employing this approach, I was able to isolate novel pre-40S intermediates containing classical pre-40S but also a few residual 90S AFs, which in overall opened the door to clarify the long-sought 90S-to-pre-40S transition.

2. Results

2.1 Identification and characterization of the Noc4-Nop14-Emg1-Enp1-Rrp12 module on the 90S particle

The 90S pre-ribosome typically consists of biochemically stable subcomplexes, or modules, which are grouped together through RNA molecules (rRNA, snoRNA) to form this huge particle. Several such modules have been identified such as the UTP-A, UTP-B, UTP-C and Mpp10 module (see Introduction). With the identification of a new subcomplex consisting of Noc4, Nop14, Emg1, Enp1 and Rrp12 and subsequent isolation of pre-ribosomal particles, we were able to identify and biochemically characterize a novel pre-40S intermediate.

The protein Noc4 contains a Noc-domain, which is a conserved stretch of about 45 amino acids involved in binding of its binding partner. Besides Noc4, there are 3 other AFs, Noc1, Noc3, which contain a Noc-domain and participate in the production of the large subunit (Milkereit et al., 2001). We found Noc4 as part of an interaction cluster in Y2H assays with Nop14, Enp1, Emg1 and Rrp12 (Supplemental Figure S1). Nop14, Emg1 and Noc4 are exclusive 90S factors, while Enp1 and Rrp12 have a function in 90S biogenesis and remain in the 40S production pathway on late pre-40S particles. CRAC analysis (Cross-linking and cDNA Analysis) showed that Enp1 and Rrp12 associate with the 3' domain of the 18S rRNA and later cryo-EM analysis confirmed this interaction with structural models of late pre-40S particles (Ameismeier et al., 2018; Granneman et al., 2010). Hence, this finding motivated us to further investigate whether these AFs form a biochemically stable module together and whether we can find out how a module consisting of 90S and pre-40S factors participates in ribosome biogenesis. Specifically, we were intrigued by the possibility that a potential 90S module, which also consists of pre-40S AFs, could be involved in the so far poorly understood process that results in the transformation of 90S particles into pre-40S subunits.

To further investigate if these proteins form a complex and can act as a larger module, we aimed to reconstitute the proteins in a dimeric, trimeric and pentameric complex. For that, the corresponding proteins from *Chaetomium thermophilum* were used, which often show superior biochemical properties compared to the ones from yeast or other eukaryotes. These factors were overexpressed under a galactose

inducible promoter (GAL promoter) and affinity purified via the tagged proteins. If binding occurs, the untagged overexpressed assembly factors are pulled down as well. Indeed, a pentameric complex of Noc4-Nop14-Emg1-Enp1-Rrp12 could be isolated (Fig. 2.1 A). In the case of Rrp12, only the HEAT repeat domain (residues 1-1,039) was used for reconstitution assays because of better biochemical behavior compared to the full-length protein. With this biochemical approach we could define and expand the Noc4-module from Noc4-Nop14-Emg1 to a set of five assembly factors: Noc4-Nop14-Emg1-Enp1-Rrp12. Furthermore, a series of 90S pre-ribosomes from *Chaetomium thermophilum* was isolated with a split-tag affinity-purification approach, using Kre33-TEV-protA as first bait and Noc4-FLAG as second bait.

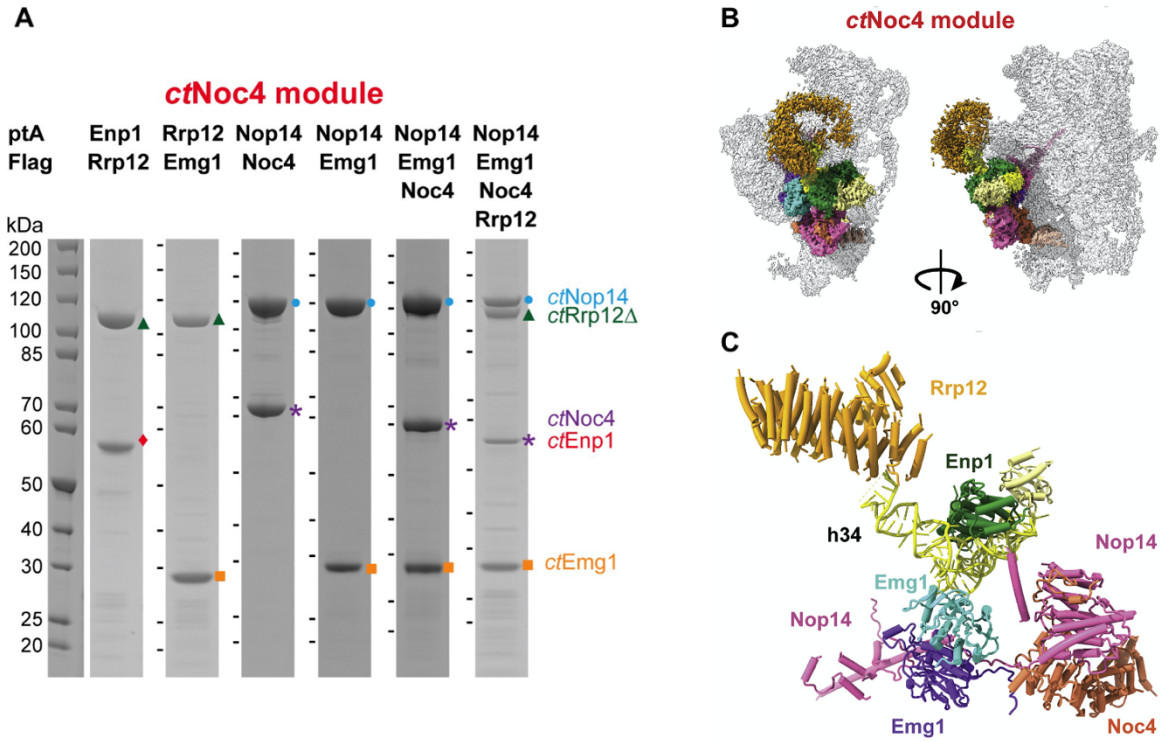

Figure 2.1 The Noc4 module on 90S particles consists of both typical 90S AFs (Noc4, Nop14, Emg1) as well as 90S/pre-40S factors (Enp1, Rrp12). (A) Biochemical reconstitution of the Noc4-Nop14-Emg1-Enp1-Rrp12 module. Indicated thermophilic proteins were tagged with ProtA-TEV, the Flag epitope or untagged as indicated. Proteins were overexpressed under the control of a galactose inducible promoter in *Saccharomyces cerevisiae* and tandem affinity purified. Eluates were analyzed by SDS-PAGE and Coomassie staining. (B) Cryo-EM density of the thermophilic 90S pre-ribosome with highlighted Noc4 module in different colors (yellow, Rrp12; green, Enp1; cyan/purple, Emg1; pink, Nop14; orange, Noc4). (C) Organization of the Noc4-Nop14-Emg1-Enp1-Rrp12 module around 18S rRNA helix h32-34 (yellow). A poly-Ala model is provided for Rrp12 as a placeholder. Figure was adapted from (Cheng et al., 2019).

Combined with cryo-EM analysis and modelling, we could refine the already existing 90S particle as well as its maturation and gain structural information on the Noc4 module, among other new features of the 90S pre-ribosome (Fig 2.1 B). State B1 clearly shows all five module members of the Noc4 module and their organization on the 90S pre-ribosome. In the depicted model for the Noc4 module, a poly-alanine model for Rrp12 and Enp1 was used (Fig 2.1 C), meaning that the molecular models could be positioned lacking side-chain information. The pentameric complex is seen organized around helix h32-34 of the 18S rRNA (Fig. 2.1 B and C). This might serve as a recruiting platform for the whole Noc4 module as one entity. Alternatively, subcomplexes of the Noc4 module, e.g. Noc4-Nop14-Emg1 and Rrp12-Enp1, could assemble upon accessibility and organization of helix h32-34. The cryo-EM structure shows members of the Noc4 module protein-protein interaction network in close proximity to their binding partners, or even visualizes direct interaction surfaces of the proteins (Noc4-Nop14; Nop14-Emg1).

2.2 The 90S>pre-40S transition occurs in novel pre-ribosomal intermediates

2.1.2 Novel pre-40S biogenesis particles contain the Noc4-module

To isolate pre-ribosomal intermediates at the transition from a 90S pre-ribosome to the primordial pre-40S particle, we employed the approach of a split-tag tandem-affinity purification. We chose the assembly factor Noc4 as first bait due to its association with a broad range of 90S intermediates, which is corroborated by the fact that the Noc4 module contains the dual 90S/pre-40S AFs Enp1 and Rrp12, as well as by structural information of the module on the 90S particle. To catch pre-ribosomal during the transition period, it was important to choose an AF as second bait, which is known to regulate early key events in the pre-40S biogenesis pathway. For that, we chose the DEAH-box RNA helicase Dhr1, which releases distinct RNA heteroduplexes between the U3 snoRNA and 18S rRNA. The dissociation of U3 snoRNA is presumed to cause the formation of 18S rRNA pseudo knot (CPK), which is a hallmark in the maturation of pre-40S particles (Boneberg et al., 2019; Sardana et al., 2015; Zhu et al., 2016) (see Introduction). Moreover, it was shown before that a catalytic mutant of Dhr1, *dhr1* K420A, accumulates stalled pre-40S intermediates, which sediment at around 45-55S and contain the 20S pre-rRNA but also U3 snoRNA

as well as some 90S biogenesis factors (Mpp10, Imp4, Utp14) (Zhu et al., 2016). Additionally, it regulates A_1 cleavage. This indicated that Dhr1 is present on pre-ribosomes, which undergo the changes necessary to transform a 90S particle into the pre-40S intermediate.

With these two selected baits, Noc4 and Dhr1, we could enrich pre-ribosomal particles with a band pattern characteristic of 90S particles and indeed further separate them on a sucrose gradient into a pre-40S and 90S pool (Figure 2.2 A). This observation was unusual and a key step to my PhD study, since normally, isolated 90S pre-ribosomes separate into a heavy pool (fraction 11-13) and, if the 90S particle was isolated via a member of a 90S module, into a pool of free modules running in the first fractions of the gradient. We therefore analyzed protein bands of the 90S and pre-40S fractions (#8 and #12) by MALDI (Matrix-Assisted Laser-Desorption-Ionization) mass spectrometry.

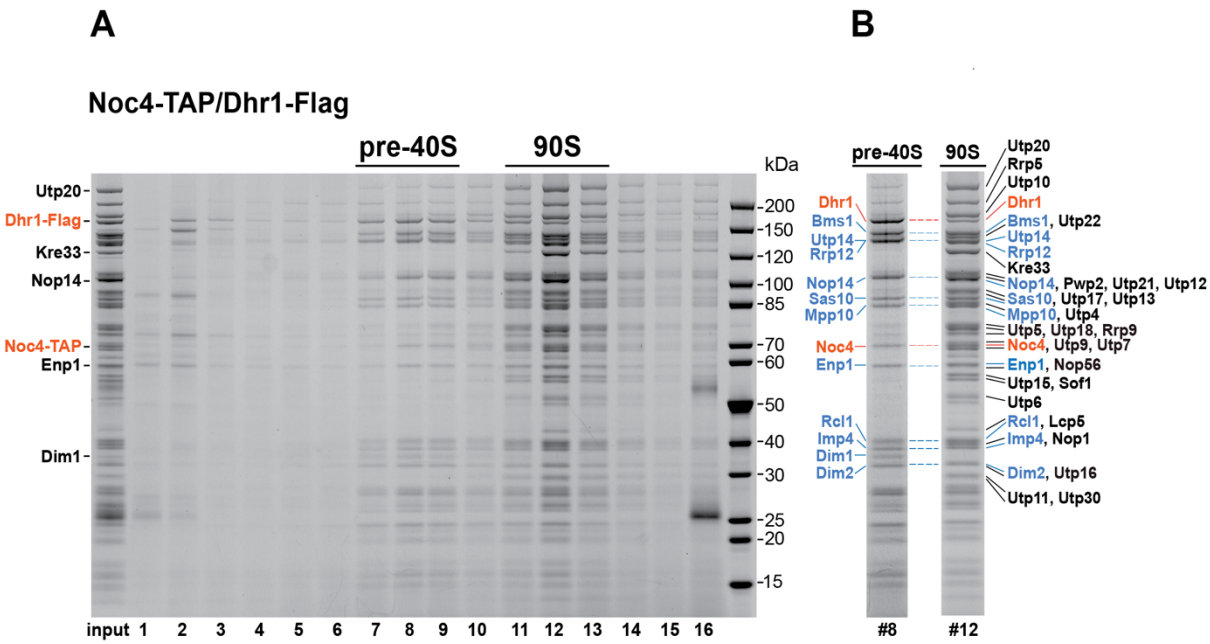

Figure 2.2 Noc4-Dhr1 split tandem-affinity purification contains 90S and unusual pre-40S particles. (A) Sucrose gradient centrifugation of Noc4-Dhr1 eluate. Input and fraction 1-15 were analyzed by SDS-PAGE and Coomassie staining. Lanes 7-9 and 11-13 contain the pre-40S and the 90S, respectively. (B) Side by side comparison of pre-40S and 90S factors (90S factors, black; dual 90S and pre-40S factors, blue; baits, orange). Labeled factors were excised from the gel and identified by mass spectrometry. Figure was adapted from (Cheng et al., 2020).

The 90S fraction revealed a protein composition similar to what was observed in other studies for a classical 90S pre-ribosome, with the exception that Dhr1 was found in

stoichiometric amounts on the 90S particle (Kornprobst et al., 2016). To our surprise, the pre-40S pool enriched not only classical dual 90S and pre-40S factors (e.g., Enp1, Rrp12, Pno1), but also contained AFs like Bms1 and Mpp10, which were thought to be exclusively associated with the 90S pre-ribosome. These factors were not only present as single assembly factors on the pre-40S particle, but with their respective binding partners or module members. For example, the whole Mpp10 module (Mpp10, Imp3, Imp4, Sas10) and Bms1 hetero-dimer (Bms1 and Rcl1) were present on the isolated pre-40S particles (Figure 2.2 B). The migration behavior of this unusual intermediate together with the identified proteins, which are found in distinct Coomassie-stainable bands by SDS-PAGE reflects the composition, mass and size of pre-ribosomal particles and hence correlates well with pre-40S intermediates. Moreover, the methyltransferase Dim1 was strongly enriched in the pre--40S pool, indicating a recruitment of this assembly factor specifically during the process of transition from the 90S to pre-40S pre-ribosome (Figure 2.2 B).

To further characterize the isolated 90S and unconventional pre-40S particles, we wanted to analyze their rRNA species. For that, we performed Northern blotting of the Noc4-Dhr1 purification separated in fractions on a sucrose gradient by using one half of each fraction for protein analysis by SDS-PAGE (Figure 2.3 B upper panel) and one half for RNA analysis by northern blotting (Figure 2.3 B lower panels). The Northern probes used for hybridization are indicated in a schematic overview of processing events occurring within small subunit maturation, which displays all rRNA molecule intermediates with indicated cleavage sites (Figure 2.3 A). The 90S fraction from the Noc4-Dhr1 purification contains the 5'-ETS A_0 fragment, which was observed before in other 90S purifications (e.g., Enp1-FTpA, Pwp2-FTpA, or Utp22-FTpA (Kornprobst et al., 2016)). The cleavage at site A_0 is performed before cleavage at site A_1 and thus the 5'-ETS A_0 molecule is the predominant 5'-ETS species in 90S particles (Barandun et al., 2018; Chaker-Margot et al., 2017; Kornprobst et al., 2016; Sun et al., 2017). Moreover, the 90S fraction contains the 23S pre-rRNA species, which is a 5' end-A_3 fragment indicating no cleavage in 5'-ETS. In addition, the 90S fraction carries a 21S pre-rRNA which has been generated by cleavage at site A_1. Together these two rRNA species of isolated 90S particles are indicative of both pre-A_1 and post-A_1 cleavage states.

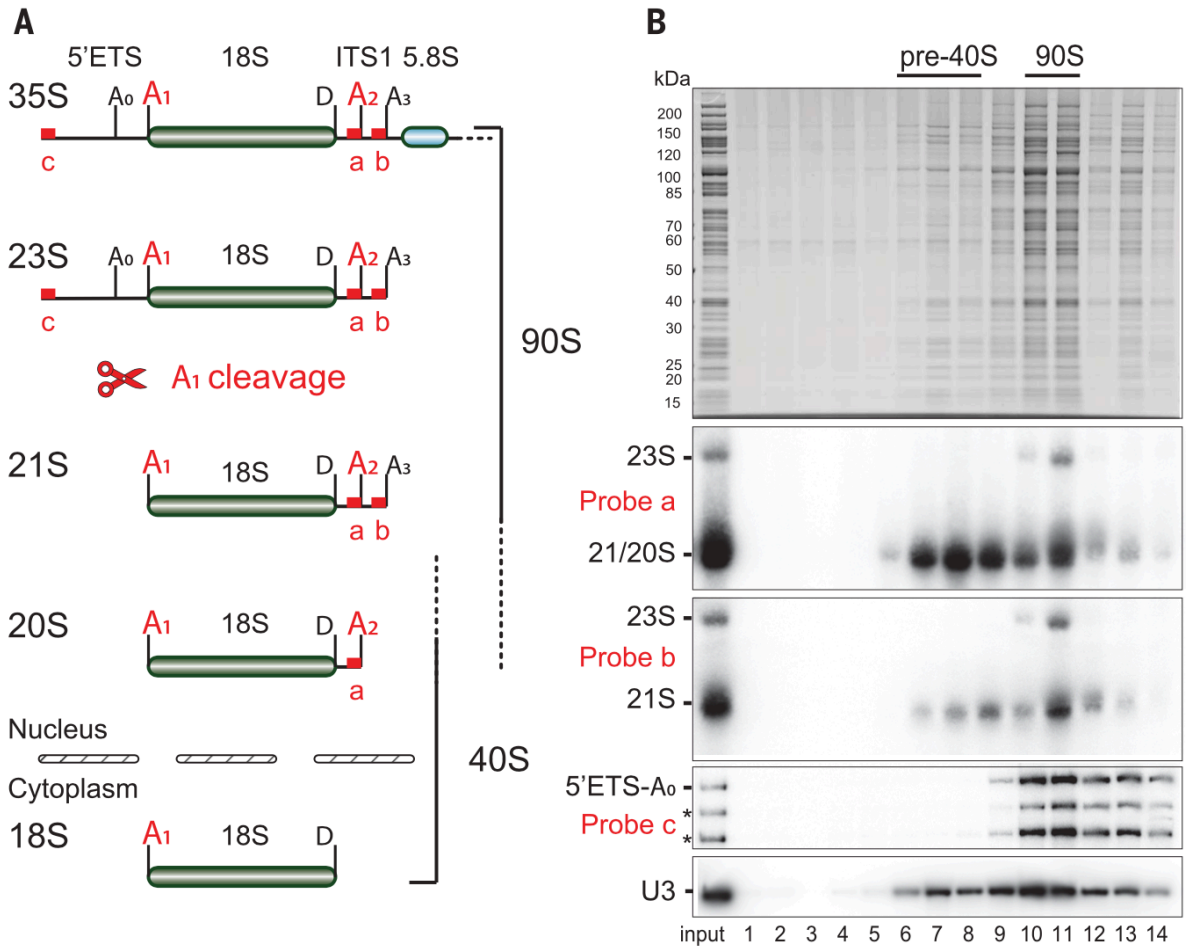

Figure 2.3 Purification of Noc4-Dhr1 transition particles and analysis of the associated pre-rRNA intermediates. (A) Schematic overview of rRNA processing in yeast during 40S subunit biogenesis with hybridization sites of probe a, b and c on 35S rRNA indicated. (B) Noc4-Dhr1 split-tag affinity-purified intermediates separated by sucrose gradient, followed by SDS-PAGE and Coomassie staining (upper panel) and Northern blotting (four lower panels). The two upper panels show a 1.2% agarose gel for separation of larger rRNA species (23S/21S/22S rRNA), the two lower panels show the 5'-ETS and U3 snoRNA and were resolved on a 6% polyacrylamide gel, respectively. Probes from (A) are indicated as well as the different pre-rRNA species. Northern blot analysis was performed by Dr. Giuseppe La Venuta. Figure taken from (Cheng et al., 2020).

In contrast, the unconventional pre-40S fractions contains predominantly 20S pre-rRNA, which is derived from cleavage at site A_1 and A_2. This suggests that the species is derived from a 21S rRNA molecule cleaved at site A_2, leading to a release of 20S pre-rRNA. Both states, the 90S and pre-40S, contain the endonuclease Utp24 which has been speculated to perform cleavage at site A_1 and/or at site A_2 (An et al., 2018; Bleichert et al., 2006; Tomecki et al., 2015; Wells et al., 2016b). Moreover, both the 90S and pre-40S fractions contain the U3 snoRNA as well as the RNA helicase Dhr1, which is supposed to release the U3 snoRNA (Figure 2.3 B). This finding

strongly suggested that the unusual pre-40S intermediate was undergoing a transition from 90S particles, which contain the U3 snoRNA, to classical pre-40S particles, which do not contain the U3 snoRNA (Sardana et al., 2015). Motivated by the finding of a novel ribosome biogenesis intermediate, we further tried to enrich the unusual pre-40S particle. For that, we performed a split-tag affinity purification with Dhr1 as first bait together with Dim1 as second bait, because we found Dim1 strongly enriched in the pre-40S pool. Again, we were able to separate this preparation on a sucrose gradient into a 90S and unusual pre-40S pool, essentially confirming the previous results (Figure 2.4).

Taken together, with the split-tag purification approach, we were able to isolate novel ribosome biogenesis intermediates using the bait combination Noc4-TAP-Dhr1-Flag. Sucrose gradient analysis combined with Northern Blotting revealed an unusual composition of a pre-40S pool containing 20S pre-rRNA. We were able to enrich the novel pre-40S particle performing split-tag affinity purification with AFs, which were found in high amounts in the pre-40S pool (Dhr1-TAP-Dim1-Flag). However, the overall yield was lower than in the Noc4-TAP-Dhr1-Flag sample. This is indicative of a rather small cellular pool of the identified pre-ribosomal intermediates.

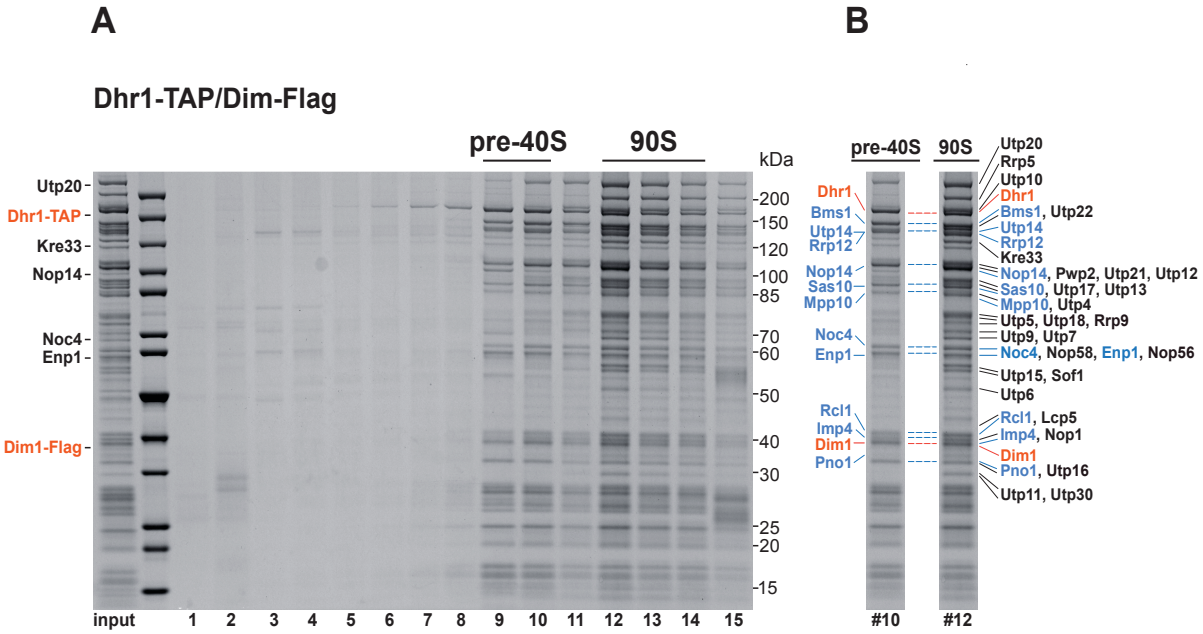

Figure 2.4 Isolation of 90S pre-ribosomes and unusual pre-40S particles based on split-tag affinity purification using Dhr1-Dim1 as baits. (A) Sucrose gradient centrifugation of the Dhr1-Dim1 Flag eluate and subsequent analysis by SDS-PAGE and Coomassie staining. (B) Side by side comparison of pre-40S and 90S factors (90S factors, black; dual 90S and pre-40S factors, blue; baits, orange). Labeled factors were excised from the gel and identified by mass spectrometry. Figure was adapted from (Lau et al., 2021).

2.2 Cryo-EM reveals a series of structures 90S structures that finally lead to the formation of primordial pre-40S ribosomes

The discovery of a novel and very early pre-40S particle and its biochemical analysis prompted us to reveal its cryo-EM structure, which was done in collaboration with the Prof. Roland Beckmann and the Beckman Lab at the Gene Center Munich. To provide them with our biochemical isolates, we affinity-purified by split-tag, either Noc4-Dhr1 or Dhr1-Dim1 bait combinations, from yeast cultures of 48 liters per preparation to ensure sufficient amounts for cryo-EM analysis. These samples contained a series of pre-ribosomal particles covering small subunit biogenesis from the early 90S particles until the transition into a primordial pre-40S particle after A_1 processing is completed.

2.2.1 Maturation of 90S particles culminates in A_1 cleavage by the Utp24 endonuclease

3D classification of the samples containing both 90S and the unusual pre-40S pre--ribosomes revealed seven distinct and well-defined classes of pre-ribosomal particles, which could be placed in a chronological order (Figure 2.5). For states B2, pre- A_1, post- A_1 and Dis-C, the average resolution was between 3.5 Å and 3.9 Å, which made it possible to build and refine complete models of the states. States A, Dis-A, and Dis-B showed an average resolution between 4.4 Å and 7.1 Å, which allowed rigid-body docking of molecular models. State A and B2 essentially resemble state A, B1 and B2 from the *Chaetomium thermophilum* sample upon Kre33-TAP-Noc4-FLAG split-tag affinity purification and cryo-EM analysis. Moreover, they share the characteristics that are common to pre-ribosomal particles with a non-cleaved A_1 site (Chaker-Margot et al., 2017; Cheng et al., 2017; Kornprobst et al., 2016; Sun et al., 2017).

In state A, the Kre33 module, Utp20 and the ES6 of the 18S rRNA could not be resolved, arguing that they are either not associated with or loosely attached to the pre-ribosome. Moreover, much of the 5’ domain rRNA is not visible. In state B2, these factors and rRNAs are more stably attached and thus can be visualized by cryo-EM analysis and modeling. This not only confirms the idea that maturation in terms of stable association and compaction proceeds in reverse order of transcription, where the first to be transcribed rRNA domain (5’ domain) is the last to be stably incorporated

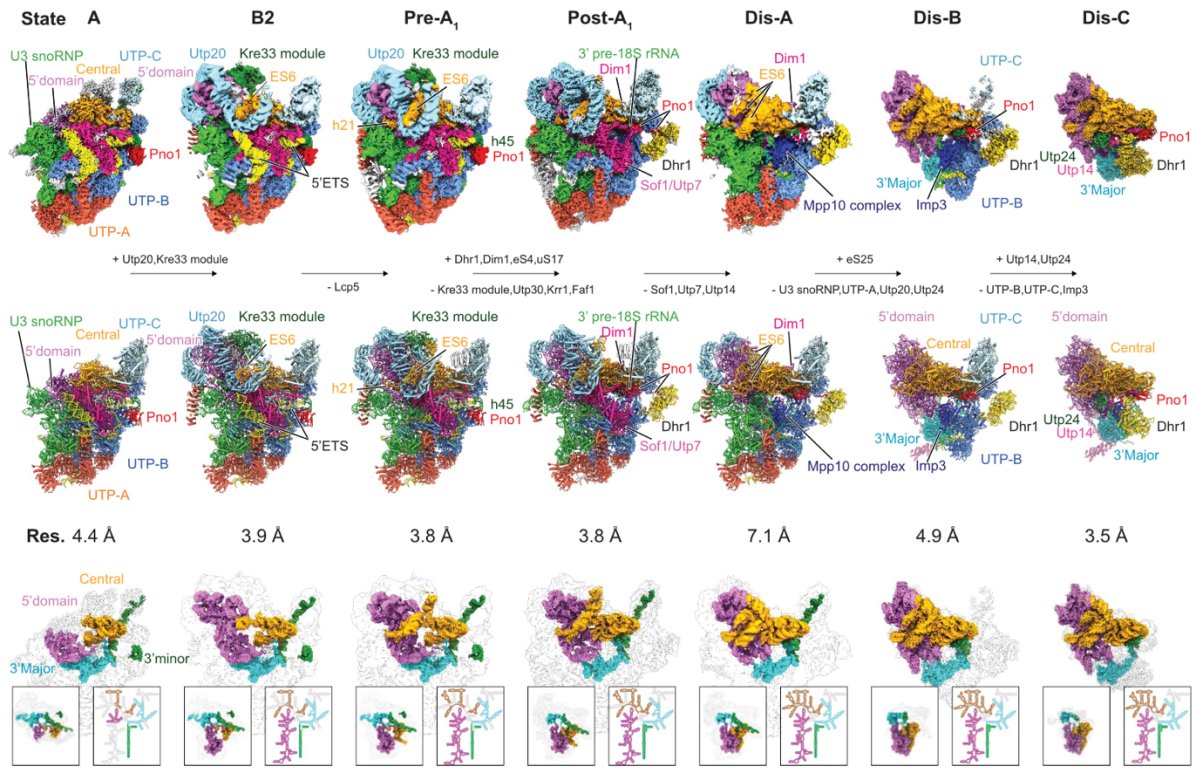

Figure 2.5 Cryo-EM states of 90S to pre-40S conversion intermediates. EM densities (upper panel) and molecular models (middle panel) of seven isolated states in transition from 90S pre-40S from yeast. Depicted biogenesis factors and models are labeled and compositional changes are indicated. 18S rRNA density and compaction (lower panel) and corresponding secondary structure in transition to pre-40S. 40S views are shown in boxes. (color code: green, 3' minor domain; cyan, 3' major domain; orange, central domain; magenta, 5' domain). Figure was taken from (Cheng et al., 2020).

into the pre-ribosome. Moreover, it appears that ES6 integration is coupled to the recruitment of Kre33 and Utp20 and hence, the maturation of the 5' domain.

Moving from state B2 to state pre-A_1, a further compaction of the particle as a whole can be observed (Supplemental Figure S2). The 5' domain moves closer towards the central domain with helix h21 in the ES6 of the 18S rRNA moving to its mature conformation. The tightening of the particle comprises the Kre33 module and Utp20. Lcp5 however as part of the Kre33 module disappears to make room for h21. Moreover, helix h9 of the 5'-ETS becomes dislodged, a trend that continues into the next state. State pre-A_1 is the last state with an intact A_1 site. The particle series from state A to pre-A_1 shows how a higher compaction of the particle with a starting dislodgement of the 5'-ETS prepares the 90S pre-ribosome for A_1 cleavage.

Moving from state pre-A_1 to the post-A_1 state, many structural rearrangements can be observed in a series of pre-ribosomal particles visualized for the first time.

Perhaps the most dramatic one is the dissociation of some AFs that have seemingly completed their job in the biogenesis pathway. The Kre33 module dissociates from the 90S particle and now, the 5' domain and the central domain interact in a close to mature conformation (Figure 2.6 A). Moreover, Krr1 and Faf1 dissociate, and enable a relocation of Pno1 together with helix h45 from the periphery to the center of the particle, with Pno1 now occupying Krr1's place and h45 recruiting the dimethyltransferase Dim1 (Figure 2.6 B). This relocation results in Dhr1 appearing at the site in the periphery of the particle previously occupied by Pno1.

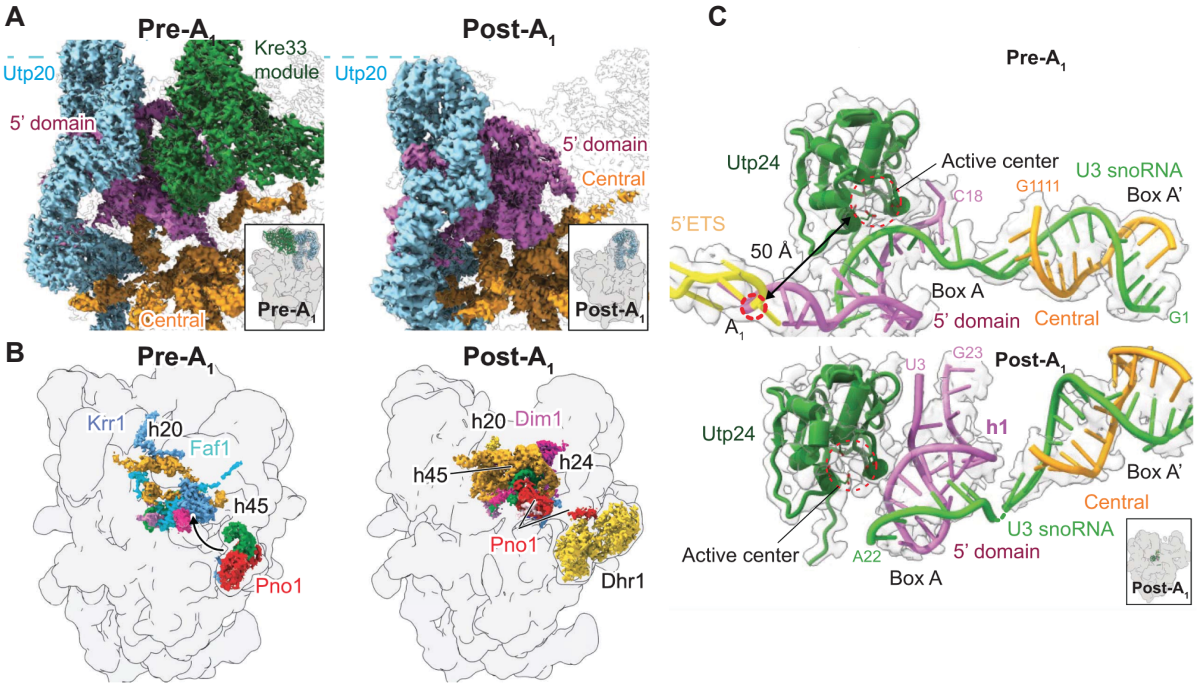

Figure 2.6 Compaction of 18S central domain and conformational changes upon A_1 cleavage. (A) Compaction of 5' (purple) and central (orange) domain of 18S pre-rRNA with volume representation of Utp20 and Kre33 module in Pre-A_1 (left) and post-A_1 states (right). Dashed lines indicating the rearrangement of Utp20. The boxes at the bottom right indicate position at 90S pre-ribosome for better orientation. (B) Changes and rearrangements of 18S pre-rRNA central domain region are highlighted in states pre-A_1 (left) and post-A_1 (right). (C) Model of the region around helix h1 of 18S pre-rRNA and the position relative to Utp24 before (upper panel, state Pre-A_1) and after A_1 (lower panel, state Post-A_1) cleavage. Catalytic domain of Utp24 and A_1 rRNA cleavage site are indicated by dashed red circles. The box at the bottom right shows the position of A_1 cleavage within the 90S pre-ribosome for better orientation. Figure was taken from (Cheng et al., 2020).

Moreover, the C terminus of Utp7, which interacted extensively with h7 of the 5'-ETS in the pre-A1 state, is transformed into an extended helix in the post-A1 state. This long helix now helps stabilize the new Pno1-h45 conformation and additionally shields

the D cleavage site (not shown). The observed differences in the degree of compaction of the particle as a whole offers a clue for the mechanism behind A_1 cleavage. The last noncleaved state pre-A_1 shows a distance of approximately 50 Å between the catalytic center of endonuclease Utp24 and the A_1 cleavage site, which is the suggested PIN domain enzyme performing this rRNA processing (An et al., 2018; Bleichert et al., 2006; Tomecki et al., 2015; Wells et al., 2016b) (Figure 2.6 C). Interestingly, the 5' end of the 18S rRNA in the post-A_1 state has already adopted helix h1, which is a short RNA stem loop structure. The initial formation of this structure may have led to endonucleolytic cleavage, since this loop formation probably brought the A_1 cleavage site in close proximity to the catalytic center of endonuclease Utp24 (Figure 2.6 C).

Moreover, we can follow the RNA sequence of the cleaved and now released 5' end of 18S rRNA until the third nucleotide from the base of the newly formed mature helix h1 stem loop (Figure 2.6 C, lower panel, U3 corresponds to third nucleotide (uridine)).To our surprise, the formation of helix h1 and subsequent A_1 cleavage does not require unwinding of the two pre-18S rRNA – U3 snoRNA heteroduplex structures, called Box A and Box A'. These two prominent structures retain in the pos-A_1 state (Figure 2.6 C). Noteworthy, our data show that remodeling and relocation of pre-18S rRNA is the triggering step for A_1 cleavage by moving the substrate RNA to the stably positioned endonuclease Utp24. Moreover, the overall conformational state not only gains a higher compaction as the particle approaches A_1 processing. The 5'-ETS is increasingly flexible or dislodged, as discussed in section 2.3, which contributes to a dynamic enabling the decisive A_1 cleavage step.

Taken together, A_1 processing seems to require and/or result in two somewhat opposite developments. On the one side, the conformation of the three 18S rRNA subdomains (5' domain, central domain, 3' domain) gradually tightens as the subdomains are stably integrated into the pre-ribosome in the reverse order of rRNA transcription (3' domain first, 5' domain last). The integration of the 5' domain ultimately leads to the dissociation of the Kre33 module, while bringing h45 of the 3' minor domain to its mature conformation forces Krr1-Faf1 to leave the 90S particle. On the other hand, the 5'-ETS increasingly disappears, providing a certain degree of dynamic of the pre-rRNA (see section 2.3).

2.2.2 A_1 processing sets off the 90S>pre-40S transition through step-wise reduction of the huge 90S particle

The incipient dissociation of AFs observed in state post-A_1 continues with more dramatic, incremental reductions of the huge 90S particle in the states Dis-A, Dis-B and Dis-C (Dis for dissociation) (Figure 2.7). Moving from state post-A_1 to state Dis-A, the Sof1 module (Sof1, Utp7, and Utp14) has been released together with Utp6 (part of the UTP-B module). Dissociation of the UTP-A module as a whole together with Utp18 (part of the UTP-B module) and the U3 snoRNP leads to the state Dis-B. However, the U3 snoRNA remains attached to the pre-ribosome in this state. Finally, release of the UTP-B core and the remaining UTP-C module now gives rise to state Dis-C. In line with the fact that the 5'-ETS is a scaffold for the UTP-A, UTP-B and U3 snoRNP, the last bit of the 5'-ETS (3' hinge region) is not visible any more in state Dis-C.

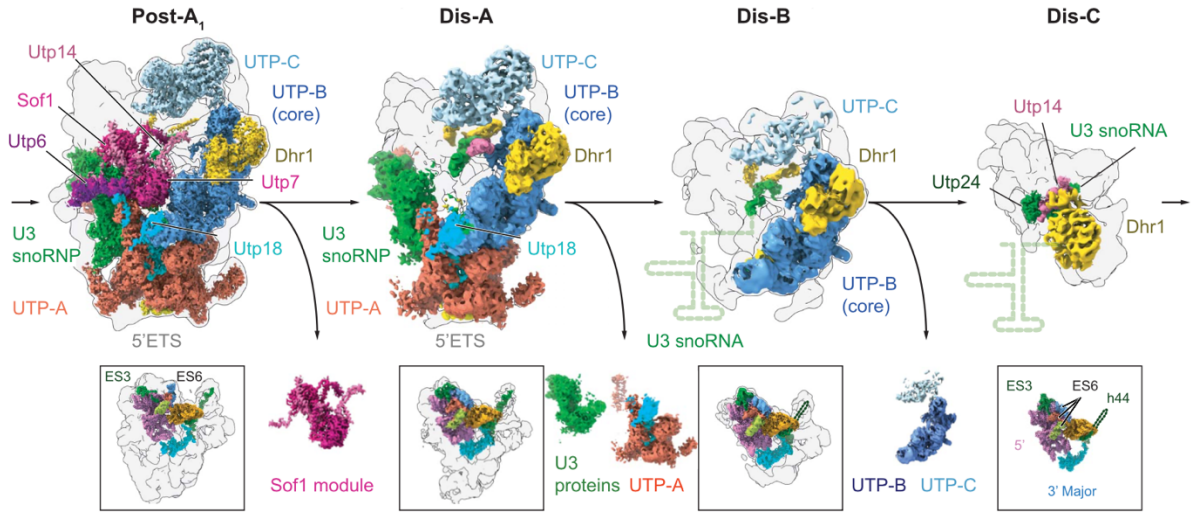

Figure 2.7 Consecutively shedding of biogenesis factors during the 90S pre-ribosome to a primordial pre-40S transition. The shedding process visualized by cryo-EM models reveals the dissociation of 90S assembly modules during the transition from state Post-A_1 to state Dis-C. Proteins, modules and remaining 5'-ETS (H1-H2) being dissociated in the transition process are colored and labeled. RNA helicase Dhr1 is colored in yellow to demonstrate relocation from state Dis-B to Dis-C. The boxes indicate the maturation of the pre-18S RNA (color code: magenta, 5' domain; orange, central domain; cyan, 3' major domain; green, 3' minor domain; light green and light blue, ES6) and released assembly modules, respectively. The figure was taken from (Cheng et al., 2020).

The U3 snoRNA is mostly detached in the particle states Dis-B and Dis-C. However, only the first 5' nucleotides stay localized on the particles, tethered by their

involvement in forming a heteroduplex with the 18S rRNA. Interestingly, there is rather a limited maturation of the pre-40S rRNA domains in the process of shedding. Thus, only the expansion segments ES3a, ES3b, and ES6a to ES6d undergo rearrangements to adopt mature conformations. They are displayed later on the solvent site of the 40S subunit, whereas all other domains stay unchanged during the dramatic loss of 90S biogenesis factors and modules (Figure 2.7 boxes).

Beneath the successive shedding of the protein modules, release of 5'-ETS rRNA and remodeling of 18S rRNA, additional structural changes can be observed. One of them is the relocation of RNA helicase Dhr1 form its distal UTP-B binding site in state Dis-B towards a more central location in the state Dis-C, where the Utp-B module has already been released (Figure 2.7 and 2.8 A and B). This new location of Dhr1 brings the helicase in strategic position for unwinding the last remaining U3::18S pre-rRNA hetero-duplex. Furthermore, endonuclease Utp24, which was not visible in state Dis-B, becomes detectable again in state Dis-C, where it occupies the binding site for ribosomal protein uS5. Interestingly, the assembly factor Utp14, previously bound to Utp6 and helix h9 of the 5'-ETS, disappears as part of the Sof1 module in state Dis-A, just to appear again in state Dis-C at a new location, binding Pno1 and Dhr1 via four α helices. Known to be a co-factor of the helicase Dhr1, Utp14 relocates in a position tethered to Dhr1 in state Dis-C, where Dhr1 has been attached to its substrate U3. Furthermore, relocated Utp14 inhibits the endonuclease Utp24 with two of its arginine residues coordinating the active center of Utp24, thus inactivating the enzymatic activity of the endonuclease (Supplemental Figure S3).

Following Dhr1 during the maturation process leading towards a primordial pre-40S particle sheds light on the enzymatic function of Dhr1 and how it is primed to unwind the last U3::18S pre-rRNA heteroduplex (called Box A) and thus release the U3 snoRNA from the 40S pre-ribosome. Visible for the first time in State post-A_1 as taking the place vacated by Pno1, Dhr1 is anchored via two invariant N-terminal helices interacting with Dim1 and the Box A heteroduplex. However, the catalytic domain of Dhr1, which is located on the C-terminus, is located far away from the N-terminus (Figure 2.8 C-E). With the exception of state Dis-C, Dhr1's more compact and global C-terminus is seen interacting with UTP-B module members Utp13 and Utp21 in all states after pre-A_1. This interaction is mediated by a β barrel-like structure provided by Dhr1. When the UTP-B module leaves the pre-ribosome as part of the

shedding of 90S modules, Dhr1 occupies this empty cavity and relocates to Box A and 18S pre-rRNA helix h1, which is in close distance to its U3 snoRNA substrate. Moreover, the β barrel-like domain of Dhr1 is now attached to a new binding interface formed by Utp14, Pno1 and the 18S pre-rRNA 3' region.

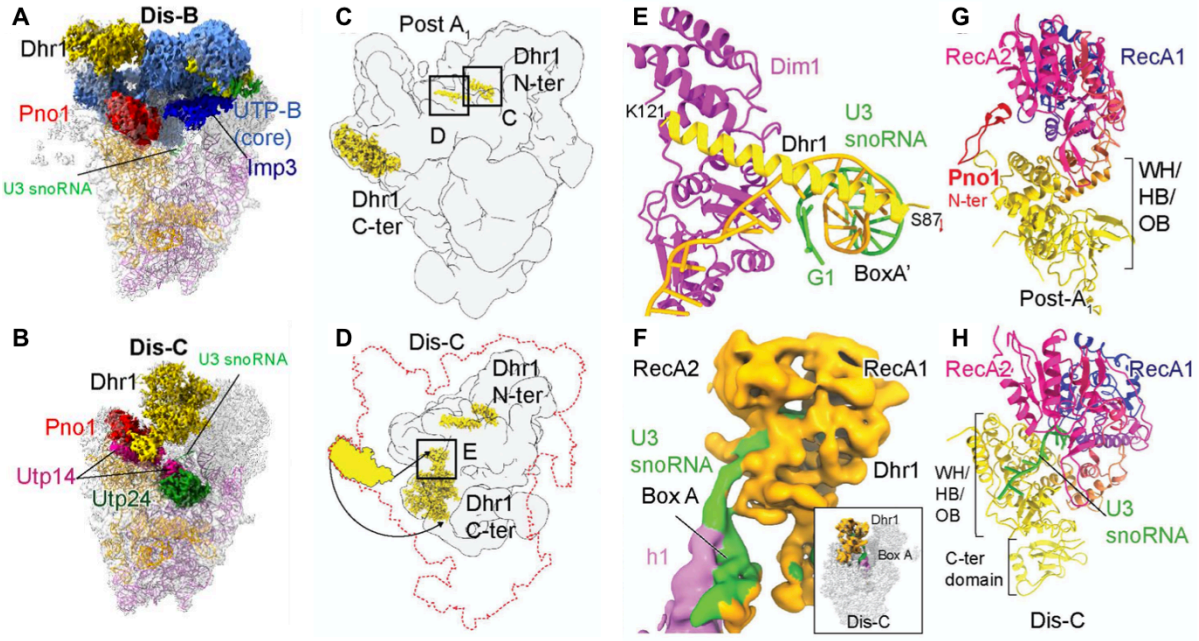

Figure 2.8 Position and conformation of RNA helicase Dhr1 in different transition states. (A-B) Density map with colored assembly factors which show a relocation or dissociate from state Dis-B (A) to state Dis-C (B). (C-D) Dhr1 is shown on density maps of state Post-A_1 (C) and Dis-C (D) with the C termini indicated. (E) Ribbon model of the N-terminal helices of Dhr1 (yellow) interacting with Box A' (gold pre-18S RNA and green U3 snoRNA) and Dim1 (purple) in all states after Pre-A_1. (F) EM densities of Dhr1 in association with U3 snoRNA directly in front of Box A duplex (purple pre-18S RNA helix h1 and green U3 snoRNA). The box at the bottom right shows the location of Dhr1 on pre-ribosomal particles from state Dis-C. (G-H) Molecular model of Dhr1 in state Post-A_1 (G) and Dis-C (H), where Dhr1 is seen in two different conformations. U3 snoRNA and Pno1 are colored in green and red, respectively. Labeled domains of Dhr1 are RecA1 and RecA2 domain, WH (Winged Helix), HB (Helical Bundle), OB (OB-fold domain) and C-terminal domain. The model of Dhr1 is multiple colored from blue to red and yellow. Figure was taken from (Cheng et al., 2020).

Dhr1's binding to its co-factor Utp14 in state Dis-C stresses the importance of Utp14 for recruitment and relocation of Dhr1 (Figure 2.8 A, B, and F). From state post-A_1 to state Dis-B, Pno1's N-terminus prevents Dhr1 from binding its substrate. Moreover, Dhr1 is attached to the 90S particle in an open conformation bound to ADP. In Dis-C, Dhr1 is visible in a closed conformation, bound to its RNA substrate and ATP-free, in

agreement with previously published data for the human homolog DHX37 (Figure 2.8 G and H) (Boneberg et al., 2019).

Taken together, A_1 processing appears to set off a dramatic series of events transforming the huge 90S particle into a smaller and simpler pre-40S intermediate. 90S modules and AFs are not releases en bloc, as previously believed for the 5'-ETS RNP, but sequentially. Moreover, the series highlights the dynamic function of helicases in ribosome biogenesis. Dhr1 is seen changing location and interaction partners, both affecting its catalytic activity. Finally, the Noc4 module as one of the larger 90S modules survives the excessive shedding of 90S factors during the transition period. Together with the Bms1-Rcl1 heterodimer, it remains associated to the 3' domain, which later forms the head of the mature 40S subunit.

2.3 The evolving 90S pre-ribosome is associated with the RNA exosome

The discovered stepwise shedding of the 90S pre-ribosome after A_1 cleavage was not compatible with the expected *en bloc* release of a 5'-ETS particle. Surprisingly, whereas the overall composition and shape of the 90S intermediate stays largely unchanged as the particle nears A_1 processing, the 5'-ETS does not. We observed a progressively disordered state of the 5'-ETS pre-rRNA, culminating in its almost complete disappearance after the A_1 site has been processed. Interestingly, we discovered large amounts of the RNA exosome on this further developed 90S pre-ribosome, providing first evidence that the RNA exosome could be mechanistically involved in the 90S biogenesis and ultimately production of pre-40S particles.

2.3.1 The RNA exosome is bound to 90S particles that undergo A_1 cleavage

During the biochemical characterization of the Noc4-Dhr1 sample, we noticed that this preparation contained unusual high amounts of RNA exosome components including Mtr4. Normally, classical 90S baits enrich only sub-stochiometric amounts of the RNA exosome, which can increase in particles isolated from cells grown under mutant conditions (Sardana et al., 2015; Sturm et al., 2017). An involvement of the RNA exosome in 90S biogenesis was proposed by several studies, as an example see (Kornprobst et al., 2016) and (Thoms et al., 2015). A direct comparison of the Noc4--Dhr1 and Dhr1-Dim1 90S particles to particles isolated via Utp10-FTpA or Krr1-FTpA showed a significantly higher association of exosome components with

pre-ribosomes, with the highest number of RNA exosome components in the Dhr1--Dim1 sample (Figure 2.9 A). Since Mtr4 co-migrates with Kre33 on SDS-PAGE gels, we monitored its co-enrichment also by Western Blot analysis, which confirmed that the 90S particles, which undergo A_1 cleavage or are in the 90S to pre-40S transition, also contain high amounts of the RNA exosome, whereas earlier 90S pre-ribosomes (e.g. Utp10 particles) do not. To further investigate if there is a direct association of the RNA exosome to 90S pre-ribosome, we performed a sucrose gradient centrifugation of the Dhr1-Dim1 preparation. The core exosome factors (Rrp46, Rrp45, Rrp44, Rrp43, Rrp42, Rrp41, Rrp40, Rrp4, Mtr3, and Csl4) together with the nuclear exonuclease Rrp6 and the RNA helicase Mtr4 were recovered from same sucrose fractions that also contained the 90S particles (Figure 2.9 B). Thus, we conclude that the nuclear RNA exosome together with its adapter protein Mtr4 stably associates with 90S particles derived from the Dhr1-Dim1 preparation. Encouraged by these data, we wanted to further validate an RNA exosome associated 90S particle and thus we analyzed the Dhr1-Dim1 preparation by negative-stain EM (nsEM). Indeed, we found a pool of 90S particles displaying an extra density with a round shape and size typical for the RNA exosome (Aloy et al., 2002). We saw that this extra density, when found on 90S particle, was positioned laterally between “head” and “body” (Figure 2.9 C). A structural comparison of the results of nsEM and the previously obtained 90S cryo-EM states (pre-A_1 and post-A_1) revealed that the exosome is located next to 18S pre-rRNA central domain and the UTP-B module (e.g., Utp6 and Utp18). These observations give evidence that the exosome was not randomly attached to the 90S pre-ribosome, but rather to a distinct recruitment site, perhaps fulfilling a specific but unknown function at this position. To further expand on these observations, we performed semiquantitative mass spectrometry analysis of the Dhr1-Dim1 preparation. The results corroborated that 90S factors are associated with the nuclear RNA exosomal subunits and Mtr4, but not with exosomal factors, which were identified to play a role in quality control or degradation of faulty RNA molecules (Supplemental Figure S4 A, e.g., TRAMP complex factors) (Tudek et al., 2018).

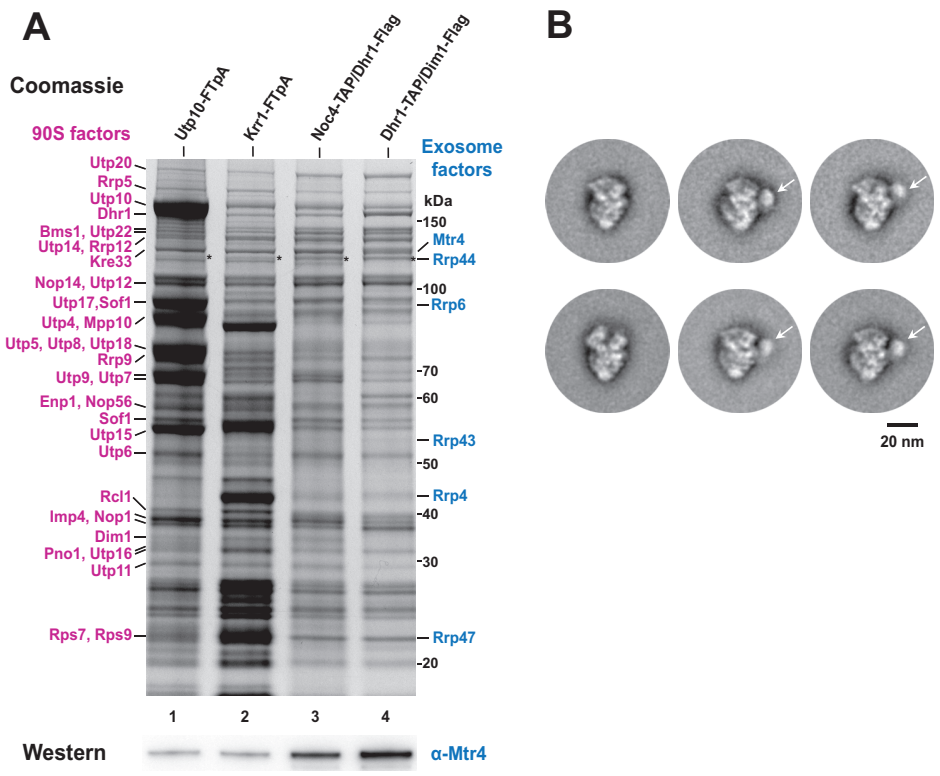

Figure 2.9 Isolation of 90S pre-ribosomes associated with the nuclear exosome and its co-factor Mtr4 helicase by affinity purification. (A) Affinity purification of different 90S pre-ribosomal particles via indicated bait proteins analyzed by SDS-PAGE and Coomassie staining (upper panel). Western blot analysis using anti-Mtr4 antibodies (lower panel). Labelled protein bands were identified by MALDI-TOF mass spectrometry (90S factors, left; exosome factors, right). (B) Negative-stain electron microscopy of fraction 12 containing 90S particles from the Dhr1-Dim1 sucrose gradient preparation. Shown are typical 2D classes of 90S particles carrying an extra density (right panel) displaying the nuclear RNA exosome (indicated by an arrow) and 90S particles without extra density (left panel). Negative-stain electron microscopy was performed by Dr. Dirk Flemming. Figure was taken from (Lau et al., 2021).

We next asked whether the exosome is recruited prior to A_1 processing and if it directly performs a role of 90S maturation rather than 5'-ETS degradation. For this, we wanted to enrich a stoichiometric 90S-exosome super-complex and performed a split-tag affinity purification using a core exosome subunit (Csl4, Rrp46, or Rrp44) as first bait and the dual 90S/pre-40S factor Dim1 as second bait. With Dim1 as second bait, we wanted to ensure that we capture particles in transition from 90S to pre-40S. The selected baits were chromosomally integrated at the corresponding gene loci. For all combinations, the corresponding yeast strains were growing normally at the temperatures tested, therefore minimizing the isolation of aberrant 90S pre-ribosomes

from such cells (Supplemental Figure S5). The exosomal subunits chosen as first bait purified predominantly the core exosome together with its known co-factors Rrp6, Mtr4, and Ski-complex (Figure 2.10 A, e.g., Ski3 and Ski7) (Halbach et al., 2013). Noteworthy, we observed 90S (e.g., Utp10) and pre-60S assembly factors in lower amounts indicating that the first exosomal baits already purify reasonable amounts of 90S-exosomal particles. Moreover, we observed members of the TRAMP complex (e.g., Air1, Air2, Trf4, and Trf5) in very low quantities, reducing the possibility of isolating particles being part of quality control and turnover of faulty RNA (Tudek et al., 2018) (Supplemental Figure S4 B). With subsequent purification via second affinity bait Dim1-Flag, the majority of 90S factors were drastically co-enriched (up to 100-fold), whereas there was no co-enrichment of pre-60S components, the Ski-complex, or TRAMP complex factors (Figure 2.10 A and Supplemental Figure S4 B). Taken together, the split-tag affinity purification approach enabled us to isolate stoichiometric amounts of a 90S-exosome super-complex containing the adaptor RNA helicase Mtr4. To further investigate this 90S-exosome super-complex we have chosen the bait combination Csl4-Dim1 for all the following experiments. We performed sucrose gradient centrifugation analysis of a Csl4-Dim1 preparation and again, similar to the Dhr1-Dim1 preparation, the core exosome together with Rrp6 and Mtr4 co-migrated with the 90S particles. Only little amounts of the core exosome complex migrated in the top fractions of the sucrose gradient. Noteworthy, there was no pre-40S pool recovered, indicating an exclusive presence of the exosome on 90S particles and a release of exosome before the 90S-to-pre-40S transition (Figure 2.10 B). Moreover, we analyzed the Csl4-Dim1 preparation by ns EM and obtained the characteristic EM density for the exosome on 90S particles, with similar size and position compared to the Dhr1-Dim1 preparation (Figure 2.10 C).

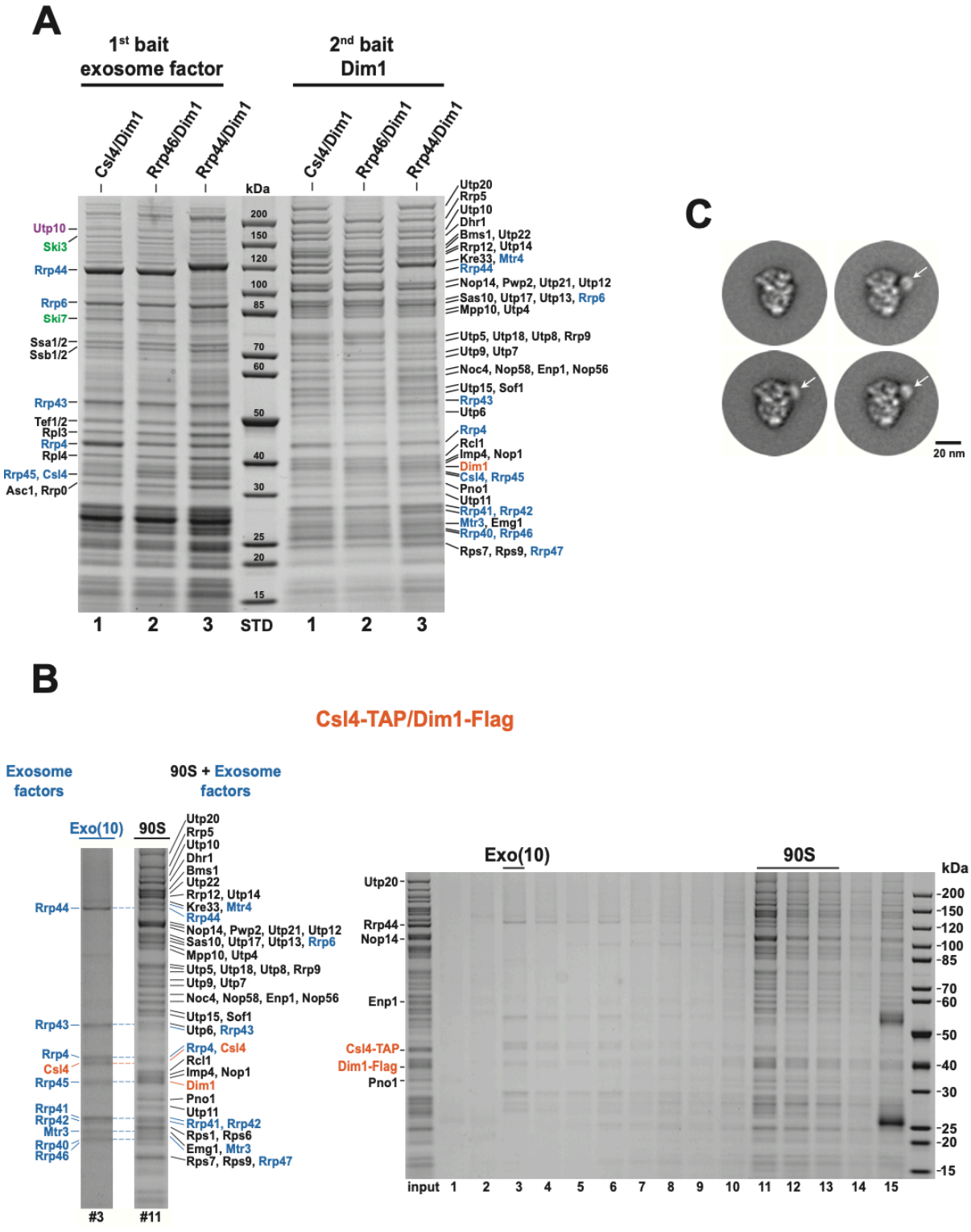

Figure 2.10 Isolation of 90S-exosome super-complexes by split-tag exosome/90S affinity purification. (A) Affinity purification of different exosome factors and Dim1 as second bait. SDS-PAGE and Coomassie staining of different TEV eluates (left panel lane 1-3, first bait used exosome factors are indicated) as well as of the Flag eluates via second bait Dim1 (right panel lane 1-3). Labelled protein bands were identified by MALDI-TOF mass spectrometry. (B) Sucrose gradient ultracentrifugation of the Csl4-Dim1 Flag eluate with subsequent analysis by SDS-PAGE and Coomassie staining showing

the input and fraction 1-15. Exosome containing 90S particles of fraction 11 and the free exosome of fraction 3 are displayed side by side (left). Labelled protein bands were identified by MALDI-TOF mass spectrometry (exosome factors, blue; 90S factors, black; baits, red). (C) Negative-stain electron microscopy of fraction 11 containing 90S particles from the Csl4-Dim1 sucrose gradient preparation. Shown are typical 2D classes of 90S particles carrying an extra density displaying the nuclear RNA exosome (indicated by an arrow) and 90S particles without extra density. Negative-stain electron microscopy was performed by Dr. Dirk Flemming. Figure was adopted from (Lau et al., 2021).

Taken together, these data indicate that the RNA exosome is associated with the 90S pre-ribosome *in vivo* and is most likely performing a distinct role on these particles. These results and the continuous shedding of 90S factors during the 90S-to-pre-40S transition are in contrast to our current thinking that the exosome is degrading the 5'-ETS RNA, after A_1 cleavage, on an already released, so called 5'-ETS particle (Barandun et al., 2018; Klinge and Woolford, 2019; Kornprobst et al., 2016).

2.3.2 Remodeling of the 5'-ETS pre-rRNA during A_1 processing on the 90S-exosome super-particles

Encouraged by our finding that it is possible to isolate 90S-exosome super-particles, which can be visualized by nsEM, we performed single-particle cryo-EM analysis in collaboration with the Beckmann lab at the LMU in Munich. For that we used isolated Csl4-Dim1 particles, which showed the highest amount of exosome together with Mtr4 attached to the 90S pre-ribosome (Figure 2.10 D). Extensive 3D classification revealed two main states, with the RNA exosome density positioned at the 90S pre-ribosome as observed by nsEM, namely pre-A_1-exosome and post-A_1-exosome. The overall refinement revealed final maps with average resolution of 4.6 Å (pre-A_1-exosome) and 3.8 Å (post-A_1-exosome), respectively. This resolution enabled an unambiguous fitting of the already existing 90S pre-ribosome models derived from pre-A_1 and pos-A_1 cleavage states (Figure 2.11). The exosome bound to 90S particle was observed at lower resolution, most likely due to flexibility and perhaps incomplete occupancy, but was nonetheless sufficient for unambiguous fitting as rigid bodies by molecular models for the entire yeast (or human) nuclear exosome complex (Figure 2.11) (Makino et al., 2013; Weick et al., 2018). Moreover, both states showed the very characteristic arch domain of Mtr4, thus allowing a rather precise assignment of the

exosome on 90S particles (Figure 2.11 and 2.12 A) (Schuller et al., 2018; Thoms et al., 2015).

Prompted by these results, we re-investigated the Dhr1-Dim1 cryo-EM data with intense sorting and special focus on the region of expected exosome attachment. Our data revealed in the post-A_1 state an extra EM density. This density could be assigned to the Mtr4-exosome bound to the 90S pre-ribosome, albeit in a smaller pool of particles compared to the Csl4-Dim1 preparation (Supplemental Figure S6 A and B). Interestingly, the post-A_1 state of both samples, Dhr1-Dim1 and Csl4-Dim1, reveals Mtr4 together with the exosome in the same conformation and recruited at same docking site of 90S pre-ribosome (Supplemental Figure S6 C).

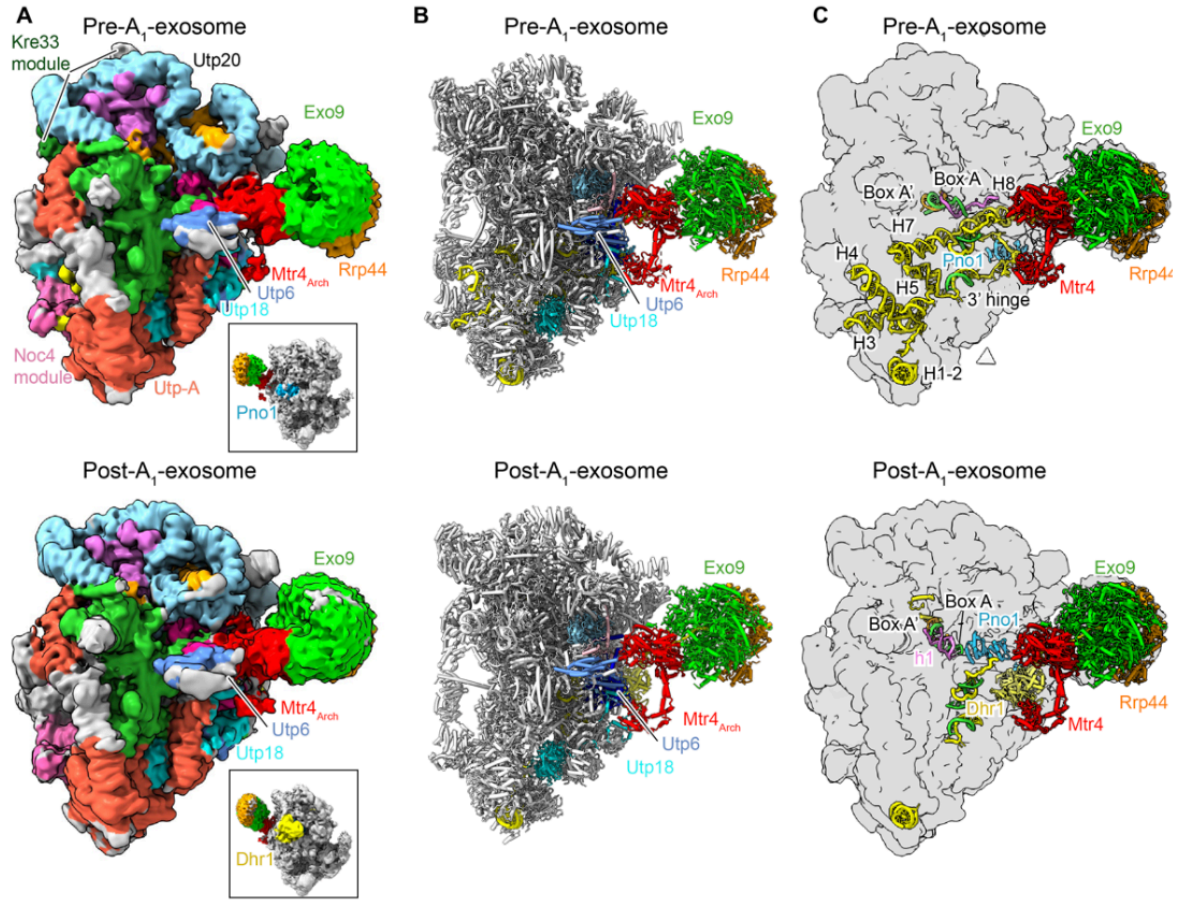

Figure 2.11 Cryo-EM structure and molecular model of the 90S-exosome super-complex. (A and B) Cryo-EM density and molecular model of the 90S in association with the exosome. Shown are Pre-A_1 (top) and Post-A_1 (bottom) states, derived from a Csl4-Dim1 tandem-affinity purification. The boxes at the bottom right depict the back views highlighting the position of Dhr1 (yellow) and Pno1 (blue). (C) Structural model of the Pre-A_1 (top) and Post-A_1 (bottom) states displaying the Mtr4-exosome and illustrating differences in 5'-ETS RNA (yellow), Dhr1 (yellow) and Pno1 (blue). Figure was taken from (Lau et al., 2021).

Noteworthy, the cryo-EM densities suggest that there is no direct physical interaction between the exosome and 90S pre-ribosome, with Mtr4 mediating all contact as an adopter between them (Figure 2.11). In all three presented cryo-EM states with attached exosome (Csl4-Dim1 pre-A_1, Csl4-Dim1 post-A_1, and Dhr1-Dim1 post-A_1) we observed that Mtr4 is docking at the 90S particle at same position. This finding is in line with previous studies showing that the exosome can be recruited to its targets via the adaptor protein Mtr4 helicase (Lingaraju et al., 2019; Thoms et al., 2015).

With our new structural information, we found that the protruding Utp6 α-solenoid provides a platform for the recruitment of Mtr4 with the associated exosome at the region of dislodged helix h9-9' of 5'-ETS (Figure 2.11, 2.12 A and 2.13). Furthermore, several short α-helical elements (residue 324-408) of assembly factor Utp14 are seen interacting with different regions of Utp6 as reported previously (Barandun et al., 2017), and thereby could help stabilizing Utp6, which in turn could favour the Mtr4-exosome binding (Figure 2.10 A-C). However, the close-by amino-terminus of 90S assembly factor Utp18 seems to be a key element for initial tethering of Mtr4 to the 90S particle. It comprises the so-called AIM motif, not visible in our cryo-EM density. This motif is described to show an efficient binding to the KOW domain of Mtr4, which is part of the characteristic Mtr4 arch (Figure 2.10 A and D) (Falk et al., 2017; Thoms et al., 2015). Interestingly, Mtr4 is positioned at the interface of the Sof1 module (Sof1, Utp7, and Utp14) and Utp6. This binding region also comprises the 3' end of the 5'-ETS RNA and thus Mtr4 is in close proximity to the A_1 cleavage site of 5'-ETS (Figure 2.10 C). Thus, Mtr4 appears to be strategically positioned in a way that the Mtr4 RNA binding tunnel can access the 5'-ETS RNA at the endo-nucleolytic cleavage site A_0, which in principle could enable a channeling of the 5'-ETS RNA forward to the Mtr4 helicase domain. The A_0 cleavage site of 5'-ETS is positioned downstream of helix h9' and is approximately 90 nucleotides 5' upstream of the A_1 site (Figure 2.10 C and Supplemental Figure S7 A) (Chen et al., 2020; Kufel et al., 1999).

Due to this strategic position of Mtr4 and because 90S particles in the pre-A_1 state already show cleavage at A_0, we postulate that the RNA is channeled from the 3' end of the 5'-ETS-A_0 fragment through Mtr4 into the exosome channel for subsequent degradation. This would be in accordance with the observation of dismantling of 5'-ETS helix h9-9' in this area. Noteworthy, Mtr4 binds in an open and thus active conformation to the 90S particle, while the arch domain shows a distal position. This could allow channeling and unwinding of the 5'-ETS RNA duplex and

finally guiding the single stranded RNA into the exosome. Consistent with the open conformation of Mtr4, the arch domain in addition can contact the nearby Utp18 AIM motif via the Mtr4 KOW domain (KOW domain is part of Mtr4 arch (Falk et al., 2017; Thoms et al., 2015)). In a next step, we wanted to confirm these structural observations. For that, we tested whether the Mtr4-exosome recruitment is impaired in mutant cells on a Dhr1-Dim1 particle, which carries the exosome in the post-A_1 state. Therefore, we expressed in yeast cells a mutated Utp18 AIM motif (*utp18-5xAla*) (Thoms et al., 2015) or deleted the non-essential *RRP6* gene, which is a subunit of the nuclear RNA exosome. Indeed, the biochemical and genetic analysis revealed a decrease in Mtr4 and exosome recruitment to the 90S pre-ribosome, when isolated from mutant cells (Supplemental Figure S7 B and C), supporting our conclusions from the structural cryo-EM analysis.

Taken together, we were able to provide direct evidence that the RNA exosome is recruited to the 90S particle. This recruitment happens before the A_1 cleavage site is processed, concomitantly with the observed initiation of 5'-ETS dislodgment in the state pre-A_1. Moreover, we show that in agreement with previously reported data, Mtr4 is the adaptor protein mediating contact between the 90S pre-ribosome and the RNA exosome. In agreement with the observation that a mutated AIM motif of Utp18 does not completely abolish Mtr4 binding to the 90S, we found that Mtr4 exploits a more complex binding platform consisting of the Sof1 module, Utp6 and Utp18.

To our surprise the exosome was recruited before A_1 cleavage, speaking for a task on the 90S pre-ribosome prior to this cleavage event. The pre-A_1-exosome state is essentially similar to the previously described pre-A_1 state, which did not yet reveal the Mtr4-exosome complex. Comparing the states pre-A_1 and post-A_1 from the Dhr1-Dim1 preparation, we observed an extensive 5'-ETS remodeling. In this process helix h9 of 5'-ETS is the first to become detached in state pre-A_1. With subsequent A_1 cleavage (state post-A_1) 5'-ETS helices h3-h8 become disordered, displaying empty cavities in these regions for the 90S post-A_1 intermediate (Figure 2.12 A). Only helix h1 and h2, which are closely attached to the UTP-A module stay visibly in this 90S, as well as two short segments (3' and 5' hinge regions) of the 5'-ETS involved in heteroduplex formation with the U3 snoRNA, the (Figure 2.12 B).

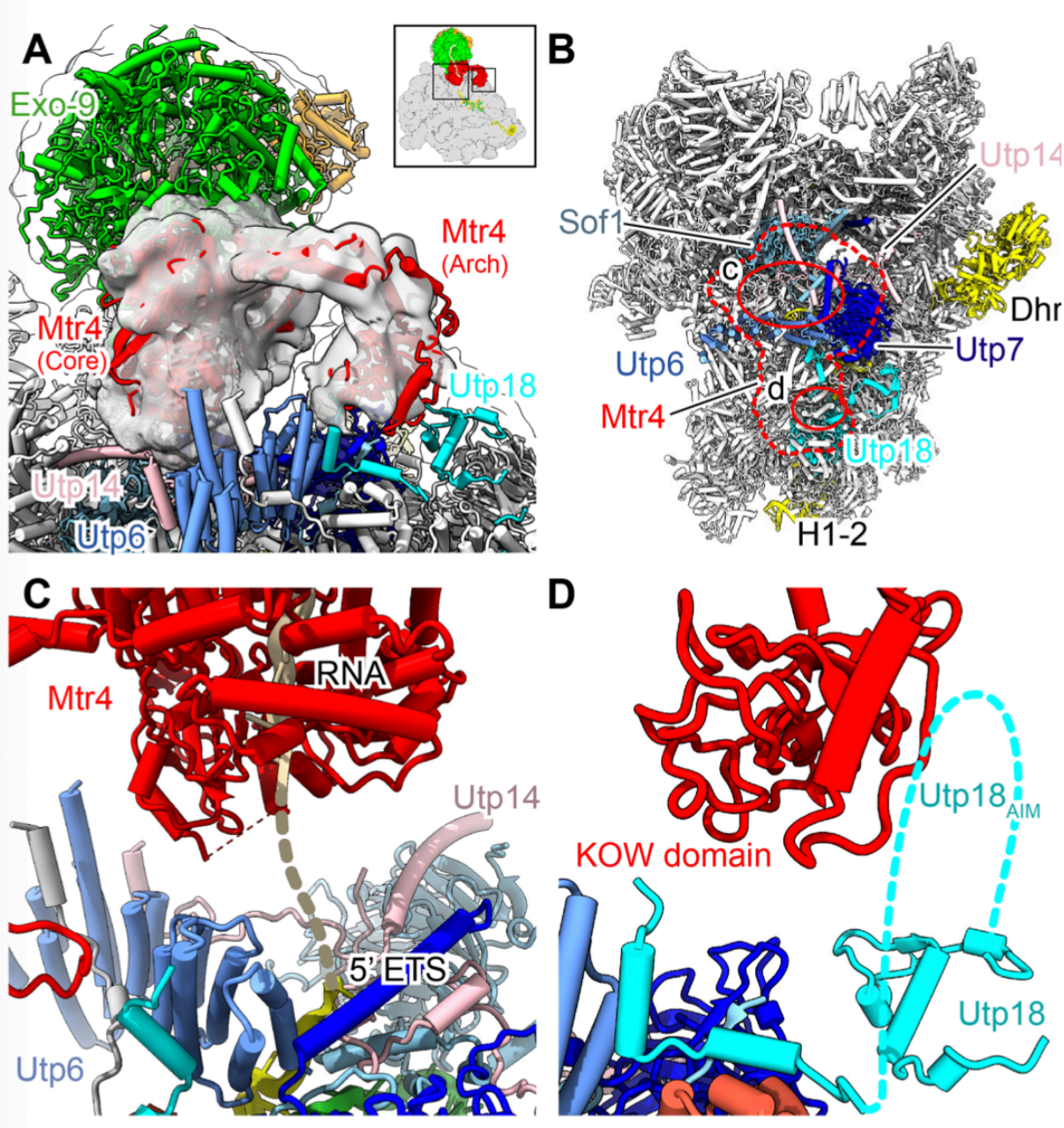

Figure 2.12 Mtr4 provides the bridge between 90S pre-ribosome und RNA exosome. (A) Zoom of Mtr4 bound to the 90S pre-ribosome showing the density of the Mtr4 helicase core and arch domain. The Mtr4 density is lowpass filtered to 10 Å and was isolated from a Dhr1-Dim1 map. The box at the top right shows full view of Mtr4, the exosome and the 90S pre-ribosome for better orientation. (B) Mtr4 (outlined in red) binding interface and selected colored biogenesis factors are depicted in an overall view of the 90S pre-ribosome. (C) Close-up view of the Mtr4-Utp6 binding interface is shown in a molecular model. The 3' end of 5'-ETS RNA (yellow) is in close vicinity to the RNA binding tunnel in the exosome. Model of the RNA exosome bound to substrate RNA is from PDB 6FSZ. The dashed lines indicate a potential connection between 5'-ETS RNA and RNA bound to the exosome. (D) Zoom of Mtr4 and its KOW domain being in close distance to the AIM motive of Utp18. The AIM motive of Utp18 on the 90S pre-ribosome structure is not visible and therefore indicated in dashed lines. Figure was taken from (Lau et al., 2021).

Noteworthy, both pre-A_1 states from the Dhr1-Dim1 as well as Csl4-Dim1 sample display dislodged helix h9-9' of the 5'-ETS RNA and matured helix h21 of the 18S pre-rRNA. The RNA helicase Mtr4 is recruited to the 90S pre-ribosome via its ATPase/helicase domain, which is tethering at a site previously occupied by the base of helix h9-9' of the 5'-ETS in state B2 (Figure 2.12 A) (Barandun et al., 2017; Cheng et al., 2019). Thus, we suggest that the dislodged helix h9-9' of the 5'-ETS is a prerequisite for the recruitment of the Mtr4-exosome. Alternatively, Mtr4 as helicase has the ability to relocate helix h9-9' by docking to the 90S pre-ribosome (Figure 2.9 middle panel).

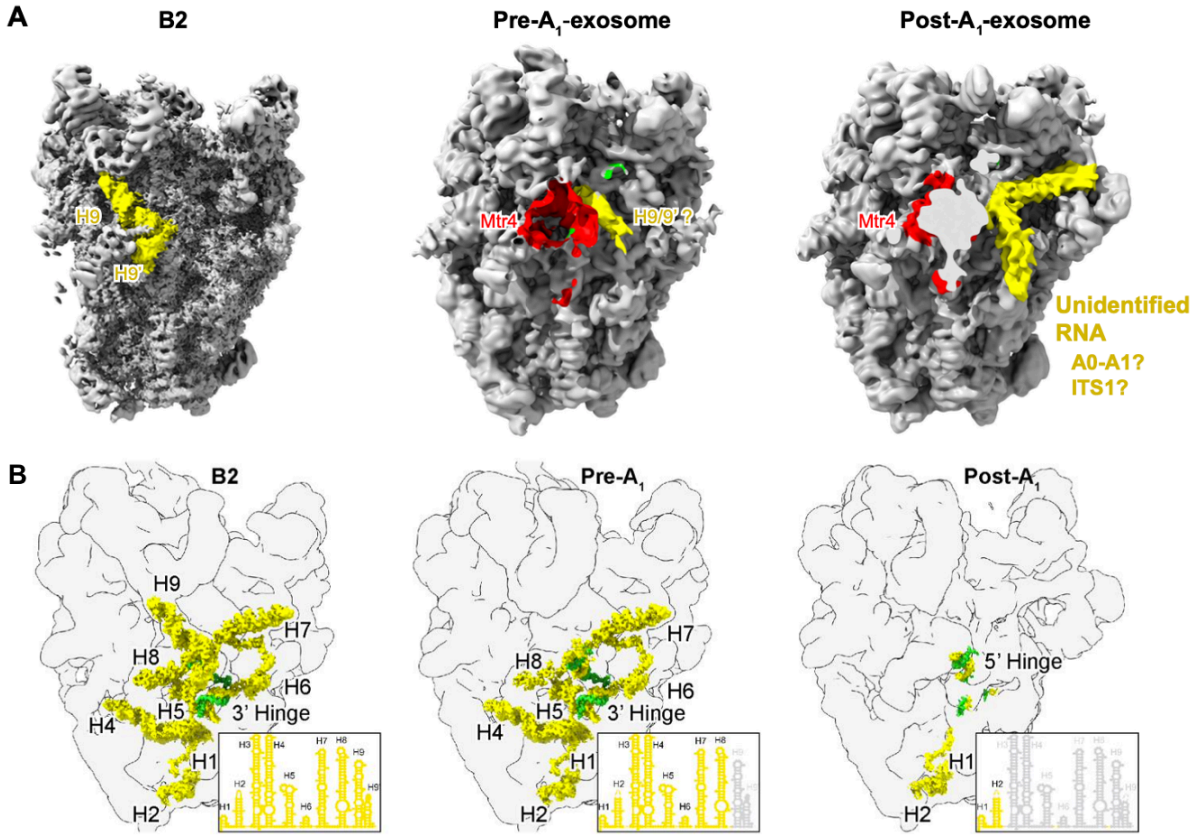

Figure 2.13 Cryo-EM structure displaying position of 5'-ETS RNA, helix H9-9' and Mtr4 helicase upon 90S maturation. (A) Cryo-EM maps and conformational changes in transition states (B2, left; Pre-A_1, middle; Post-A_1, right) from 90S particles displaying the 5'-ETS regions of H9-9'. Highlighted yellow densities represent 5'-ETS RNA helix H9-9' in state B2 (left). Yellow densities in state Pre-A_1 (middle) represent potential new position of H9-9', yellow densities in Post-A_1 (right) an unidentified newly visible RNA density. Red densities show a sectional view of the Mtr4 helicase. (B) Cryo-EM maps of state B2 (left), Pre-A_1 (middle) and Post-A_1 with 90S particles shown in grey and 5'-ETS RNA in yellow. The boxes at the bottom right indicate the secondary structure diagram of the 5'-ETS. Dislodged or digested helices are shown in grey, whereas visible helices are colored in yellow. Figure was taken from (Lau et al., 2021) and (Cheng et al., 2020).

As discussed in section 2.2, A_1 cleavage is accompanied by major structural changes on the 90S particle. Pno1 together with helix h45 of 18S pre-rRNA relocates from the periphery to a central position, the RNA helicase Dhr1 is recruited to the periphery of the 90S particle, while the 5'-ETS supports a sufficient range of motion so that the cleavage site A_1 moves close enough to the catalytic center of the endonuclease Utp24. Nevertheless, the position of the Mtr4-exosome is highly similar in both states. Of the structural changes in the core of the post-A_1 90S particle, perhaps the most striking is the nearly complete dislodgment of the 5'-ETS pre-rRNA, leaving behind only a remainder of helix h1-2 and the 3' hinge and 5' hinge regions (Figure 2.8 and 2.9). The exosome has been suggested in the literature to be the major RNA degradation machinery for the 5'-ETS RNA (Delan-Forino et al., 2020; Klinge and Woolford, 2018; Kobylecki et al., 2018; Kornprobst et al., 2016). Therefore, it is possible that the observed 5'-ETS dismantling/degradation is performed by the Mtr4-exosome attached to the 90S pre-ribosome, starting close to the previously dislodged helix h9-9' of 5'-ETS. Noteworthy, we observed an RNA like density in the post-A_1-exosome state (Figure 2.12 A right panel) close to Mtr4. We cannot unambiguously assign the density to a specific piece of rRNA, but we speculate to be either part of the ITS1 rRNA or the 5'-ETS A_0-A_1 fragment. If this RNA would be ITS1 it would be very close to the endonuclease Utp24, which then could cleave at the nearby site A_2 (3' extension at 3' end of 18S pre-rRNA), while the 5'-ETS A_0-A_1 fragment would be still bound after both 5'-ETS cleavages (A_0 and A_1) to post-A_1 particles as observed via Northern blot (Supplemental Figure S8).

Taken together, our biochemical and structural data suggests that the decisive A_1 cleavage step takes place within a 90S-exosome super-complex. Surprisingly, the recruitment of the RNA exosome mediated by Mtr4 occurs before the A_1 site is processed to the 90S pre-ribosome in the pre-A1 state and not to a free 5'-ETS RNP as suggested in literature. Moreover, we observed a dislodgment of the 5'-ETS already, which is initiated in the pre-A1 state close to the docking site of the RNA exosome. This finding suggests that the RNA exosome could fulfill a role not only in 5'-ETS degradation but also in its remodeling, which gives this pre-rRNA region enough flexibility for the A_1 site to reach the catalytic center of the endonuclease Utp24.

3. Discussion

Understanding the exact steps, which drive ribosome biogenesis, has been investigated with tremendous effort in the past 50 years. Genetic and biochemical analysis of wild type and mutant yeast cells has allowed to come to a basic understanding of this process and many further tools could be developed to investigate a large number of pre-ribosomal particles, each representing a snapshot of the biogenesis pathway. In the past decade, these pre-ribosomal particles became the subject of structural studies by cryo-EM analysis and modelling. With my PhD study, I was able to discover new pre-ribosomal particles of the pathway leading to the 40S subunits. While it was recognized for a long time that the 90S pre-ribosome contains the pre-rRNA and many r-proteins as well as AFs necessary for pre-40S biogenesis, the processes as well as requirements for the pre-40S to emerge from the huge 90S complex were poorly understood. In combination with cryo-EM studies performed in the Beckman lab, we were able to depict for the first time 90S particles after A_1 cleavage has occurred. Moreover, we visualized the so far mysterious 90S to pre-40S transition in great detail. During the course of the biochemical characterization of the new pre-ribosomal particles, we were able to enrich the RNA exosome on 90S particles with the split-tag purification approach, thereby making it possible to visualize a 90S-exosome super-complex by cryo-EM analysis. The results from my PhD work give a detailed insight into how particle compaction, structural rearrangements following A_1 cleavage, productive 5'-ETS degradation by the RNA exosome and sequential shedding of 90S AFs gives rise to the primordial pre-40S particle (Figure 3.1).

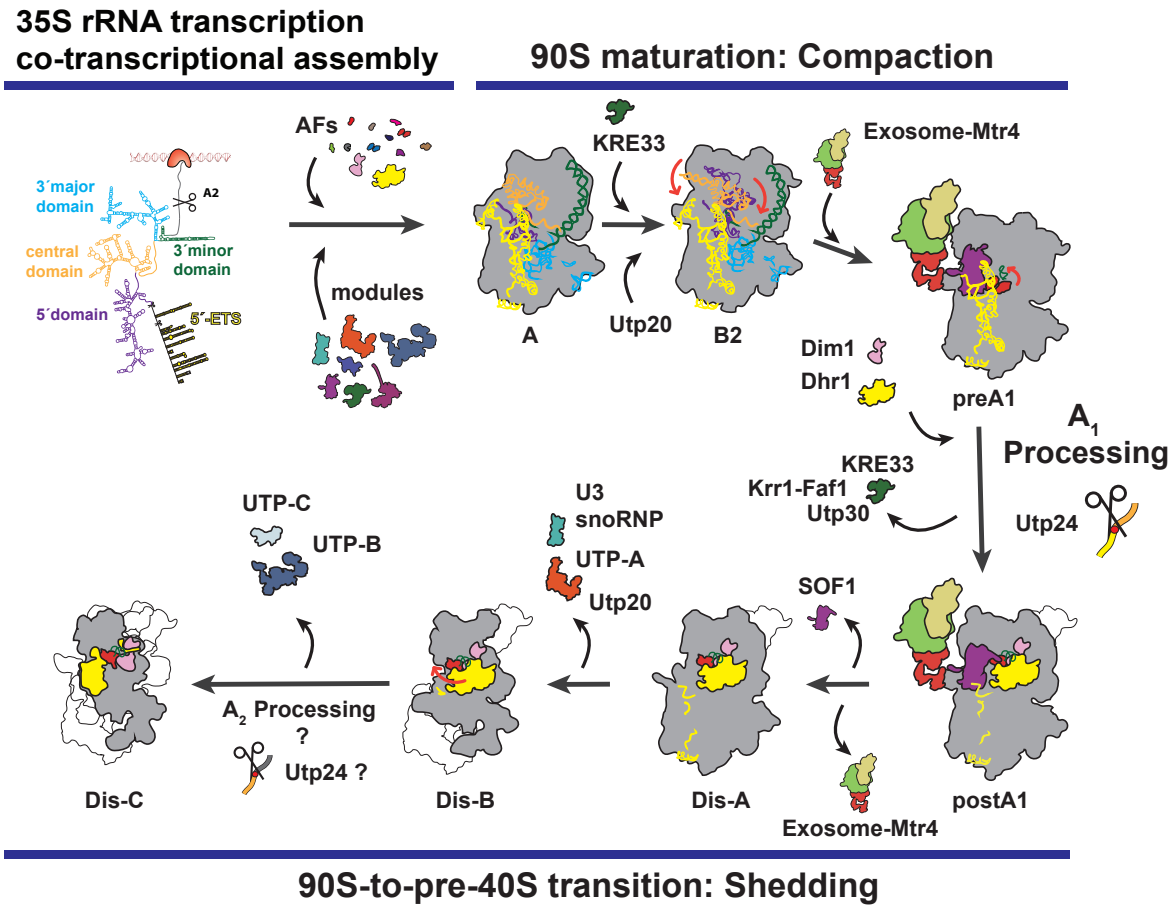

Figure 3.1 Dynamic model of 90S biogenesis and 90S to pre-40S transition. The first biochemically stable pre-ribosomal intermediates are assembled co-transcriptionally as AFs and modules bind the nascent 35S pre-rRNA (Upper panel, left side). The 90S pre-ribosome undergoes a process of compaction (upper panel), which culminate in recruitment of the Exosome-Mtr4 complex, the helicase Dhr1 as well as the dimethyltransferase Dim1, remodeling of 5'-ETS and finally, the processing of the A1 site (right side). This in turn sets off a process of reduction, in which a serial shedding of modules results in a first primordial pre-40S subunit (Dis-C). The 5'-ETS: yellow, 5' domain: magenta, central domain: orange, 3' major domain: cyan, 3' minor domain (H45): forest green. Exosome core: green, Rrp44: khaki, Mtr4: red. Red arrows indicate conformational changes within the 90S pre-ribosome. For better overview, only the 5'-ETS is visualized from state pre-A1 onwards. See text for details.

3.1 90S particle compaction and RNA exosome recruitment precedes A_1 cleavage

The biogenesis of both ribosomal subunits has been described by the order of pre-rRNA processing steps as well as sequential maturation of regions within pre-ribosomal particles, including assembly and disassembly events of r-proteins and

AFs. Recently published single-particle cryo-EM models of 90S pre-ribosomes from the thermophile *Chaetomium thermophilum* in combination with the results presented in this work highlight local structural rearrangements as well as more regional and global compaction processes of the 90S particle with simultaneously increased flexibility of the 5'-ETS as crucial drivers of the competence for A_1 cleavage. Moreover, the series of 90S states from *Chaetomium thermophilum* and yeast revealed that the subdomains of the 18S rRNA (in the order of transcription: 5' domain, central domain, 3' major domain and 3' minor domain) are assembled individually with their set of AFs and r-proteins as the pre-rRNA is transcribed, while their stable integration into the 90S pre-ribosome occurs in the reverse order, starting with the 3' domain, followed by the central and then 5' domain. The reverse order of stable integration of the rRNA subdomains could be an elegant way to prevent the products of premature Pol I termination or rRNA degradation (which are truncated at their 3' end) from further engaging in ribosome biogenesis.

Here, the Noc4-module plays an integral part as it is attached to parts of the 3' domain and hence involved in the earliest compaction processes of the 90S biogenesis involving the pre-formed 5'-ETS scaffold, or base region, and the 3' domain. Moreover, incorporation of the heterodimer Bms1-Rcl1 depends on the 3' domain and at the same time Bms1 establishes ties between the 3' domain and the 5' domain via its interaction with the distal copy of the acetyltransferase Kre33. The 5' domain of the 18S rRNA becomes stably integrated and hence visible in 90S cryo-EM models as the Kre33 module members appear in the head region of the pre-ribosome. They are located at strategic positions and contributing if not driving this integrative assembly step. The body, or central domain of the 90S pre-ribosome, is linked with the 5' domain via Lcp5's C-terminus and additionally via the U3 snoRNP and Rrp9. Moreover, the C-terminus of Bfr2 and Enp2 form an interface to which the KH domain containing protein Krr1 reaches out from the 90S central domain with an extended C-terminal helix. In addition to the Kre33 module, the huge α-helical protein Utp20 can be seen wrapped around the whole 5' domain and interacting with Utp10, another elongated α-solenoid element containing protein coming from the base region of the 90S particle. As 90S maturation continues, Utp20 adopts a more closed and hence compact conformation. This compaction of the head region, as well as Kre33 module's movement towards the central domain, appear to be driven by the immature 5' domain, which gradually moves closer towards the central domain. At the same time, in the

base region of the 90S pre-ribosome, the 5'-ETS rRNA gains an increased flexibility or is degraded as helices of the 5'-ETS disappear in the cryo-EM models.

It is not clear, how both seemingly opposed events, compaction of the 18S rRNA and remodeling of the 5'-ETS pre-rRNA, are connected or depend on each other. However, the interconnectivity of individual rRNA subdomains as well as their stable integration status could serve as a checkpoint along the 90S biogenesis pathway, enabling further compaction processes of the 90S pre-ribosome as a whole and simultaneously increasing 5'-ETS flexibility, which are observed as the 90S pre-ribosome approaches A_1 cleavage. This checkpoint as a bottleneck in the 90S biogenesis pathway could be an explanation for why 90S pre-ribosomes with an intact A_1 site were easier to obtain with biochemical methods and stable enough to result in high-resolution cryo-EM structural models. Within this context, UTP-C likely plays an important role. In the 90S particle series from yeast and *Chaetomium thermophilum*, the interaction network of the module increases to rRNA helices of the central domain and 3' domain, strengthening its association with the 90S pre-ribosome. At the same time, the strategic location in the central domain, with contacts to the 3' domain as well as the 5' domain via Krr1-Enp2 and hence the Kre33 module, could enable UTP-C to sense the integration status of each subdomain individually and relative to each other. The ability to monitor 90S biogenesis progression via rRNA subdomain integration together with a link to global cellular regulatory pathways via the CURI complex indeed opens an intriguing connection between ribosome production and global transcriptional regulation.

Interestingly, our findings showed that the RNA exosome is recruited to a sufficiently matured 90S pre-ribosome before the A_1 site has been processed (Pre-A_1 state). In contrast to what was described in literature, the RNA exosome is bound to the 90S particle, forming a 90S-exosome super-complex, arguing that its role is not restricted to just RNA degradation. The Mtr4-RNA exosome machinery could use the already processed A_0 site in the 5'-ETS as entry and progressively channel the RNA in an ATP dependent manner into the exosome core for subsequent degradation in a 3'>5' direction. To facilitate complete degradation of the 5'-ETS, the Mtr4-RNA exosome machinery could remain bound to the 90S particle until later dismantling steps set free the modules and factors interacting with the last parts of the 5'-ETS. It is possible that RNA exosome recruitment prior to A_1 processing entails the remodeling of the 5'-ETS observed in the cryo-EM structures described in this work and thus

contribute to the competence of the 90S pre-ribosome for endonucleolytic cleavage at the A_1 site. Supporting this idea, in a recent publication it was shown that by depletion of essential Dhr1, the exosome was recruited to 90S particle with intact A_1 cleavage site but not fully rotated Pno1-H45 (Du et al., 2020), whereas upon Pno1 depletion Dhr1 together with the exosome was accumulated on a 90S pre-ribosome (Sturm et al., 2017). Another possibility is that the Mtr4-RNA exosome machinery positions itself at the 90S particle with a relatively flexible 5'-ETS, waiting for A_1 cleavage to occur as the signal for 5'-ETS degradation.

Taken together, the 90S particle series shows a clear structural compaction of the 18S rRNA subdomains, which seems to be driven by stable integration of the 5' domain. Nevertheless, major parts of the 90S pre-ribosome and the associated AFs remain unresolved. The maturation of the central domain and ES6 for example involves many crucial AFs, including helicases like Rok1 and its cofactor Rrp5 as well as snoRNAs such as the essential snR30. None of these factors were so far located within the 90S particles analyzed by cryo-EM, with the exception of a small part of Rrp5 close to the UTP-C module. Moreover, we can observe remodeling of the 5'-ETS pre-rRNA and the Mtr4-RNA exosome associated with significantly developed 90S pre-ribosomes. Both ultimately culminate in the cleavage of the A_1 site, which is accompanied by major structural rearrangements as well as relocation and dissociation of some AFs (see next section).

3.2 A_1 cleavage is accompanied by major structural changes in the 90S-exosome super-particle

Previously published cryo-EM models of 90S pre-ribosomes were obtained from particles containing an intact A_1 cleavage site, similar to the states A to Pre-A_1 from our study. In the Pre-A_1 state, the A_1 processing site is clamped between α-helices of Sof1 and Utp7, circa 50 Å away from the PIN domain containing AF Utp24 and thus too far to reach for the catalytic center of the endonuclease. Our results are the first studies providing structural and biochemical evidence of the mechanisms leading up to A_1 cleavage as described in the previous paragraph. Moreover, the series of cryo-EM models resulting from this work depicts for the first time pre-ribosomal stages after A_1 cleavage. We see that in the Post-A_1 state, the A_1 site moved closer to the catalytic center of endonuclease Utp24 while a short RNA stem loop (h1) can be observed at the now mature 5' end of the 18S rRNA, which can be traced in the

cryo-EM model until Uridine 3, i.e., the third nucleotide of the mature 18S rRNA. This finding is in line with studies previously describing A_1 processing as sequence-independent but stem-loop dependent, with a three-nucleotide spacer relative to the stem loop base as crucial (Sharma and Tollervey, 1999). Moreover, our findings show that 18S rRNA remodeling leads to substrate availability for Utp24 rather than a relocation of Utp24 close to the A_1 processing site, again arguing for the compaction of rRNA subdomains as major pre-requisite for A_1 cleavage.

In addition to the rRNA compaction and remodeling events leading up to A_1 processing, A_1 cleavage is accompanied by loss of several AFs (Kre33 module, Krr1, Faf1) as well as recruitment and relocation of other AFs (Dhr1, Dim1, and Pno1). Major structural rearrangements take place in the base region upon A_1 processing. First, the 5'-ETS is mostly not visible in the Post-A_1 state. Whether this is caused by a higher flexibility or degradation is not clear. However, the overall structure and organization of the 90S scaffold in the base region remains the same, pointing to a higher degree of flexibility of the pre-rRNA region rather than its complete absence. Notably, Utp7, which together with Sof1 contributed to keeping the A_1 site in place prior to A_1 cleavage, undergoes a conformational change in its C-terminus. In the Pre-A_1 state, the C-terminus has extensive interactions with the helix H7 of the 5'-ETS. Upon A_1 processing, this C-terminal region transforms into an extended helix, now contacting the newly recruited Pno1 and shielding processing site D of the 20S pre-rRNA. Pno1 is a KH domain containing protein with high homology to the KH domains of Krr1, but lacking Krr1's C-terminal extension. It has been described to replace Krr1 in a recent study by our lab (Sturm et al., 2017). During the events surrounding A_1 processing, Krr1 together with Faf1 dissociates from the 90S pre-ribosome and Pno1 occupies the KH domain binding site. Its relocation from the periphery of the 90S pre-ribosome to the central domain designates the first step of the 90S to pre-40S transition. Prior to A_1 cleavage, Pno1 binds as peripheral 90S AF to Utp14, a cofactor of the Dhr1 RNA helicase, and thus contributes to the activation of the helicase as previously reported (Sturm et al., 2017). The empty cavity upon relocation of Pno1 and H45 provides now a binding interface for Dhr1 and leads to its recruitment. Post A_1 processing, Pno1 has adopted its pre-40S location, bringing H45 to its mature conformation and later recruiting the endonuclease Nob1. Notably, the relocation of Pno1 is accompanied by a change of the binding mode to H45. This novel binding is stabilized by the newly constructed C-terminal helix of Utp7. How this is achieved remains unclear. Pno1 could

dissociate from the 90S particle or remain loosely attached during the relocation and this flexibility could enable a new binding to H45. The relocation of Pno1-H45 also marks recruitment of Dim1, a dimethyltransferase that adds a dimethyl-group to the helix tip of H45, a modification, which is highly conserved and is even found in bacteria. Since these rearrangements take place at the boarder of the base and body region, where the 5'-ETS and central domain are located, respectively, it can be assumed that the global compaction processes of the rRNA subdomains and 5'-ETS remodeling events both play a role in setting the A_1 cleavage and the described rearrangements in motion.

Taken together, our findings have revealed in great structural detail the maturation events surrounding A_1 processing. These include particle compaction, 5'-ETS remodeling as well as release and recruitment of AFs. Considering the dramatic remodeling events, A_1 processing can be regarded as the starting point for the 90S to pre-40S transition (see next section), which highlights the removal of the 5'-ETS as the decisive step enabling the pre-40S particle to emerge from the huge 90S pre-ribosome.

3.3 The pre-40S particle is liberated from the 90S pre-ribosome by continuous shedding of 90S assembly factors

The events driving the conversion of the 90S pre-ribosome into a pre-40S particle were poorly described prior to this study. The former view on this was that upon A_1 cleavage a so called 5'-ETS particle is released *en bloc*, thereby generating the first pre-40S intermediate (Klinge and Woolford, 2019; Kornprobst et al., 2016). This 5'-ETS particle was suggested to consist of the 5'-ETS rRNA, the U3 snoRNA attached to most of the 90S AFs and modules (e.g., UTP-A, UTP-B, Mpp10, U3 snoRNP, and unclassified AFs). Further, it was suggested that the released AFs can be recycled upon 5'-ETS RNA degradation, mediated by the RNA exosome, for further engagement in 90S pre-ribosome biogenesis.

Here, we describe in great detail the process of the 90S-to-pre-40S transition by analyzing three isolated cryo-EM intermediates, which contradict the common understanding of this process. The first transition particle Dis-A, which is derived from the post-A_1 state, has released the Sof1 module together with Utp6. Noteworthy, this module was keeping the A_1 site of 18S rRNA in place before formation of H1 and subsequent cleavage. We speculate that A_1 cleavage is a prerequisite for the release

of this module and thus on the other hand the cleavage can initiate the transition process. Next, the Dis-B intermediate is emerging as a continuation of the shedding process by dissociation of the UTP-A module together with Utp18 and all protein components of the U3 snoRNP. Interestingly, the UTP-A module not only dissociates as whole, but presumably with the 5'-ETS rRNA remainder H1-H2 still bound, which is observed in state Dis-A. In this scenario, the released UTP-A module could be recycled and reactivated upon 5'-ETS rRNA degradation by an exonuclease (e.g., Xrn1, Rat, or Mtr4-exosome). Moreover, the UTP-A module dissociates in combination with Utp18, which on the other hand can recruit Mtr4 together with the exosome, an ideal candidate for H1-H2 of 5'-ETS degradation. Thus, the recycled UTP-A module, which is the first 90S module to be recruited to the newly transcribed 35S rRNA, could engage again in the process of nascent 90S pre-ribosome formation. This would be an elegant way to provide feedback on the status of 90S particle biogenesis, as UTP-A is successfully released from particles, which have experienced the transition to pre-40S intermediates and are hence past the decisive A_1 processing step. In the Dis-B state, the U3 snoRNP proteins have also been released, leaving behind the U3 snoRNA attached to the particle via heteroduplex formation with the 18S pre-rRNA. With this massive shedding of AFs, the Dis-B state has been strongly reduced in size compared to a classical 90S pre-ribosome. From the final transition intermediate Dis-C, the UTP-B and UTP-C module have been dissociated, together with the last piece of the 5'-ETS (3' hinge region). This step leaves behind a particle, which for the first time has a shape reminiscent of a classical pre-40S particle with head, beak and body features. It was previously reported that a catalytically lethal *dhr1*$_{K420A}$ mutant accumulates a ~ 45S particle with some 90S factors still bound (e.g., Mpp10 module, U3 snoRNP, Utp14) and thus giving evidence that enzymatic activity of Dhr1 is essential for such a stalled particle (Sardana et al., 2015). Noteworthy, the dissociation of the UTP-B module from the state Dis-B now allows the RNA helicase Dhr1 to fill this vacant position and relocate to a segment of the U3 snoRNA, where final release can be initiated. Not only is Dhr1 now bound to its substrate, the U3 snoRNA, but it also changed the conformation to a closed apo-state, meaning that Dhr1 has RNA bound in a closed conformation but is still awaiting ATP binding to carry out a pulling force on the U3 snoRNA. In the previous cryo-EM states, where Dhr1 is visualized, the RNA helicase is seen in an open conformation with no RNA bound but presumably complexed with ADP. Thus, we could reveal for the first time, how this helicase *in vivo* changes

conformations from an inactive closed to an open apo-conformation in the process of shedding 90S AFs and modules. This exciting observation shows Dhr1 now acting on its substrate, the U3 snoRNA. Most likely every cycle of ATP hydrolysis leads to Dhr1 pulling the U3 snoRNA a bit further apart from the Dis-C particle, thus releasing the last U3 – 18S rRNA heteroduplex, so that the U3 snoRNA can finally dissociate from the Dis-C particle.

Taken together, the findings from my PhD study could reveal a successive release of AFs from a 90S particle after A_1 has been carried out. This could be observed on three distinct transition intermediates (Dis-A, Dis-B and Dis-C), whereas the last one already has the shape of a primordial pre-40S with relocated Dhr1, now ready for unwinding the U3-18S rRNA hybrid.

3.4 Conclusion and outlook

This work describes for the first time the 90S-to-pre-40S ribosome transition and how the RNA exosome is engaged in this process. This could be shown through a series of cryo-EM in combination with biochemical analyses, which together challenge our common thinking of an *en bloc* release of a 5'-ETS particle during the birth of the pre-40S intermediate. We change this view by demonstrating that the 90S-to-pre-40S transition is a successive shedding of AFs and modules until a first primordial pre-40S emerges. Moreover, we could isolate a 90S-exosome super-complex and show that the 5'-ETS rRNA is processed by the exosome on the 90S particle. This process coincides with the A_1 cleavage, which we could observe for the first time on corresponding 90S particles by cryo-EM. Furthermore, we have first evidence that the exosome fullfills, beside its general RNA degradation role, an additional remodeling function of the 90S pre-ribosome prior to A_1 cleavage. Noteworthy, we could observe how the RNA helicase Dhr1 adopts an open apo-conformation upon relocation to its substrate U3 snoRNA on the primordial pre-40S particle, which is our last isolated transition state.

By elucidating the complex 90S-to-pre-40S transition some aspects of this conversion process remain still unclear and need further scientific investigation. Moreover, with the presented insights into this transition process some new questions arise. One of these questions is the role of the large Kre33 module in this process. We could demonstrate that the successive compaction of the 5' domain toward the central domain of 18S pre-rRNA leads to the dissociation of the Kre33 module, which is coupled with the A_1 cleavage of 5'-ETS rRNA observed in the post-A_1 state. It would be interesting to know if the release of the Kre33 module by the described compaction is forcing this process further until it culminates in a conformation of the 18S pre-rRNA sufficient for A_1 cleavage. Alternatively, A_1 cleavage could be forcing further compaction and causing the release of the Kre33 module. Answering these questions would help to understand if A_1 cleavage is the final checkpoint, which if successfully overcome, causes a cascade of irreversible maturation steps as described in the results sections. Here, a better temporal resolution of between the two snapshots "pre-A1"and "post-A1" would be beneficial.

Regarding the 90S-exosome super-complex further questions arise regarding the precise role of the exosome and especially Mtr4 in the 90S pre-ribosome processing. Our data show that the 90S recruitment of Mtr4 is mediated not only by

the AIM motif containing protein Utp18, but also by Utp6. Thus, exosome recruitment is more complex as compared to events within the pre-60S particle maturation involving Nop53 and Mtr4. We do not know in detail how Mtr4 is recruited to the 90S pre-ribosome in state pre-A_1, why there is the need for a redundancy (Utp18 plus Utp6 interface) or which maturation state of the 90S particle is sufficient for Mtr4 to dock at the specific interface. Mtr4 could, together with the exosome, have an additional remodeling function on the 90S pre-ribosome. Therefore, the recruitment of RNA helicase Mtr4 could not be simply to guide the helicase to a 3' end of 5'-ETS rRNA, it could furthermore be to position Mtr4 strategically on the 90S pre-ribosome to carry out its remodeling reaction. This idea is supported by our data that the Mtr4-exosome is recruited already to the 90S pre-A_1 particle, before A_1 cleavage has occurred, but the 5'-ETS has not been processed or dislodged. Concomitant to this observation an additional question came up, for example if the Mtr4-exosome recruitment, remodeling and processing on the 90S particle is a prerequisite for the A_1 cleavage and if so, how does the remodeling work in detail?

A major finding of this work is the observation that the RNA helicase Dhr1 shows two different conformations on the 90S, one is the open inactive and the other one the closed but active apo-conformation, which Dhr1 adopts upon relocation and substrate binding. In a broader sense, the question to this conformational switch on a pre-ribosomal particle could be, whether this could be a more general mechanism for RNA helicases continuously positioned on macromolecular complexes, which can be activated upon certain remodeling of the structure and how this is accomplished. A recent publication showed the dual role of essential Dhr1 upon depletion, which leads to a stalled 90S particle before A_1 cleavage (Du et al., 2020) giving evidence of an additional function of Dhr1 on the 90S particle besides the U3 snoRNA release from the primordial pre-40S. We can show *in vivo* that the helicase activity of Dhr1 functions as a checkpoint of completed 90S-to-pre-40S transition and that the helicase is adopting an active conformation by production of the primordial pre-40S intermediate. One important role of the relocation of Dhr1 on the ribosomal particles plays its long N-terminal domain, which could be also the case for other RNA helicases with large N-or C-terminal extensions. Another interesting outlook regarding Dhr1 is the question, what causes the release of the U3 snoRNA from the primordial pre-40S particle. One very certain event would be the formation of the central pseudoknot but in addition we speculate that this massive RNA remodeling event causes the release of the remaining

90S associated AFs from the primordial pre-40S (e.g., Mpp10, Sas10, Imp4, Utp14 and Utp24), resulting a first classical pre-40S intermediate as already described by others (Ameismeier et al., 2020; Heuer et al., 2017).

Moreover, this study shows mechanistically how the endonuclease Utp24 performs the A_1 cleavage of 5'-ETS. Furthermore, we could observe how Utp24 dislocates from the Dis-B particle, just to relocate to a different position on the subsequent state Dis-C. Therefore, we speculate that Utp24 might dislocate from particle Dis-B to perform another endonucleolytic cleavage on ITS1 at site A_2. Our Northern blot analysis supports this idea with the observation that state Dis-C has a 20 rRNA species, which has A_2 site cleaved, whereas the remaining particles show largely intact A_2 sites by 21S or 23S rRNA species (Figure 2.3 B).

The presented data and mechanisms contribute to a better understanding of the biogenesis of the small subunit and shed light on the 90S-to-pre-40S transition. However, the presented cryo-EM data show only snapshots in ribosome biogenesis and not the whole entity of one pre-ribosomal particle can be displayed. Several AFs and rRNA segments could not be visualized due to their flexibility and so the picture of the presented particles stays incomplete. Thus, additional biochemical analysis could fill some of these open questions and complement the mechanistic details presented in this study.

Last but not least, our presented data were derived from yeast and *Chaetomium thermophilum*, but we think that this could be relevant also for humans, as the eukaryotic ribosome biogenesis is highly conserved. Therefore, the growing scientific field dealing with ribosomopathies, which describes human disorders of genetic abnormalities by causing impairment in ribosome biogenesis and thus resulting in specific clinical phenotypes, could be supported with our presented biochemical and structural insights to describe ribosome biogenesis in molecular detail. Thus, the transformation of our approach to a specific genetic disorder could help in a better understanding of ribosomopathies and related human diseases.

4. Materials and Methods

4.1 Molecular biology and genetic methods

4.1.1 Construction of plasmids and common molecular methods

Constructed plasmids and used molecular methods were performed as follows. PCR products were amplified using Phusion High-Fidelity DNA Polymerase (NEB) and separated by agarose gel electrophoresis followed by purification with Gel Extraction kit (SIGMA). DNA constructs were digested with restriction enzymes and subsequently ligated with T4 DNA Ligase (NEB) and finally transformed into *E. coli* Dh5α strain [F– endA1 glnV44 thi-1 recA1 relA1 gyrA96 deoR nupG purB20 φ80dlacZΔM15 Δ(lacZYA-argF)U169, hsdR17(rK–mK+), λ–] (Inoue et al., 1990). Amplified plasmid DNA was isolated with the GenElute TM HP Plasmid Miniprep Kit (SIGMA) and correct insert was verified by test digest and DNA sequencing (Eurofins MWG-Operon; Ebersberg, Germany). For a complete list of used plasmids see table 1.

4.1.2 Growth and construction of *S. cerevisiae* strains

Cultivation of haploid *S. cerevisiae* strains was performed in YPD media at standard growth conditions at 30°C. Introducing a C-terminal tag to a gene or gene disruption was done by PCR-based homologous recombination as described before (Ito et al., 1983; Janke et al., 2004; Longtine et al., 1998). Correct genetic modification was confirmed by colony PCR and/or detection of the tag by western blot. *S. cerevisiae* cells were monitored for a growth phenotype by incubating cells in a serial dilution on YPD plates at 23°C, 30°C and 37°C. For isolation of ribosomal particles cells were grown to logarithmic growth phase and harvested at an OD_{260} = 2.0. Yeast strains used in this study are listed in table 2.

YPD (yeast extract, peptone, dextrose) medium (pH 5.5):
1% (w/v) yeast extract, 2% (w/v) glucose (Merck), 2% Bacto™ peptone

YPG (yeast extract, peptone, galactose) medium (pH 5.5):
1% (w/v) yeast extract, 2% (w/v) galactose (Merck), 2% Bacto™ peptone

SDC-X (synthetic dextrose complete) medium (pH 5.5):
2% (w/v) glucose (Merck), 0.67% yeast nitrogen base w/o amino acids complemented with amino acids lacking X for selection.

Solid media for plates was supplemented with 22 g/l agar.

Table 1 Recombinant DNA used in this study.

Strains: Saccharomyces cerevisiae	Source	Published
$P_{GAL1-10}$-*ct rrp12* (1-1039) TEV-ProtA, LEU2, 2µ, *AmpR*	This study	(Cheng et al., 2019)
$P_{GAL1-10}$-ProtA-TEV-*ctENP1*, LEU2, 2µ, *AmpR*	This study	(Cheng et al., 2019)
$P_{GAL1-10}$-ProtA-TEV-*ctNOP14*, LEU2, 2µ, *AmpR*	This study	(Cheng et al., 2019)
$P_{GAL1-10}$-Flag-*ctENP1*, TRP1, 2µ, *AmpR*	This study	(Cheng et al., 2019)
$P_{GAL1-10}$-*ct rrp12* (1-1039) Flag, TRP1, 2µ, *AmpR*	This study	(Cheng et al., 2019)
$P_{GAL1-10}$-3xFlag-*ctEMG1*, TRP1, 2µ, *AmpR*	This study	(Cheng et al., 2019)
$P_{GAL1-10}$-3xFlag-*ctNOC4*, TRP1, 2µ, *AmpR*	This study	(Cheng et al., 2019)
$P_{GAL1-10}$-3xFlag-*ctEMG1*, $P_{GAL1-10}$-*ctNOC4* TRP1, 2µ, *AmpR*	This study	(Cheng et al., 2019)
$P_{GAL1-10}$-HA-*ctNOP14*, URA3, 2µ, *AmpR*	This study	(Cheng et al., 2019)
$P_{GAL1-10}$-HA-*ctNOC4*, URA3, 2µ, *AmpR*	This study	(Cheng et al., 2019)

4.1.2 Expression of recombinant proteins in yeast

For heterologous co-expression of *Chaetomium thermophilum* proteins in yeast, a high copy yeast vector (2µ) under control of a GAL promotor, carrying the protein of interest, was transformed into cells. An SDC-X pre-culture was transferred into YPG media and protein was expressed for 6 hours.

Table 2 Strains used in this study.

Strains: Saccharomyces cerevisiae	Source	Published
W303, *trp1-1, leu2-3, 112, his3-11, 15, ura3-1, can1-100*	(Thomas and Rothstein, 1989)	(Thomas and Rothstein, 1989)
NOC4-TAP::HIS3, *DHR1*-Flag::natNT2, W303	This study	(Cheng et al., 2020)
DHR1-TAP::HIS3, *DIM1*-Flag::natNT2, W303	This study	(Cheng et al., 2020)
CSL4-TAP::HIS3, *DIM1*-Flag::natNT2, W303	This study	(Lau et al., 2021)
RRP46-TAP::HIS3, *DIM1*-Flag::natNT2, W303	This study	(Lau et al., 2021)
RRP44-TAP::HIS3, *DIM1*-Flag::natNT2, W303	This study	(Lau et al., 2021)
DIM1-Flag::natNT2, W303	This study	(Lau et al., 2021)
UTP10-FTpA::natNT2, W303	(Kornprobst et al., 2016)	(Kornprobst et al., 2016)
KRR1-FTpA::HIS3, pno1::natNT2 shuffle, W303	(Sturm et al., 2017)	(Sturm et al., 2017)

4.2 Biochemical methods

4.2.1 Tandem-affinity purification of ribosomal particles

Yeast cells were harvested and stored at -80°C. Frozen cells were mechanically disrupted by a cryogenic grinding mill (Retsch MM400). For lysis cells were resuspended in 15ml buffer A and lysate was cleared twice by centrifugation (10 min at 5000 rpm followed by 20 min at 17000 rpm, 4°C). For first affinity purification step lysate was incubated on pre-equilibrated immunoglobulin G Sepharose 6 Fast Flow beads (GE Healthcare) for 2 hours followed by washing with 25 ml of Buffer B in batch and additional washing with 4 ml Buffer B on column. Bound proteins were eluted from beads by TEV cleavage at 16°C for 45 min (Parks et al., 1994).

Buffer A:
50 mM Tris-HCl (pH 7.5), 100 mM NaCl, 1.5 mM $MgCl_2$, 5% glycerol, 0.1% IGEPAL CA-630, 1 mM DTT, SIGMAFAST complete protease inhibitor cocktail (Sigma-Aldrich)

Buffer B:
50 mM Tris-HCl (pH 7.5), 100 mM NaCl, 1.5 mM $MgCl_2$, 5% glycerol, 0.01% IGEPAL CA-630, 1 mM DTT (samples for cryo-EM contained 2% glycerol).

4.2.2 Sucrose gradient ultracentrifugation

Eluate of a tandem-affinity purification was transferred to a linear 10%-40% (w/v) sucrose gradient. Gradient was made in buffer B1 by use of a Gradient Master device (BioComp Instruments). Sucrose gradient was centrifuged for 16 hours, 129,300 xg at 4°C. Gradient was fractionated into equal volume fractions and used for SDS-PAGE, Northern blot analysis or negative-stain electron microscopy.

Buffer B1:
50 mM Tris-HCl (pH 7.5), 100 mM NaCl, 1.5 mM $MgCl_2$, 0.003% IGEPAL CA-630, 1 mM DTT

4.2.3 Mass spectrometry

MALDI-TOF: Bands of interest from an 4-12% SDS-polyacrylamide gel, stained with colloidal Coomassie (Roti-Blue), were excised from gel, digested with trypsin and analyzed with Mass Spectrometry (BZH mass spectrometry facility, Heidelberg, Germany) as previously described (Bassler et al., 2001)
FingerPrint proteomics: Eluates of a tandem-affinity purification was separated on 4-12% polyacrylamide gel at 180V for 6 minutes. Gel was incubated in fixing solution (50% methanol, 10% acidic acid) for 1 hour and subsequently stained with colloidal Coomassie (Roti-Blue) for 15 minutes. Gel was incubated in water for 30 minutes and lanes with loaded sample was cut out till 1 cm below running front. Gel pieces were trypsin digested and analyzed by MS/MS FingerPrints proteomics (1D nLC-ESI-MS-MS, University of Dundee, UK). Raw data was analyzed by MaxQuant software (Cox & Mann, 2008) and IBAQ values were used for quantification as indicated in figures.

4.2.4 RNA extraction and Northern blot analysis

All tandem-affinity purifications where RNA was extracted, purification buffers were supplemented with RiboLock RNase inhibitor (Thermo Fisher Scientiffic). RNA from Flag-eluates or sucrose gradient fractions were extracted and precipitated with ethanol (Kos & Tollervey, 2005) and subsequently resolved on a 1.2% agarose gel after denaturation with glyoxal or on a 6% polyacrylamide gel (with 8M Urea) as previously described (Kornprobst et al., 2016). For northern analysis, the following 5'end γ32P-ATP radiolabeled probes (DNA oligonucleotides) were used: probe a (OMK002) 5'-CGGTTTTAATTGTCCTA-3', probe b (OMK800) 5'-GCAAAGATATGAAAACTCCAC-3‘, probe c (OMK1455) 5'- GTCTTCAACTGCTTTCGCA-3' and probe for U3 5'-GGTTATGGGACTCATCA-3'.

4.3 Electron microscopy

4.3.1 Negative-stain electron microscopy

Negative-stain, data collection and processing were performed by Dr. Dirk Flemming as described previously (Gasse et al., 2015). In brief, 5µl of the sucrose fractions were applied to a glow-discharged carbon-coated grid for 10 seconds. The sample was washed three times with water and subsequently stained with 3% aqueous uranyl acetate. Images of negatively stained particles were acquired either on a Thermo

Fisher Talos L120C electron microscope equipped with a Ceta 16M camera or a FEI Tecnai F20 electron microscope, operated at 200 kV, equipped with a field-emission gun and bottom-mounted 4K camera resulting in a magnification of 36,000x (4.13 Å/pixel) or 22,000x (4.46 Å/pixel), respectively. Particle selection for 2D classification was done by using boxer in EMAN2 (Tang et al., 2007). Image processing was performed using the IMAGIC-4D package (van Heel et al., 1996). Particles were band-pass filtered and mass centered. Two-dimensional alignment was carried out, classification and iterative refinement of class averages was performed as described previously (Liu and Wang, 2011). Total number of particles picked for 2D classification and averaging were 5,400 and 15,000 for Dhr1-Dim1 and Csl4-Dim1, respectively.

4.3.2 Cryo-electron microscopy and image processing

Cryo-electron microscopy (Cryo-EM), data processing and analysis was performed by the Beckmann group (Beckmann Lab, LMU Munich). In Brief, 3.5 µl Flag eluate of Noc4-Dhr1, Dhr1-Dim1 and Csl4-Dim1 preparations were directly applied onto pre-coated R3/3 holey-carbon-supported copper grids (Quantifoil), blotted for 2-3 seconds at 4° C and plunge-frozen in liquid ethane by an FEI Vitrobot Mark IV. Data for cryo-EM was acquired on a FEI Titan Krios transmission electron microscope at 300 kV under low dose conditions. Data collection, model building, and refinement was performed as described in detail in Cheng et al., 2020 and Lau et al., 2021, respectively. The corresponding density maps were deposited at the Electron Microscopy Data Bank (EMDB) and the coordinated files containing the fitted models at the Protein Data Base (PDB), respectively. All accession codes are listed in table 3.

Table 3 Cryo-EM accession codes

Cryo- EM state	EMDB code	PDB code
state A	11357	6ZQA
state B2	11358	6ZQB
state pre-A_1	11359	6ZQC
state pre-A_1 Exosome	11807	7AJT
state post-A_1	11360	6ZQD
state post-A_1 Exosome (Csl4-Dim1)	11808	7AJU
state post-A_1 Exosome (Dhr1-Dim1)	11809	
state Dis-A	11361	6ZQE
state Dis-B	11362	6ZQF
state Dis-C	11363	6ZQG

5. Supplemental Information

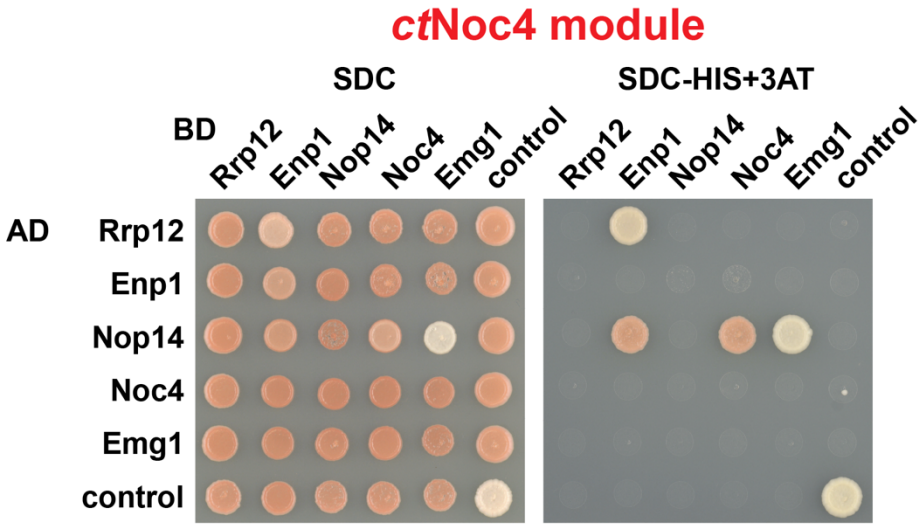

Figure S1. Yeast-two-hybrid interaction network of thermophilic Noc4 module. All protein-protein interactions of members from the Noc4 module were analyzed. All protein-protein pairs were transformed into yeast strain PJ69-4. Growth was analyzed after 4 days of incubation at 30° C on SDC-LEU-TRP (left block) or SDC-LEU-TRP-HIS+1 mM 3-AT. Figure was adapted from (Cheng et al., 2019).

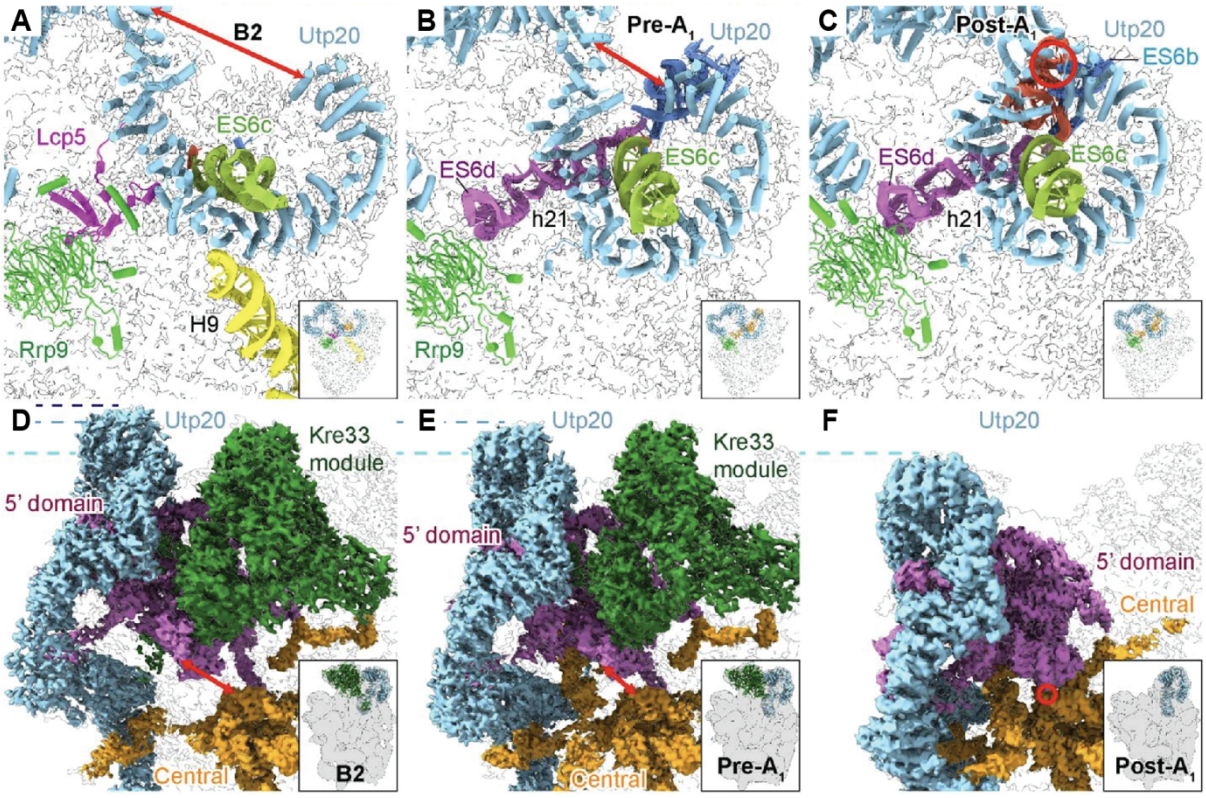

Figure S2. Remodeling and compaction events of 90S particle upon A_1 cleavage. (A-C) Molecular models of Rrp9 (green), Lcp5 (purple), and Utp20 (light blue) in association to 5'-ETS rRNA helix h9 (yellow) and pre-18S rRNA ES6 in state B2 (A), pre-A_1 (B), and post-A_1 (C). Showing dissociation of Lcp5 domain and structural change of Utp20 C-terminal region (indicated by red arrow and circle), concomitant relocation of 18S rRNA expansion segment 6 (ES6a, ES6b, ES6c, and ES6d) and disappearance of 5'-ETS rRNA helix h9. (D-F) Successive compaction of 5' domain (purple) and central domain (orange) of 18S pre-rRNA from state B2 (D) over subsequent state pre-A_1 (E), and state post-A_1 (F) with additional release of Kre33 module (green). The movement of Utp20 is indicated by dashed lines, while compaction of 18S pre-rRNA domains is indicated by red arrow and circle. Figure was adapted from (Cheng et al., 2020).

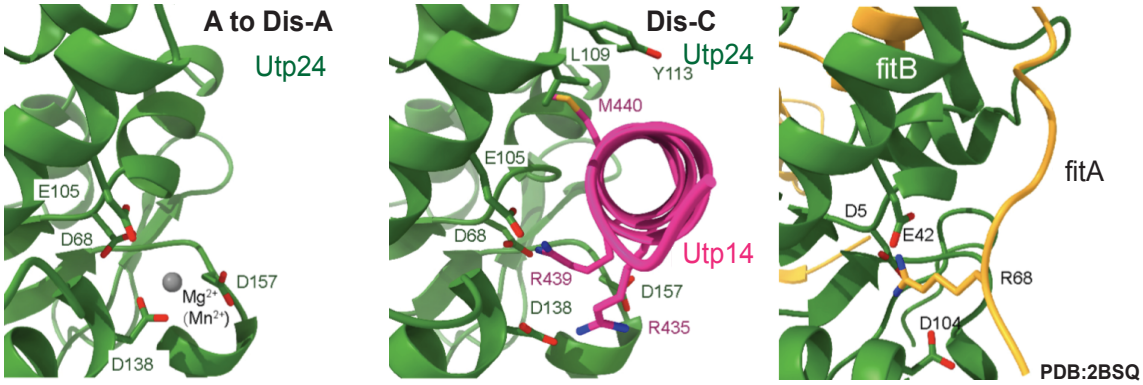

Figure S3. Utp14 inhibits upon relocation on Dis-C particle the endonuclease Utp24 by two arginine residues. The catalytic center of Utp24 with coordinated Mg^{2+} or Mn^{2+} ion shown as molecular model in the states A to Dis-A (left panel). The catalytic center of Utp24 is inhibited in state Dis-C (middle panel) by R435 and R439 of Utp14. A similar mechanism is described where an arginine finger of bacterial fitA protein protruding into the catalytic center of PIN domain endonuclease fitB (right panel). Figure was adapted from (Cheng et al., 2020).

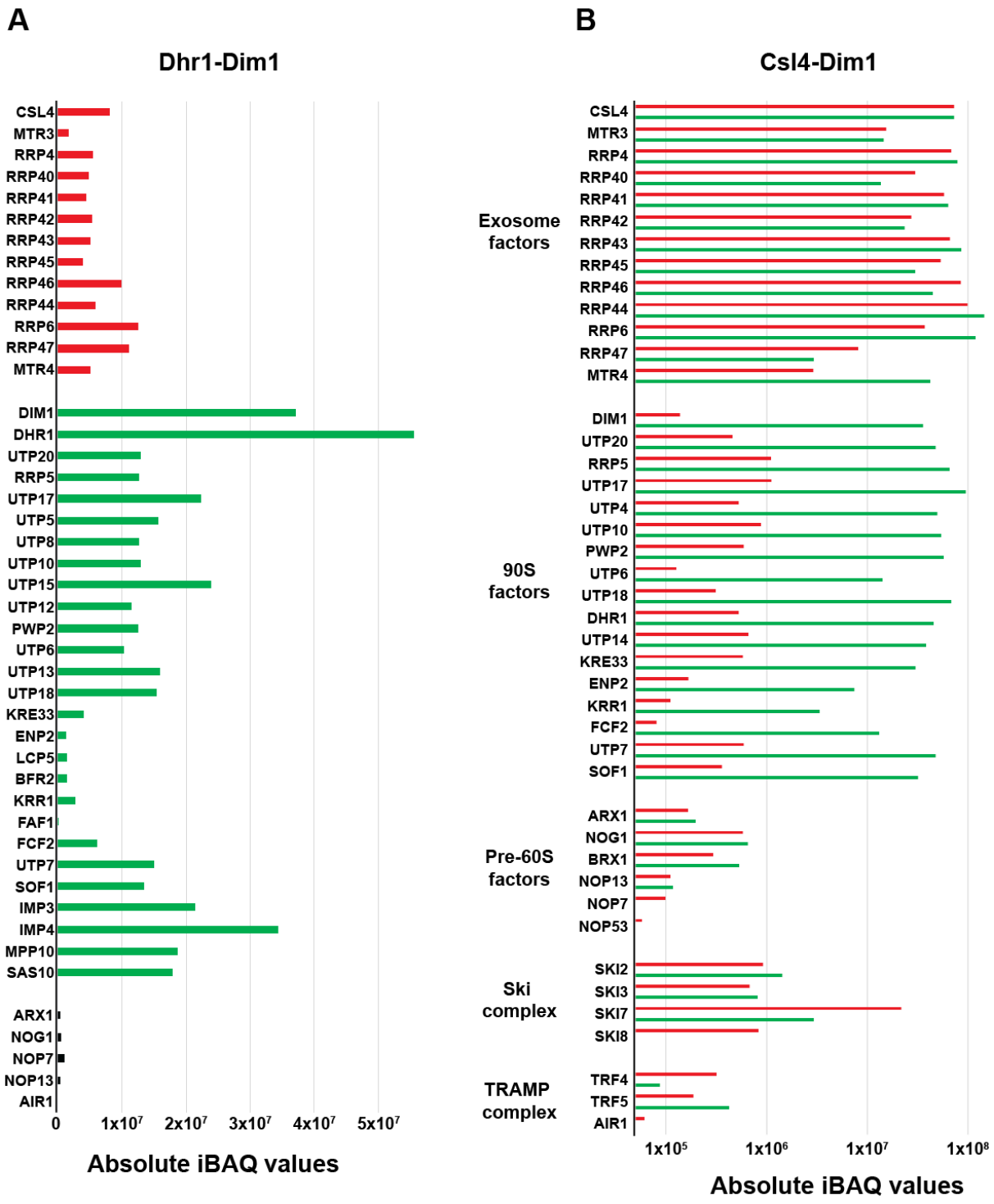

Figure S4. Semi-quantitative mass spectrometry of isolated Dhr1-Dim1 and Csl4-Dim1 particles. (A) Intensity-based absolute quantification (iBAQ) values from Dhr1-Dim1 isolated flag-eluates. Bars representing iBAQ intensity of detected proteins, red for exosomal proteins and Mtr4, green for 90S pre-ribosome assembly factors, and black for putative contaminants. (B) Comparison of the absolute iBAQ values, representing the Csl4 TEV eluate (red) against the Dim1-Flag eluate (green), both derived from the same Csl4-Dim1 preparation. Values were normalized to that of Csl4 from the TEV eluate, which was set to 1. In the second affinity step the 90S assembly factors where strong enriched, whereas the values for pre-60S factors, Ski-complex, or TRAMP complex stayed constant or were reduced. Figure was taken from (Lau et al., 2021).

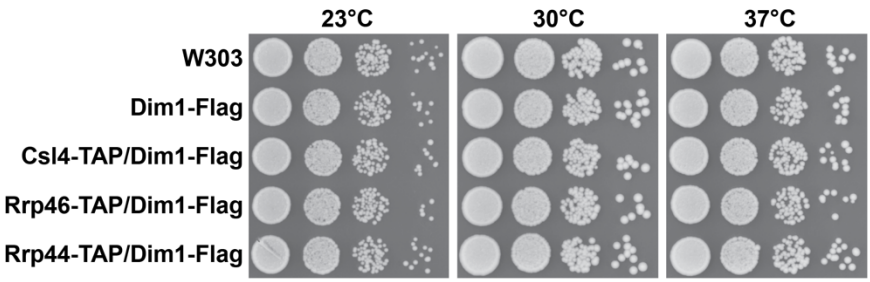

Figure S5. Growth analysis of yeast strains carrying chromosomally integrated tag bait. Growth analysis yeast strains with exosome-Dim1 split-tag used for tandem affinity purification and cryo-EM sample preparation in comparison to wild-type W303 yeast. Strains were spotted in a 10-fold serial dilution on YPD plates and growth at indicated temperatures was recorded after two days. Figure was adapted from (Lau et al., 2021).

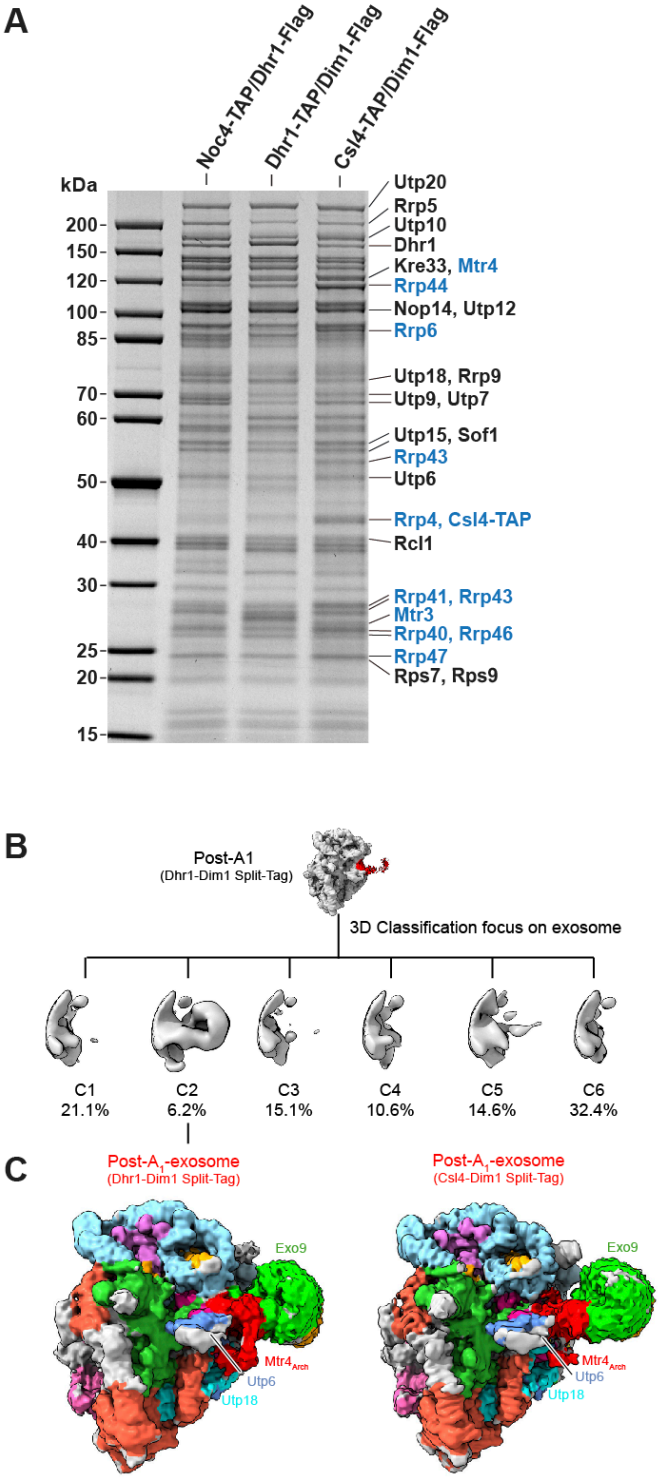

Figure S6. Comparison of 90S-exosome particles and Dhr1-Dim1 and Cls4-Dim1 cryo-EM maps. (A) Comparison split-tag affinity purified particles enriching the nuclear exosome on the 90S pre-ribosome, analyzed by SDS-PAGE and Coomassie staining. The labeled bands (90S factors, black and exosome factors, blue) were excised from the gel and identified by MALDI-TOF mass spectrometry. (B) The post-A_1 state of the Dhr1-Dim1 sample was sorted with focus on the exosome region, using tau factor value 4. Only class 2 (C2) exhibited a defined density for the exosome, which was used for final reconstitution. (C) Comparison of the cryo-EM volumes, in same orientation, from the Dhr1-Dim1 (left) and Csl4-Dim1 (right) post-A_1 exosome states. Both particles were identically color-coded and low pass filtered to 10 Å, displaying a similar conformation. Figure was adapted from (Lau et al., 2021).

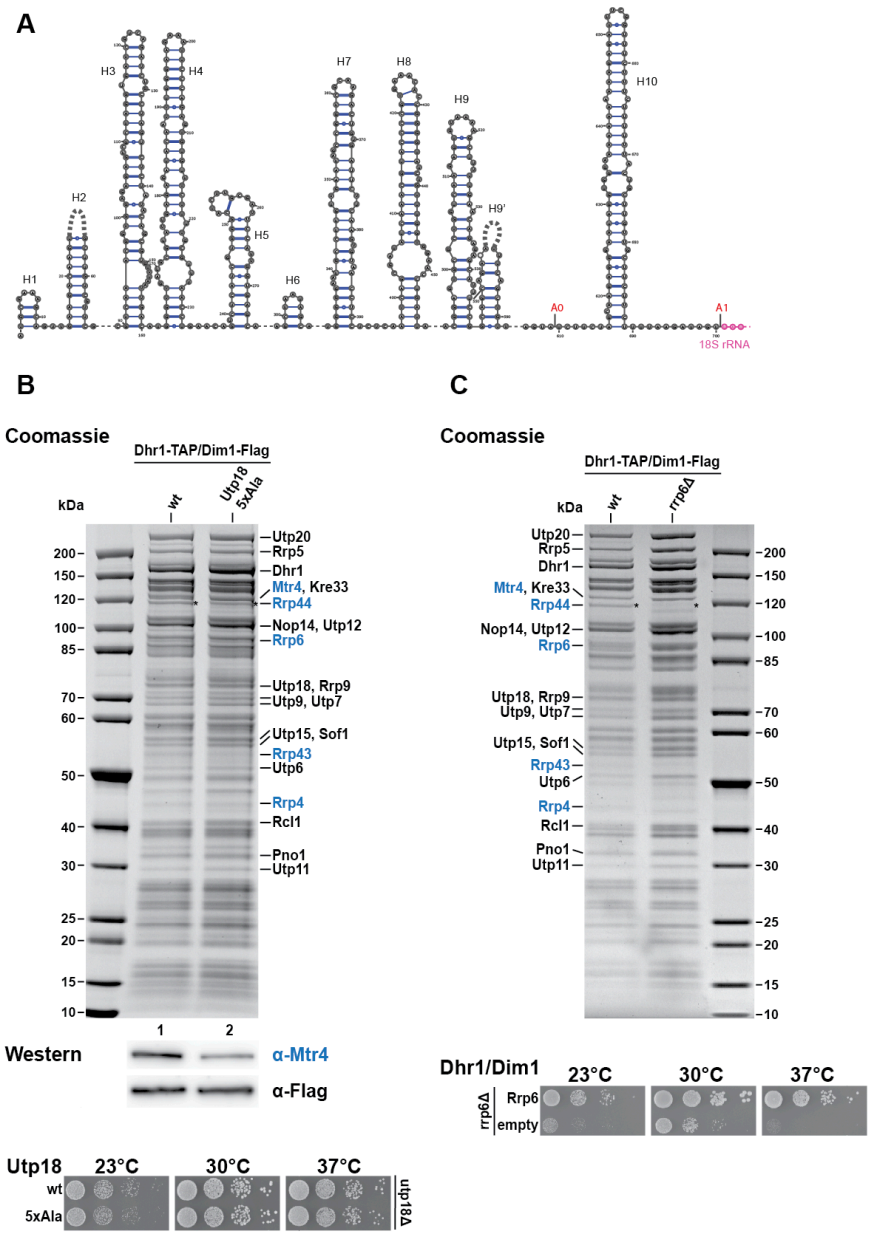

Figure S7. Yeast 5'-ETS rRNA secondary structure and genetic studies of exosome-Mtr4 recruitment to the 90S particles. (A) Yeast 5'-ETS rRNA sequence (nucleotides 1-700) and secondary structure with folding into helices h1 to h10. In addition, A_0 and A_1 cleavage sites are indicated. (B) Isolation of split-tag affinity-purified Dhr1-Dim1 90S particles from *UTP18* (wild-type) and *utp18-AIM* mutant cells (*utp18-5xAla*; see Thoms et al., 2015). Final eluates were analyzed by SDS-PAGE and subsequent Coomassie staining (upper panel), and additional Western blotting using anti-Mtr4 and anti-Flag (Dim1 bait as loading control) antibodies (middle panel). The labeled bands (90S factors, black and exosome factors, blue) were excised from the gel and identified by MALDI-TOF mass spectrometry in previous experiments. Growth analysis for yeast *UTP18* (wild-type) and *utp18-AIM* mutant strain have been performed (lower panel), therefor strains were spotted in a 10-fold serial dilution on YPD plates and growth at indicated temperatures was recorded after two days. (C) Isolation of split-tag affinity-purified Dhr1-Dim1 90S particles from *RRP6* (wild type) and *rrp6Δ* cells. Final eluates were analyzed by SDS-PAGE and subsequent Coomassie staining (upper panel). The labeled bands (90S factors, black and exosome factors, blue) were excised from the gel and identified by MALDI-TOF mass spectrometry in previous experiments. For growth analysis of RRP6 (plasmid-based *RRP6* in strain *rrp6Δ*) and *rrp6Δ,* strains were spotted in a 10-fold serial dilution on SDC-LEU plates and growth at indicated temperatures was recorded after two days. Figure was adapted from (Lau et al., 2021).

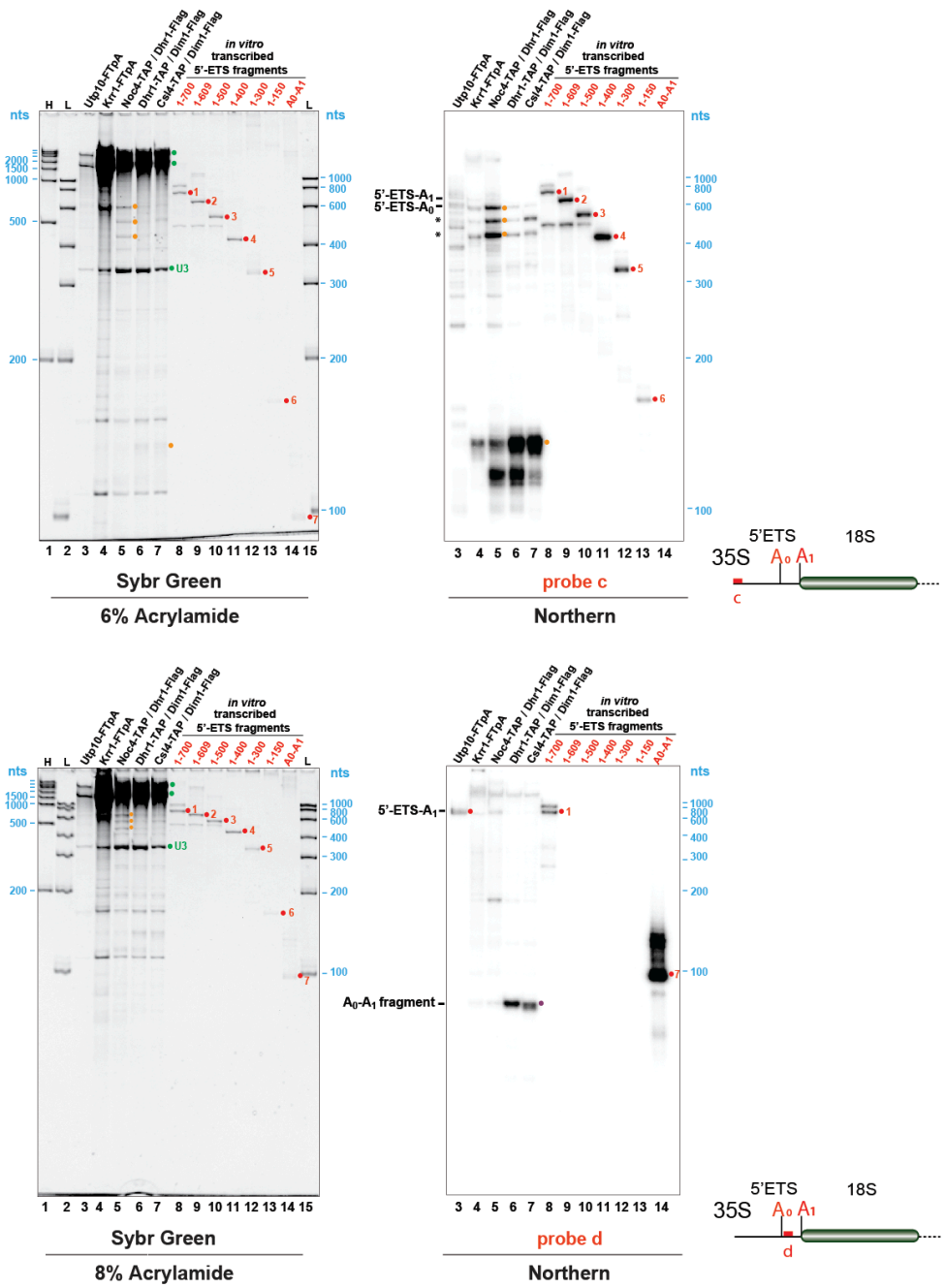

Figure S8. Northern blot analysis of the 5'-ETS fragments as comparison of different 90S particles. 5'-ETS rRNA comparison by northern blot of the affinity purified Utp10-FTpA, Krr1-FTpA, Noc4-TAP-Dhr1-Flag, Dhr1-TAP-Dim1-Flag, and Csl4-TAP-Dim1-Flag particles. The RNA derived from the different FLAG eluates (lane 3-7), two different RNA standards (H and L; lane 1, 2, and 15), and *in-vitro*-transcribed 5'-ETS fragments of various length (lanes 8-14) were separated on a denaturing 6% (top panel) and 8% polyacrylamide gel (bottom panel). The gels were stained with Sybr Green II fluorescent dye to visualize all present RNA (left), labeling the U3 snoRNA (green), 5'-ETS (orange dots), and high-molecular-weight pre-RNAs (i.e., 20S/21S/23S pre-rRNA) (green dots). The RNA was subsequently blotted on a nylon membrane for northern blot analysis and further hybridized with the probes c and d, which anneal to the 5'-ETS, as indicated in the schemes. Probe c displays all 5'-ETS molecules with intact 5' end, including smaller 3' truncated fragments (fragments ~ 130-150 nt long, labeled with orange dots), whereas probe d detects full-length 5'-ETS-A_1 and the ~ 90-nt-long A_0-A_1 fragment (labeled with a violet dot), retained only in the 8% polyacrylamide gel. As size reference an A_0-A_1 RNA molecule was *in vitro* transcribed with additional 17 nt and loaded on the gel (lane 14). Northern blot analysis was performed by Dr. Giuseppe La Venuta. Figure was taken from (Lau et al., 2021).

6. Appendix

6.1 List of Abbreviations

°C: degree Celsius

2D: two-dimensional

2µ: two-micron (high copy plasmid)

3D: three-dimensional

5-FOA: 5-fluoroorotic acid

Å: angstrom (10-10 m)

aa: amino acids

AF: assembly factor

Amp: ampicillin

ARS: autonomously replicating sequence

ATP: adenosine triphosphate

bp: basepairs

C-terminus: carboxy-terminus

C.t./Ct: Chaetomium thermophilum

CBP: calmodulin binding protein

cDNA: complementary DNA

CEN: 125bp centromeric DNA sequence

CP: central protuberance

CRAC: UV crosslinking and analysis of cDNA

CURI: CK2-Utp22-Rrp7-Ifh1 (complex)

DFC: dense fibrillar component (nucleolus)

DNA: deoxyribonucleic acid

DTT: dithiothreitol

EM: electron microscopy

ESs: expansion segments (rRNA)

ES6: expansion segment 6 (18S rRNA)

ETS: external transcribed spacer

FC: fibrillar center (nucleolus)

FTpA: Flag-TEV-ProteinA (tag)

GC: granular component (nucleolus)

GDP: guanosine diphosphate

GFP: green flourescent protein

GTP: guanosine triphosphate

HEAT: huntingtin, EF3, PP2A, TOR1 (motif)

His: histidine

iBAQ: intensity-based absolute quantification (mass spectrometry)

ITS: internal transcribed spacer

Kan: kanamycin

kDa: kilo-Dalton (10^3 Da)

KH: K-homology (domain)

LB: lysogeny broth (Escherichia coli medium)

Leu: leucine

LSU: large subunit (ribosome)

M: molar concentration (1 M = 1 mol/l)

MDa: mega-Dalton (10^6 Da)

mRNA: messenger RNA

MS: mass spectrometry

N-terminus: amino-terminus

NLS: nuclear localization sequence

nm: nanometer (10^{-9} m)

ns-EM: negative-stain EM

nt: nucleotides

ORF: open reading frame

ProtA: protein A

PCR: polymerase chain reaction

PDB: protein data bank

pGAL: galactose inducible promoter (yeast)

PIN: PilT N-terminus (domain)

Pol I: RNA polymerase I

PPI: protein-protein interaction

PTC: peptidyl transferase center

RecA: recombinase A-like

rDNA: ribosomal DNA/chromatin

RNA: ribonucleic acid

RNP: ribonucleoprotein particle

RPLs: ribosomal proteins of the large subunit

rpm: rounds per minute

R-proteins: ribosomal proteins

RPSs: ribosomal proteins of the small subunit

rRNA: ribosomal RNA

S: Svedberg unit (sedimentation rate)

S.c./Sc: Saccharomyces cerevisiae

SDC: synthetic yeast growth media (synthetic dextrose complete)

SDS-PAGE: sodium dodecyl sulfate polyacrylamide gel electrophoresis

Sec: second

snoRNA: small nucleolar RNA

SSU: small subunit(ribosome)

TAP: tandem-affinity purification

TAP-Flag: proteinA-TEV-CBP-Flag (tag)

TCA: trichloroacetic acid

TEV: tobacco etch virus (protease or cleavage site)

TORC1: target of rapamycin 1

tRNA: transfer RNA

Trp: tryptophan

Ura: uracil

Utp: U three protein

UV: ultraviolet

WD40: tryptophan-aspartic acid (W-D) motif

X-link: crosslink

xg: standard gravity (9.81 m/s2)

YPD: complete yeast growth media (yeast extract, peptone, dextrose)

YPG: complete yeast growth media (yeast extract, peptone, galactose)

6.2 List of Figures

6.3 Own Publications

(1) “Thermophile 90S Pre-ribosome Structures Reveal the Reverse Order of Co-transcriptional 18S rRNA Subdomain Integration” Jingdong Cheng*, Jochen Baßler*, Paulina Fischer*, Benjamin Lau, Nikola Kellner, Ruth Kunze, Sabine Griesel, Martina Kallas, Otto Berninghausen, Daniela Strauss, Roland Beckmann, Ed Hurt. Molecular Cell 2019. doi: 10.1016/j.molcel.2019.06.032. As author I retain the right to include the Figures in my thesis without explicit permission or license.

(2) “90 S pre-ribosome transformation into the primordial 40 S subunit” Benjamin Lau*, JIngdong Cheng*, Giuseppe La Venuta, Michael Ameismeier, Otto Berningshausen, Ed Hurt, Roland Beckmann. Science 2020. doi: 10.1126/science.abb4119 * Co-First Authorship. As author I retain the right to include the Figures in my thesis without explicit permission or license.

(3) “Structure of the maturing 90 S pre-ribosome in association with the RNA exosome.” Benjamin Lau*, Jingdong Cheng*, Dirk Flemming, Giuseppe La Venuta, Otto Berninghausen, Roland Beckmann, Ed Hurt. Molecular Cell 2021. doi: 10.1016/j.molcel.2020.11.009 * Co-First Authorship. As author I retain the right to include the Figures in my thesis without explicit permission or license.

7. References

Albert, B., Knight, B., Merwin, J., Martin, V., Ottoz, D., Gloor, Y., Bruzzone, M.J., Rudner, A., and Shore, D. (2016). A Molecular Titration System Coordinates Ribosomal Protein Gene Transcription with Ribosomal RNA Synthesis. Mol Cell *64*, 720-733.

Albert, B., Kos-Braun, I.C., Henras, A.K., Dez, C., Rueda, M.P., Zhang, X., Gadal, O., Kos, M., and Shore, D. (2019). A ribosome assembly stress response regulates transcription to maintain proteome homeostasis. eLife *8*.

Allmang, C., Petfalski, E., Podtelejnikov, A., Mann, M., Tollervey, D., and Mitchell, P. (1999). The yeast exosome and human PM-Scl are related complexes of 3' --> 5' exonucleases. Genes Dev *13*, 2148-2158.

Aloy, P., Ciccarelli, F.D., Leutwein, C., Gavin, A.C., Superti-Furga, G., Bork, P., Bottcher, B., and Russell, R.B. (2002). A complex prediction: three-dimensional model of the yeast exosome. EMBO Rep *3*, 628-635.

Ameismeier, M., Cheng, J., Berninghausen, O., and Beckmann, R. (2018). Visualizing late states of human 40S ribosomal subunit maturation. Nature *558*, 249-253.

Ameismeier, M., Zemp, I., van den Heuvel, J., Thoms, M., Berninghausen, O., Kutay, U., and Beckmann, R. (2020). Structural basis for the final steps of human 40S ribosome maturation. Nature *587*, 683-687.

An, W., Du, Y., and Ye, K. (2018). Structural and functional analysis of Utp24, an endonuclease for processing 18S ribosomal RNA. PloS one *13*, e0195723.

Axt, K., French, S.L., Beyer, A.L., and Tollervey, D. (2014). Kinetic analysis demonstrates a requirement for the Rat1 exonuclease in cotranscriptional pre-rRNA cleavage. PloS one *9*, e85703.

Bammert, L., Jonas, S., Ungricht, R., and Kutay, U. (2016). Human AATF/Che-1 forms a nucleolar protein complex with NGDN and NOL10 required for 40S ribosomal subunit synthesis. Nucleic Acids Res *44*, 9803-9820.

Barandun, J., Chaker-Margot, M., Hunziker, M., Molloy, K.R., Chait, B.T., and Klinge, S. (2017). The complete structure of the small-subunit processome. Nat Struct Mol Biol *24*, 944-953.

Barandun, J., Hunziker, M., and Klinge, S. (2018). Assembly and structure of the SSU processome - a nucleolar precursor of the small ribosomal subunit. Current Opinion in Structural Biology *49*, 85-93.

Barrio-Garcia, C., Thoms, M., Flemming, D., Kater, L., Berninghausen, O., Bassler, J., Beckmann, R., and Hurt, E. (2016). Architecture of the Rix1-Rea1 checkpoint machinery during pre-60S-ribosome remodeling. Nat Struct Mol Biol *23*, 37-44.

Bassler, J., Ahmed, Y.L., Kallas, M., Kornprobst, M., Calvino, F.R., Gnadig, M., Thoms, M., Stier, G., Ismail, S., Kharde, S*., et al.* (2017). Interaction network of the ribosome assembly machinery from a eukaryotic thermophile. Protein Sci *26*, 327-342.

Bassler, J., and Hurt, E. (2018). Eukaryotic Ribosome Assembly. Annu Rev Biochem.

Bassler, J., Kallas, M., Ulbrich, C., Thoms, M., Pertschy.B., and Hurt, E. (2010). The AAA-ATPase Rea1 drives removal of biogenesis factors during multiple stages of 60S ribosome assembly. Mol Cell *38*, 712-721.

Beltrame, M., Henry, Y., and Tollervey, D. (1994). Mutational analysis of an essential binding site for the U3 snoRNA in the 5' external transcribed spacer of yeast pre-rRNA. Nucleic Acids Res *22*, 5139-5147.

Beltrame, M., and Tollervey, D. (1992). Identification and functional analysis of two U3 binding sites on yeast pre-ribosomal RNA. EMBO J *11*, 1531-1542.

Ben-Shem, A., Jenner, L., Yusupova, G., and Yusupov, M. (2010). Crystal structure of the eukaryotic ribosome. Science *330*, 1203-1209.
Bernstein, K.A., Gallagher, J.E., Mitchell, B.M., Granneman, S., and Baserga, S.J. (2004). The small-subunit processome is a ribosome assembly intermediate. Eukaryot Cell *3*, 1619-1626.
Bleichert, F., Granneman, S., Osheim, Y.N., Beyer, A.L., and Baserga, S.J. (2006). The PINc domain protein Utp24, a putative nuclease, is required for the early cleavage steps in 18S rRNA maturation. Proc Natl Acad Sci U S A *103*, 9464-9469.
Boneberg, F.M., Brandmann, T., Kobel, L., van den Heuvel, J., Bargsten, K., Bammert, L., Kutay, U., and Jinek, M. (2019). Molecular mechanism of the RNA helicase DHX37 and its activation by UTP14A in ribosome biogenesis. RNA *25*, 685-701.
Boria, I., Garelli, E., Gazda, H.T., Aspesi, A., Quarello, P., Pavesi, E., Ferrante, D., Meerpohl, J.J., Kartal, M., Da Costa, L*., et al.* (2010). The ribosomal basis of Diamond-Blackfan Anemia: mutation and database update. Hum Mutat *31*, 1269-1279.
Bradatsch, B., Katahira, J., Kowalinski, E., Bange, G., Yao, W., Sekimoto, T., Baumgartel, V., Boese, G., Bassler, J., Wild, K*., et al.* (2007). Arx1 functions as an unorthodox nuclear export receptor for the 60S preribosomal subunit. Mol Cell *27*, 767-779.
Bradatsch, B., Leidig, C., Granneman, S., Gnadig, M., Tollervey, D., Bottcher, B., Beckmann, R., and Hurt, E. (2012). Structure of the pre-60S ribosomal subunit with nuclear export factor Arx1 bound at the exit tunnel. Nat Struct Mol Biol *19*, 1234-1241.
Braun, C.M., Hackert, P., Schmid, C.E., Bohnsack, M.T., Bohnsack, K.E., and Perez-Fernandez, J. (2020). Pol5 is required for recycling of small subunit biogenesis factors and for formation of the peptide exit tunnel of the large ribosomal subunit. Nucleic Acids Res *48*, 405-420.
Briggs, M.W., Burkard, K.T.D., and Butler, J.S. (1998). Rrp6p, the yeast homologue of the human PM-Scl 100-kDa autoantigen, is essential for efficient 5.8 S rRNA 3 ' end formation. Journal of Biological Chemistry *273*, 13255-13263.
Campbell, M.G., and Karbstein, K. (2011). Protein-protein interactions within late pre-40S ribosomes. PloS one *6*, e16194.
Cate, J.H., Yusupov, M.M., Yusupova, G.Z., Earnest, T.N., and Noller, H.F. (1999). X-ray crystal structures of 70S ribosome functional complexes. Science *285*, 2095-2104.
Chaker-Margot, M., Barandun, J., Hunziker, M., and Klinge, S. (2017). Architecture of the yeast small subunit processome. Science *355*.
Champion, E.A., Lane, B.H., Jackrel, M.E., Regan, L., and Baserga, S.J. (2008). A direct interaction between the Utp6 half-a-tetratricopeptide repeat domain and a specific peptide in Utp21 is essential for efficient pre-rRNA processing. Mol Cell Biol *28*, 6547-6556.
Charette, J.M., and Baserga, S.J. (2010). The DEAD-box RNA helicase-like Utp25 is an SSU processome component. RNA *16*, 2156-2169.
Chen, J., Zhang, L., and Ye, K. (2020). Functional regions in the 5' external transcribed spacer of yeast pre-rRNA. RNA *26*, 866-877.
Cheng, J., Bassler, J., Fischer, P., Lau, B., Kellner, N., Kunze, R., Griesel, S., Kallas, M., Berninghausen, O., Strauss, D*., et al.* (2019). Thermophile 90S Pre-ribosome Structures Reveal the Reverse Order of Co-transcriptional 18S rRNA Subdomain Integration. Mol Cell *75*, 1256-1269 e1257.
Cheng, J., Kellner, N., Berninghausen, O., Hurt, E., and Beckmann, R. (2017). 3.2-A-resolution structure of the 90S preribosome before A1 pre-rRNA cleavage. Nat Struct Mol Biol *24*, 954-964.
Cheutin, T., O'Donohue, M.F., Beorchia, A., Vandelaer, M., Kaplan, H., Defever, B., Ploton, D., and Thiry, M. (2002). Three-dimensional organization of active rRNA genes within the nucleolus. J Cell Sci *115*, 3297-3307.

Chlebowski, A., Lubas, M., Jensen, T.H., and Dziembowski, A. (2013). RNA decay machines: the exosome. Biochim Biophys Acta *1829*, 552-560.
Choudhury, P., Hackert, P., Memet, I., Sloan, K.E., and Bohnsack, M.T. (2019). The human RNA helicase DHX37 is required for release of the U3 snoRNP from pre-ribosomal particles. RNA biology *16*, 54-68.
Colley, A., Beggs, J.D., Tollervey, D., and Lafontaine, D.L. (2000). Dhr1p, a putative DEAH-box RNA helicase, is associated with the box C+D snoRNP U3. Mol Cell Biol *20*, 7238-7246.
Conconi, A., Widmer, R.M., Koller, T., and Sogo, J.M. (1989). Two Different Chromatin Structures Coexist in Ribosomal RNA Genes throughout the Cell Cycle. Cell *57*, 753-761.
Correll, C.C., Bartek, J., and Dundr, M. (2019). The Nucleolus: A Multiphase Condensate Balancing Ribosome Synthesis and Translational Capacity in Health, Aging and Ribosomopathies. Cells *8*.
Dammann, R., Lucchini, R., Koller, T., and Sogo, J.M. (1993). Chromatin structures and transcription of rDNA in yeast Saccharomyces cerevisiae. Nucleic Acids Res *21*, 2331-2338.
de la Cruz, J., Karbstein, K., and Woolford, J.L., Jr. (2015). Functions of ribosomal proteins in assembly of eukaryotic ribosomes in vivo. Annu Rev Biochem *84*, 93-129.
Decatur, W.A., Liang, X.H., Piekna-Przybylska, D., and Fournier, M.J. (2007). Identifying effects of snoRNA-guided modifications on the synthesis and function of the yeast ribosome. Method Enzymol *425*, 283-+.
Delan-Forino, C., Spanos, C., Rappsilber, J., and Tollervey, D. (2020). Substrate specificity of the TRAMP nuclear surveillance complexes. Nature communications *11*, 3122.
Dennis, P.P., Ehrenberg, M., and Bremer, H. (2004). Control of rRNA synthesis in Escherichia coli: a systems biology approach. Microbiol Mol Biol Rev *68*, 639-668.
Dragon, F., Gallagher, J.E., Compagnone-Post, P.A., Mitchell, B.M., Porwancher, K.A., Wehner, K.A., Wormsley, S., Settlage, R.E., Shabanowitz, J., Osheim, Y.*, et al.* (2002). A large nucleolar U3 ribonucleoprotein required for 18S ribosomal RNA biogenesis. Nature *417*, 967-970.
Du, Y., An, W., Zhu, X., Sun, Q., Qi, J., and Ye, K. (2020). Cryo-EM structure of 90S small ribosomal subunit precursors in transition states. Science *369*, 1477-1481.
Dunbar, D.A., Wormsley, S., Agentis, T.M., and Baserga, S.J. (1997). Mpp10p, a U3 small nucleolar ribonucleoprotein component required for pre-18S rRNA processing in yeast. MolCellBiol *17*, 5803-5812.
Dziembowski, A., Lorentzen, E., Conti, E., and Seraphin, B. (2007). A single subunit, Dis3, is essentially responsible for yeast exosome core activity. Nat Struct Mol Biol *14*, 15-22.
Emery, B., De la Cruz, J., Rocak, S., Deloche, O., and Linder, P. (2004). Has1p, a member of the DEAD-box family, is required for 40S ribosomal subunit biogenesis in Saccharomyces cerevisiae. Mol Microbiol *52*, 141-158.
Faber, A.W., Van Dijk, M., Raue, H.A., and Vos, J.C. (2002). Ng12p is a Ccr4p-like RNA nuclease essential for the final step in 3'-end processing of 5.8S rRNA in Saccharomyces cerevisiae. Rna *8*, 1095-1101.
Falk, S., Tants, J.N., Basquin, J., Thoms, M., Hurt, E., Sattler, M., and Conti, E. (2017). Structural insights into the interaction of the nuclear exosome helicase Mtr4 with the preribosomal protein Nop53. RNA *23*, 1780-1787.
Fatica, A., Oeffinger, M., Dlakic, M., and Tollervey, D. (2003). Nob1p is required for cleavage of the 3' end of 18S rRNA. Mol Cell Biol *23*, 1798-1807.
Fatica, A., Tollervey, D., and Dlakic, M. (2004). PIN domain of Nob1p is required for D-site cleavage in 20S pre-rRNA. Rna *10*, 1698-1701.

Fischer, U., Schauble, N., Schutz, S., Altvater, M., Chang, Y., Faza, M.B., and Panse, V.G. (2015). A non-canonical mechanism for Crm1-export cargo complex assembly. eLife *4*.
Fromm, L., Falk, S., Flemming, D., Schuller, J.M., Thoms, M., Conti, E., and Hurt, E. (2017). Reconstitution of the complete pathway of ITS2 processing at the pre-ribosome. Nature communications *8*, 1787.
Fromont-Racine, M., Senger, B., Saveanu, C., and Fasiolo, F. (2003). Ribosome assembly in eukaryotes. Gene *313*, 17-42.
Gallagher, J.E., Dunbar, D.A., Granneman, S., Mitchell, B.M., Osheim, Y., Beyer, A.L., and Baserga, S.J. (2004). RNA polymerase I transcription and pre-rRNA processing are linked by specific SSU processome components. Genes Dev *18*, 2506-2517.
Gamalinda, M., Ohmayer, U., Jakovljevic, J., Kumcuoglu, B., Woolford, J., Mbom, B., Lin, L., and Woolford, J.L., Jr. (2014). A hierarchical model for assembly of eukaryotic 60S ribosomal subunit domains. Genes Dev *28*, 198-210.
Gasse, L., Flemming, D., and Hurt, E. (2015). Coordinated Ribosomal ITS2 RNA Processing by the Las1 Complex Integrating Endonuclease, Polynucleotide Kinase, and Exonuclease Activities. Mol Cell *60*, 808-815.
Gelperin, D., Horton, L., Beckman, J., Hensold, J., and Lemmon, S.K. (2001). Bms1p, a novel GTP-binding protein, and the related Tsr1p are required for distinct steps of 40S ribosome biogenesis in yeast. RNA *7*, 1268-1283.
Ghalei, H., Schaub, F.X., Doherty, J.R., Noguchi, Y., Roush, W.R., Cleveland, J.L., Stroupe, M.E., and Karbstein, K. (2015). Hrr25/CK1delta-directed release of Ltv1 from pre-40S ribosomes is necessary for ribosome assembly and cell growth. J Cell Biol *208*, 745-759.
Gonzales-Zubiate, F.A., Okuda, E.K., Da Cunha, J.P.C., and Oliveira, C.C. (2017). Identification of karyopherins involved in the nuclear import of RNA exosome subunit Rrp6 in Saccharomyces cerevisiae. J Biol Chem *292*, 12267-12284.
Grandi, P., Rybin, V., Bassler, J., Petfalski, E., Strauss, D., Marzioch, M., Schäfer, T., Kuster, B., Tschochner, H., Tollervey, D*., et al.* (2002). 90S pre-ribosomes include the 35S pre-rRNA, the U3 snoRNP, and 40S subunit processing factors but predominantly lack 60S synthesis factors. Mol Cell *10*, 105-115.
Granneman, S., and Baserga, S.J. (2004). Ribosome biogenesis: of knobs and RNA processing. Exp Cell Res *296*, 43-50.
Granneman, S., and Baserga, S.J. (2005). Crosstalk in gene expression: coupling and co-regulation of rDNA transcription, pre-ribosome assembly and pre-rRNA processing. Curr Opin Cell Biol *17*, 281-286.
Granneman, S., Gallagher, J.E., Vogelzangs, J., Horstman, W., van Venrooij, W.J., Baserga, S.J., and Pruijn, G.J. (2003). The human Imp3 and Imp4 proteins form a ternary complex with hMpp10, which only interacts with the U3 snoRNA in 60-80S ribonucleoprotein complexes. Nucleic acids research *31*, 1877-1887.
Granneman, S., Kudla, G., Petfalski, E., and Tollervey, D. (2009). Identification of protein binding sites on U3 snoRNA and pre-rRNA by UV cross-linking and high-throughput analysis of cDNAs. Proc Natl Acad Sci U S A *106*, 9613-9618.
Granneman, S., Nandineni, M.R., and Baserga, S.J. (2005). The putative NTPase Fap7 mediates cytoplasmic 20S pre-rRNA processing through a direct interaction with Rps14. Mol Cell Biol *25*, 10352-10364.
Granneman, S., Petfalski, E., Swiatkowska, A., and Tollervey, D. (2010). Cracking pre-40S ribosomal subunit structure by systematic analyses of RNA-protein cross-linking. EMBO J.

Granneman, S., Petfalski, E., and Tollervey, D. (2011). A cluster of ribosome synthesis factors regulate pre-rRNA folding and 5.8S rRNA maturation by the Rat1 exonuclease. The EMBO journal *30*, 4006-4019.
Halbach, F., Reichelt, P., Rode, M., and Conti, E. (2013). The yeast ski complex: crystal structure and RNA channeling to the exosome complex. Cell *154*, 814-826.
Harnpicharnchai, P., Jakovljevic, J., Horsey, E., Miles, T., Roman, J., Rout, M., Meagher, D., Imai, B., Guo, Y., Brame, C.J*., et al.* (2001). Composition and functional characterization of yeast 66s ribosome assembly intermediates. Mol Cell *8*, 505-515.
Hedges, J., West, M., and Johnson, A.W. (2005). Release of the export adapter, Nmd3p, from the 60S ribosomal subunit requires Rpl10p and the cytoplasmic GTPase Lsg1p. Embo J *24*, 567-579.
Henras, A.K., Bertrand, E., and Chanfreau, G. (2004). A cotranscriptional model for 3 '-end processing of the Saccharomyces cerevisiae pre-ribosomal RNA precursor. Rna *10*, 1572-1585.
Henras, A.K., Plisson-Chastang, C., O'Donohue, M.F., Chakraborty, A., and Gleizes, P.E. (2015). An overview of pre-ribosomal RNA processing in eukaryotes. Wiley interdisciplinary reviews RNA *6*, 225-242.
Henry, Y., Wood, H., Morrissey, J.P., Petfalski, E., Kearsey, S., and Tollervey, D. (1994). The 5' end of yeast 5.8S rRNA is generated by exonucleases from an upstream cleavage site. EMBO J *13*, 2452-2463.
Heuer, A., Thomson, E., Schmidt, C., Berninghausen, O., Becker, T., Hurt, E., and Beckmann, R. (2017). Cryo-EM structure of a late pre-40S ribosomal subunit from Saccharomyces cerevisiae. eLife *6*.
Ho, J.H.N., Kallstrom, G., and Johnson, A.W. (2000). Nmd3p is a Crm1p-dependent adapter protein for nuclear export of the large ribosomal subunit. JCell Biol *151*, 1057-1066.
Hodnett, J.L., and Busch, H. (1968). Isolation and characterization of uridylic acid-rich 7 S ribonucleic acid of rat liver nuclei. J Biol Chem *243*, 6334-6342.
Horn, D.M., Mason, S.L., and Karbstein, K. (2011). Rcl1 protein, a novel nuclease for 18 S ribosomal RNA production. J Biol Chem *286*, 34082-34087.
Houseley, J., LaCava, J., and Tollervey, D. (2006). RNA-quality control by the exosome. Nat Rev Mol Cell Biol *7*, 529-539.
Houseley, J., and Tollervey, D. (2008). The nuclear RNA surveillance machinery: the link between ncRNAs and genome structure in budding yeast? Biochim Biophys Acta *1779*, 239-246.
Hughes, J.M., and Ares, M., Jr. (1991). Depletion of U3 small nucleolar RNA inhibits cleavage in the 5' external transcribed spacer of yeast pre-ribosomal RNA and impairs formation of 18S ribosomal RNA. EMBO J *10*, 4231-4239.
Hughes, J.M.X. (1996). Functional base-pairing interaction between highly conserved elements of U3 small nucleolar RNA and the small ribosomal subunit RNA. Journal of Molecular Biology *259*, 645-654.
Hung, N.J., and Johnson, A.W. (2006). Nuclear recycling of the pre-60S ribosomal subunit-associated factor Arx1 depends on Rei1 in Saccharomyces cerevisiae. Mol Cell Biol *26*, 3718-3727.
Hunziker, M., Barandun, J., Petfalski, E., Tan, D., Delan-Forino, C., Molloy, K.R., Kim, K.H., Dunn-Davies, H., Shi, Y., Chaker-Margot, M*., et al.* (2016). UtpA and UtpB chaperone nascent pre-ribosomal RNA and U3 snoRNA to initiate eukaryotic ribosome assembly. Nature communications *7*, 12090.

Inoue, H., Nojima, H., and Okayama, H. (1990). High-Efficiency Transformation of Escherichia-Coli with Plasmids. Gene *96*, 23-28.
Jenner, L., Melnikov, S., Garreau de Loubresse, N., Ben-Shem, A., Iskakova, M., Urzhumtsev, A., Meskauskas, A., Dinman, J., Yusupova, G., and Yusupov, M. (2012). Crystal structure of the 80S yeast ribosome. Curr Opin Struct Biol *22*, 759-767.
Johnson, M.C., Ghalei, H., Doxtader, K.A., Karbstein, K., and Stroupe, M.E. (2017). Structural Heterogeneity in Pre-40S Ribosomes. Structure *25*, 329-340.
Johnson, S.J., and Jackson, R.N. (2013). Ski2-like RNA helicase structures: common themes and complex assemblies. RNA biology *10*, 33-43.
Kappel, L., Loibl, M., Zisser, G., Klein, I., Fruhmann, G., Gruber, C., Unterweger, S., Rechberger, G., Pertschy, B., and Bergler, H. (2012). Rlp24 activates the AAA-ATPase Drg1 to initiate cytoplasmic pre-60S maturation. J Cell Biol *199*, 771-782.
Karbstein, K. (2011). Inside the 40S ribosome assembly machinery. Curr Opin Chem Biol *15*, 657-663.
Karbstein, K., and Doudna, J.A. (2006). GTP-dependent formation of a ribonucleoprotein subcomplex required for ribosome biogenesis. J Mol Biol *356*, 432-443.
Karbstein, K., Jonas, S., and Doudna, J.A. (2005). An essential GTPase promotes assembly of preribosomal RNA processing complexes. Mol Cell *20*, 633-643.
Kater, L., Thoms, M., Barrio-Garcia, C., Cheng, J., Ismail, S., Ahmed, Y.L., Bange, G., Kressler, D., Berninghausen, O., Sinning, I.*, et al.* (2017). Visualizing the Assembly Pathway of Nucleolar Pre-60S Ribosomes. Cell *171*, 1599-1610 e1514.
Khatter, H., Myasnikov, A.G., Natchiar, S.K., and Klaholz, B.P. (2015). Structure of the human 80S ribosome. Nature *520*, 640-645.
Klinge, S., Voigts-Hoffmann, F., Leibundgut, M., and Ban, N. (2012). Atomic structures of the eukaryotic ribosome. Trends Biochem Sci *37*, 189-198.
Klinge, S., and Woolford, J.L., Jr. (2018). Ribosome assembly coming into focus. Nat Rev Mol Cell Biol.
Klinge, S., and Woolford, J.L., Jr. (2019). Ribosome assembly coming into focus. Nat Rev Mol Cell Biol *20*, 116-131.
Kobylecki, K., Drazkowska, K., Kulinski, T.M., Dziembowski, A., and Tomecki, R. (2018). Elimination of 01/A'-A0 pre-rRNA processing by-product in human cells involves cooperative action of two nuclear exosome-associated nucleases: RRP6 and DIS3. RNA *24*, 1677-1692.
Kornprobst, M., Turk, M., Kellner, N., Cheng, J., Flemming, D., Kos-Braun, I., Kos, M., Thoms, M., Berninghausen, O., Beckmann, R.*, et al.* (2016). Architecture of the 90S Pre-ribosome: A Structural View on the Birth of the Eukaryotic Ribosome. Cell *166*, 380-393.
Kos, M., and Tollervey, D. (2010). Yeast pre-rRNA processing and modification occur cotranscriptionally. Mol Cell *37*, 809-820.
Kos-Braun, I.C., and Kos, M. (2017). Post-transcriptional regulation of ribosome biogenesis in yeast. Microb Cell *4*, 179-181.
Kressler, D., Hurt, E., and Baßler, J. (2010). Driving ribosome assembly. Biochim Biophys Acta *1803*, 673-683.
Kressler, D., Roser, D., Pertschy, B., and Hurt, E. (2008). The AAA ATPase Rix7 powers progression of ribosome biogenesis by stripping Nsa1 from pre-60S particles. J Cell Biol *181*, 935-944.
Krogan, N.J., Peng, W.T., Cagney, G., Robinson, M.D., Haw, R., Zhong, G., Guo, X., Zhang, X., Canadien, V., Richards, D.P.*, et al.* (2004). High-definition macromolecular composition of yeast RNA-processing complexes. Mol Cell *13*, 225-239.

Kufel, J., Dichtl, B., and Tollervey, D. (1999). Yeast Rnt1p is required for cleavage of the pre-ribosomal RNA in the 3' ETS but not the 5' ETS. RNA *5*, 909-917.
Kumar, A., and Warner, J.R. (1972). Characterization of ribosomal precursor particles from HeLa cell nucleoli. J Mol Biol *63*, 233-246.
Laferte, A., Favry, E., Sentenac, A., Riva, M., Carles, C., and Chedin, S. (2006). The transcriptional activity of RNA polymerase I is a key determinant for the level of all ribosome components. Genes Dev *20*, 2030-2040.
Lamanna, A.C., and Karbstein, K. (2009). Nob1 binds the single-stranded cleavage site D at the 3'-end of 18S rRNA with its PIN domain. Proc Natl Acad Sci U S A *106*, 14259-14264.
Larrieu, D., Vire, E., Robson, S., Breusegem, S.Y., Kouzarides, T., and Jackson, S.P. (2018). Inhibition of the acetyltransferase NAT10 normalizes progeric and aging cells by rebalancing the Transportin-1 nuclear import pathway. Sci Signal *11*.
Lebaron, S., Schneider, C., van Nues, R.W., Swiatkowska, A., Walsh, D., Bottcher, B., Granneman, S., Watkins, N.J., and Tollervey, D. (2012). Proofreading of pre-40S ribosome maturation by a translation initiation factor and 60S subunits. Nature structural & molecular biology *19*, 744-753.
Lebaron, S., Segerstolpe, A., French, S.L., Dudnakova, T., de Lima Alves, F., Granneman, S., Rappsilber, J., Beyer, A.L., Wieslander, L., and Tollervey, D. (2013). Rrp5 binding at multiple sites coordinates pre-rRNA processing and assembly. Mol Cell *52*, 707-719.
Lecompte, O., Ripp, R., Thierry, J.C., Moras, D., and Poch, O. (2002). Comparative analysis of ribosomal proteins in complete genomes: an example of reductive evolution at the domain scale. Nucleic Acids Research *30*, 5382-5390.
Lee, S.J., and Baserga, S.J. (1999). Imp3p and Imp4p, two specific components of the U3 small nucleolar ribonucleoprotein that are essential for pre-18S rRNA processing. Molecular and cellular biology *19*, 5441-5452.
Lee, Y., and Nazar, R.N. (1997). Ribosomal 5 S rRNA maturation in Saccharomyces cerevisiae. J Biol Chem *272*, 15206-15212.
Lin, J., Lu, J., Feng, Y., Sun, M., and Ye, K. (2013). An RNA-binding complex involved in ribosome biogenesis contains a protein with homology to tRNA CCA-adding enzyme. PLoS Biol *11*, e1001669.
Lingaraju, M., Johnsen, D., Schlundt, A., Langer, L.M., Basquin, J., Sattler, M., Heick Jensen, T., Falk, S., and Conti, E. (2019). The MTR4 helicase recruits nuclear adaptors of the human RNA exosome using distinct arch-interacting motifs. Nature communications *10*, 3393.
Lygerou, Z., Allmang, C., Tollervey, D., and Seraphin, B. (1996). Accurate processing of a eukaryotic precursor ribosomal RNA by ribonuclease MRP in vitro. Science *272*, 268-270.
Ma, C., Wu, S., Li, N., Chen, Y., Yan, K., Li, Z., Zheng, L., Lei, J., Woolford, J.L., Jr., and Gao, N. (2017). Structural snapshot of cytoplasmic pre-60S ribosomal particles bound by Nmd3, Lsg1, Tif6 and Reh1. Nat Struct Mol Biol *24*, 214-220.
Makino, D.L., Baumgartner, M., and Conti, E. (2013). Crystal structure of an RNA-bound 11-subunit eukaryotic exosome complex. Nature *495*, 70-75.
Makino, D.L., Schuch, B., Stegmann, E., Baumgartner, M., Basquin, C., and Conti, E. (2015). RNA degradation paths in a 12-subunit nuclear exosome complex. Nature *524*, 54-58.
Malyutin, A.G., Musalgaonkar, S., Patchett, S., Frank, J., and Johnson, A.W. (2017). Nmd3 is a structural mimic of eIF5A, and activates the cpGTPase Lsg1 during 60S ribosome biogenesis. EMBO J *36*, 854-868.
Matsuo, Y., Granneman, S., Thoms, M., Manikas, R.G., Tollervey, D., and Hurt, E. (2014). Coupled GTPase and remodelling ATPase activities form a checkpoint for ribosome export. Nature *505*, 112-116.

McCaughan, U.M., Jayachandran, U., Shchepachev, V., Chen, Z.A., Rappsilber, J., Tollervey, D., and Cook, A.G. (2016). Pre-40S ribosome biogenesis factor Tsr1 is an inactive structural mimic of translational GTPases. Nature communications *7*, 11789.
Melnikov, S., Ben-Shem, A., Garreau de Loubresse, N., Jenner, L., Yusupova, G., and Yusupov, M. (2012). One core, two shells: bacterial and eukaryotic ribosomes. Nat Struct Mol Biol *19*, 560-567.
Meskauskas, A., Baxter, J.L., Carr, E.A., Yasenchak, J., Gallagher, J.E., Baserga, S.J., and Dinman, J.D. (2003). Delayed rRNA processing results in significant ribosome biogenesis and functional defects. Mol Cell Biol *23*, 1602-1613.
Miles, T.D., Jakovljevic, J., Horsey, E.W., Harnpicharnchai, P., Tang, L., and Woolford, J.L., Jr. (2005). Ytm1, Nop7, and Erb1 form a complex necessary for maturation of yeast 66S preribosomes. Mol Cell Biol *25*, 10419-10432.
Milkereit, P., Gadal, O., Podtelejnikov, A., Trumtel, S., Gas, N., Petfalski, E., Tollervey, D., Mann, M., Hurt, E., and Tschochner, H. (2001). Maturation of Pre-Ribosomes Requires Noc-Proteins and is Coupled to Transport from the Nucleolus to the Nucleoplasm. Cell *105*, 499-509.
Miller, O.L., and Beatty, B.R. (1969). Visualization of nucleolar genes. Science *164*, 955-957.
Mitchell, P., Petfalski, E., Shevchenko, A., Mann, M., and Tollervey, D. (1997). The exosome: A conserved eukaryotic RNA processing complex containing multiple 3'-->5' exoribonucleases. Cell *91*, 457-466.
Mitchell, P., Petfalski, E., and Tollervey, D. (1996). The 3' end of yeast 5.8S rRNA is generated by an exonuclease processing mechanism. Genes Dev *10*, 502-513.
Moriggi, G., Nieto, B., and Dosil, M. (2014). Rrp12 and the Exportin Crm1 participate in late assembly events in the nucleolus during 40S ribosomal subunit biogenesis. PLoS genetics *10*, e1004836.
Morton, D.J., Kuiper, E.G., Jones, S.K., Leung, S.W., Corbett, A.H., and Fasken, M.B. (2018). The RNA exosome and RNA exosome-linked disease. RNA *24*, 127-142.
Moss, T., Langlois, F., Gagnon-Kugler, T., and Stefanovsky, V. (2007). A housekeeper with power of attorney: the rRNA genes in ribosome biogenesis. Cell Mol Life Sci *64*, 29-49.
Mougey, E.B., O'Reilly, M., Osheim, Y., Miller, O.L.J., Beyer, A., and Sollner-Webb, B. (1993). The terminal balls characteristic of eukaryotic rRNA transcription units in chromatin spreads are rRNA processing complexes. Genes Dev *7*, 1609-1619.
Nerurkar, P., Altvater, M., Gerhardy, S., Schutz, S., Fischer, U., Weirich, C., and Panse, V.G. (2015). Eukaryotic Ribosome Assembly and Nuclear Export. Int Rev Cell Mol Biol *319*, 107-140.
Nissan, T.A., Bassler, J., Petfalski, E., Tollervey, D., and Hurt, E.C. (2002). 60S pre-ribosome formation viewed from assembly in the nucleolus until export to the cytoplasm. EMBO J *21*, 5539-5547.
Oeffinger, M., Zenklusen, D., Ferguson, A., Wei, K.E., El Hage, A., Tollervey, D., Chait, B.T., Singer, R.H., and Rout, M.P. (2009). Rrp17p is a eukaryotic exonuclease required for 5' end processing of Pre-60S ribosomal RNA. Mol Cell *36*, 768-781.
Osheim, Y.N., French, S.L., Keck, K.M., Champion, E.A., Spasov, K., Dragon, F., Baserga, S.J., and Beyer, A.L. (2004). Pre-18S ribosomal RNA is structurally compacted into the SSU processome prior to being cleaved from nascent transcripts in Saccharomyces cerevisiae. Mol Cell *16*, 943-954.
Palade, G.E. (1955). A small particulate component of the cytoplasm. J Biophys Biochem Cytol *1*, 59-68.

Parker, M.D., Collins, J.C., Korona, B., Ghalei, H., and Karbstein, K. (2019). A kinase-dependent checkpoint prevents escape of immature ribosomes into the translating pool. PLoS Biol *17*, e3000329.
Perez-Fernandez, J., Martin-Marcos, P., and Dosil, M. (2011). Elucidation of the assembly events required for the recruitment of Utp20, Imp4 and Bms1 onto nascent pre-ribosomes. Nucleic Acids Res *39*, 8105-8121.
Perez-Fernandez, J., Roman, A., De Las Rivas, J., Bustelo, X.R., and Dosil, M. (2007). The 90S preribosome is a multimodular structure that is assembled through a hierarchical mechanism. Mol Cell Biol *27*, 5414-5429.
Pertschy, B., Saveanu, C., Zisser, G., Lebreton, A., Tengg, M., Jacquier, A., Liebminger, E., Nobis, B., Kappel, L., van der Klei, I.*, et al.* (2007). Cytoplasmic recycling of 60S preribosomal factors depends on the AAA protein Drg1. Mol Cell Biol *27*, 6581-6592.
Phipps, K.R., Charette, J., and Baserga, S.J. (2011). The small subunit processome in ribosome biogenesis-progress and prospects. Wiley interdisciplinary reviews RNA *2*, 1-21.
Pillon, M.C., Sobhany, M., Borgnia, M.J., Williams, J.G., and Stanley, R.E. (2017). Grc3 programs the essential endoribonuclease Las1 for specific RNA cleavage. Proc Natl Acad Sci U S A *114*, E5530-E5538.
Pöll, G., Li, S., Ohmayer, U., Hierlmeier, T., Milkereit, P., and Perez-Fernandez, J. (2014). In vitro reconstitution of yeast tUTP/UTP A and UTP B subcomplexes provides new insights into their modular architecture. PloS one *9*, e114898.
Preti, M., O'Donohue, M.F., Montel-Lehry, N., Bortolin-Cavaille, M.L., Choesmel, V., and Gleizes, P.E. (2013). Gradual processing of the ITS1 from the nucleolus to the cytoplasm during synthesis of the human 18S rRNA. Nucleic Acids Research *41*, 4709-4723.
Raska, I., Shaw, P.J., and Cmarko, D. (2006). New insights into nucleolar architecture and activity. Int Rev Cytol *255*, 177-235.
Reis, F.P., Pobre, V., Silva, I.J., Malecki, M., and Arraiano, C.M. (2013). The RNase II/RNB family of exoribonucleases: putting the 'Dis' in disease. Wiley interdisciplinary reviews RNA *4*, 607-615.
Rudra, D., Mallick, J., Zhao, Y., and Warner, J.R. (2007). Potential interface between ribosomal protein production and pre-rRNA processing. Mol Cell Biol *27*, 4815-4824.
Rudra, D., Zhao, Y., and Warner, J.R. (2005). Central role of Ifh1p-Fhl1p interaction in the synthesis of yeast ribosomal proteins. EMBO J *24*, 533-542.
Sa-Moura, B., Kornprobst, M., Kharde, S., Ahmed, Y.L., Stier, G., Kunze, R., Sinning, I., and Hurt, E. (2017). Mpp10 represents a platform for the interaction of multiple factors within the 90S pre-ribosome. PloS one *12*, e0183272.
Sardana, R., Liu, X., Granneman, S., Zhu, J., Gill, M., Papoulas, O., Marcotte, E.M., Tollervey, D., Correll, C.C., and Johnson, A.W. (2015). The DEAH-box helicase Dhr1 dissociates U3 from the pre-rRNA to promote formation of the central pseudoknot. PLoS Biol *13*, e1002083.
Schäfer, T., Maco, B., Petfalski, E., Tollervey, D., Bottcher, B., Aebi, U., and Hurt, E. (2006). Hrr25-dependent phosphorylation state regulates organization of the pre-40S subunit. Nature *441*, 651-655.
Schafer, T., Strauss, D., Petfalski, E., Tollervey, D., and Hurt, E. (2003). The path from nucleolar 90S to cytoplasmic 40S pre-ribosomes. EMBO J *22*, 1370-1380.
Schäfer, T., Strauss, D., Petfalski, E., Tollervey, D., and Hurt, E.C. (2003). The path from nucleolar 90S to cytoplasmic 40S pre-ribosomes. EMBO J *22*, 1370-1380.
Schillewaert, S., Wacheul, L., Lhomme, F., and Lafontaine, D.L. (2012). The evolutionarily conserved protein Las1 is required for pre-rRNA processing at both ends of ITS2. Mol Cell Biol *32*, 430-444.

Schmeing, T.M., and Ramakrishnan, V. (2009). What recent ribosome structures have revealed about the mechanism of translation. Nature *461*, 1234-1242.
Schmitt, M.E., and Clayton, D.A. (1993). Nuclear RNase MRP is required for correct processing of pre-5.8S rRNA in Saccharomyces cerevisiae. MolCellBiol *13*, 7935-7941.
Schneider, D.A., Michel, A., Sikes, M.L., Vu, L., Dodd, J.A., Salgia, S., Osheim, Y.N., Beyer, A.L., and Nomura, M. (2007). Transcription elongation by RNA polymerase I is linked to efficient rRNA processing and ribosome assembly. Mol Cell *26*, 217-229.
Schuller, J.M., Falk, S., Fromm, L., Hurt, E., and Conti, E. (2018). Structure of the nuclear exosome captured on a maturing preribosome. Science *360*, 219-222.
Schuwirth, B.S., Borovinskaya, M.A., Hau, C.W., Zhang, W., Vila-Sanjurjo, A., Holton, J.M., and Cate, J.H. (2005). Structures of the bacterial ribosome at 3.5 A resolution. Science *310*, 827-834.
Shah, B.N., Liu, X., and Correll, C.C. (2013). Imp3 unfolds stem structures in pre-rRNA and U3 snoRNA to form a duplex essential for small subunit processing. RNA *19*, 1372-1383.
Sharma, K., and Tollervey, D. (1999). Base pairing between U3 small nucleolar RNA and the 5' end of 18S rRNA is required for pre-rRNA processing. Mol Cell Biol *19*, 6012-6019.
Sleiman, S., and Dragon, F. (2019). Recent Advances on the Structure and Function of RNA Acetyltransferase Kre33/NAT10. Cells *8*.
Sloan, K.E., Mattijssen, S., Lebaron, S., Tollervey, D., Pruijn, G.J., and Watkins, N.J. (2013). Both endonucleolytic and exonucleolytic cleavage mediate ITS1 removal during human ribosomal RNA processing. J Cell Biol *200*, 577-588.
Strunk, B., Loucks, C., Su, M., Vashisth, H., Cheng, S., Schilling, J., Brooks, C., Karbstein, K., and Skiniotis, G. (2011). Ribosome assembly factors prevent premature translation initiation by 40S assembly intermediates. Science *333*, 1449-1502.
Strunk, B.S., Novak, M.N., Young, C.L., and Karbstein, K. (2012). A Translation-Like Cycle Is a Quality Control Checkpoint for Maturing 40S Ribosome Subunits. Cell *150*, 111-121.
Sturm, M., Cheng, J., Bassler, J., Beckmann, R., and Hurt, E. (2017). Interdependent action of KH domain proteins Krr1 and Dim2 drive the 40S platform assembly. Nature communications *8*, 2213.
Sun, Q., Zhu, X., Qi, J., An, W., Lan, P., Tan, D., Chen, R., Wang, B., Zheng, S., Zhang, C*., et al.* (2017). Molecular architecture of the 90S small subunit pre-ribosome. eLife *6*.
Talkish, J., Biedka, S., Jakovljevic, J., Zhang, J., Tang, L., Strahler, J.R., Andrews, P.C., Maddock, J.R., and Woolford, J.L., Jr. (2016). Disruption of ribosome assembly in yeast blocks cotranscriptional pre-rRNA processing and affects the global hierarchy of ribosome biogenesis. RNA *22*, 852-866.
Tamaoki, T. (1966). The particulate fraction containing 45 s RNA in L cell nuclei. J Mol Biol *15*, 624-639.
Tang, L., Sahasranaman, A., Jakovljevic, J., Schleifman, E., and Woolford, J.L., Jr. (2008). Interactions among Ytm1, Erb1, and Nop7 required for assembly of the Nop7-subcomplex in yeast preribosomes. Mol Biol Cell *19*, 2844-2856.
Thiry, M., and Lafontaine, D.L. (2005). Birth of a nucleolus: the evolution of nucleolar compartments. Trends Cell Biol *15*, 194-199.
Thoms, M., Ahmed, Y.L., Maddi, K., Hurt, E., and Sinning, I. (2016). Concerted removal of the Erb1-Ytm1 complex in ribosome biogenesis relies on an elaborate interface. Nucleic Acids Res *44*, 926-939.
Thoms, M., Thomson, E., Bassler, J., Gnadig, M., Griesel, S., and Hurt, E. (2015). The Exosome Is Recruited to RNA Substrates through Specific Adaptor Proteins. Cell *162*, 1029-1038.

Thumati, N.R., Zeng, X.L., Au, H.H., Jang, C.J., Jan, E., and Wong, J.M. (2013). Severity of X-linked dyskeratosis congenita (DKCX) cellular defects is not directly related to dyskerin (DKC1) activity in ribosomal RNA biogenesis or mRNA translation. Hum Mutat *34*, 1698-1707.
Tomecki, R., Labno, A., Drazkowska, K., Cysewski, D., and Dziembowski, A. (2015). hUTP24 is essential for processing of the human rRNA precursor at site A1, but not at site A0. RNA biology *12*, 1010-1029.
Tomecki, R., Sikorski, P.J., and Zakrzewska-Placzek, M. (2017). Comparison of preribosomal RNA processing pathways in yeast, plant and human cells - focus on coordinated action of endo- and exoribonucleases. FEBS letters *591*, 1801-1850.
Toussaint, M., Levasseur, G., Tremblay, M., Paquette, M., and Conconi, A. (2005). Psoralen photocrosslinking, a tool to study the chromatin structure of RNA polymerase I--transcribed ribosomal genes. Biochem Cell Biol *83*, 449-459.
Trapman, J., Retèl, J., and Planta, R.J. (1975). Ribosomal precursor particles from yeast. ExpCell Res *90*, 95-104.
Tudek, A., Lloret-Llinares, M., and Jensen, T.H. (2018). The multitasking polyA tail: nuclear RNA maturation, degradation and export. Philos Trans R Soc Lond B Biol Sci *373*.
Turowski, T.W., Lebaron, S., Zhang, E., Peil, L., Dudnakova, T., Petfalski, E., Granneman, S., Rappsilber, J., and Tollervey, D. (2014). Rio1 mediates ATP-dependent final maturation of 40S ribosomal subunits. Nucleic Acids Res *42*, 12189-12199.
Turowski, T.W., and Tollervey, D. (2015). Cotranscriptional events in eukaryotic ribosome synthesis. Wiley interdisciplinary reviews RNA *6*, 129-139.
Udem, S.A., and Warner, J.R. (1972). Ribosomal RNA synthesis in Saccharomyces cerevisiae. J Mol Biol *65*, 227-242.
Ulbrich, C., Diepholz, M., Bassler, J., Kressler, D., Pertschy.B., K., G., Böttcher, B., and Hurt, E. (2009). Mechanochemical Removal of Ribosome Biogenesis Factors from Nascent 60S Ribosomal Subunit. Cell *138*, 911-922.
van Hoof, A., Lennertz, P., and Parker, R. (2000). Three conserved members of the RNase D family have unique and overlapping functions in the processing of 5S, 5.8S, U4, U5, RNase MRP and RNase P RNAs in yeast. Embo Journal *19*, 1357-1365.
van Nues, R.W., Venema, J., Rientjes, J.M., Dirks-Mulder, A., and Raue, H.A. (1995). Processing of eukaryotic pre-rRNA: the role of the transcribed spacers. Biochem Cell Biol *73*, 789-801.
Vanrobays, E., Gleizes, P.E., Bousquet-Antonelli, C., Noaillac-Depeyre, J., Caizergues-Ferrer, M., and Gelugne, J.P. (2001). Processing of 20S pre-rRNA to 18S ribosomal RNA in yeast requires Rrp10p, an essential non-ribosomal cytoplasmic protein. EMBO J *20*, 4204-4213.
Warner, J.R. (1999). The economics of ribosome biosynthesis in yeast. Trends BiochemSci *24*, 437-440.
Wasmuth, E.V., Zinder, J.C., Zattas, D., Das, M., and Lima, C.D. (2017). Structure and reconstitution of yeast Mpp6-nuclear exosome complexes reveals that Mpp6 stimulates RNA decay and recruits the Mtr4 helicase. eLife *6*.
Weick, E.M., Puno, M.R., Januszyk, K., Zinder, J.C., DiMattia, M.A., and Lima, C.D. (2018). Helicase-Dependent RNA Decay Illuminated by a Cryo-EM Structure of a Human Nuclear RNA Exosome-MTR4 Complex. Cell *173*, 1663-1677 e1621.
Weinberg, R.A., and Penman, S. (1968). Small molecular weight monodisperse nuclear RNA. J Mol Biol *38*, 289-304.
Wells, G.R., Weichmann, F., Colvin, D., Sloan, K.E., Kudla, G., Tollervey, D., Watkins, N.J., and Schneider, C. (2016a). The PIN domain endonuclease Utp24 cleaves pre-ribosomal RNA at two coupled sites in yeast and humans. Nucleic Acids Res *44*, 5399-5409.

Wells, G.R., Weichmann, F., Colvin, D., Sloan, K.E., Kudla, G., Tollervey, D., Watkins, N.J., and Schneider, C. (2016b). The PIN domain endonuclease Utp24 cleaves pre-ribosomal RNA at two coupled sites in yeast and humans. Nucleic Acids Res *44*, 9016.
Wilson, D.M., Li, Y., LaPeruta, A., Gamalinda, M., Gao, N., and Woolford, J.L., Jr. (2020). Structural insights into assembly of the ribosomal nascent polypeptide exit tunnel. Nature communications *11*, 5111.
Wojda, I., Cytrynska, M., Frajnt, M., and Jakubowicz, T. (2002). Protein kinases CKI and CKII are implicated in modification of ribosomal proteins of the yeast Trichosporon cutaneum. Acta Biochim Pol *49*, 947-957.
Woodson, S.A. (2008). RNA folding and ribosome assembly. Curr Opin Chem Biol *12*, 667-673.
Woodson, S.A. (2011). RNA folding pathways and the self-assembly of ribosomes. Acc Chem Res *44*, 1312-1319.
Woolford, J.L., Jr., and Baserga, S.J. (2013). Ribosome biogenesis in the yeast Saccharomyces cerevisiae. Genetics *195*, 643-681.
Wormsley, S., Samarsky, D.A., Fournier, M.J., and Baserga, S.J. (2001). An unexpected, conserved element of the U3 snoRNA is required for Mpp10p association. RNA *7*, 904-919.
Wu, S., Tan, D., Woolford, J.L., Jr., Dong, M.Q., and Gao, N. (2017). Atomic modeling of the ITS2 ribosome assembly subcomplex from cryo-EM together with mass spectrometry-identified protein-protein crosslinks. Protein Sci *26*, 103-112.
Wu, S., Tutuncuoglu, B., Yan, K., Brown, H., Zhang, Y., Tan, D., Gamalinda, M., Yuan, Y., Li, Z., Jakovljevic, J*., et al.* (2016). Diverse roles of assembly factors revealed by structures of late nuclear pre-60S ribosomes. Nature *534*, 133-137.
Yao, W., Roser, D., Kohler, A., Bradatsch, B., Bassler, J., and Hurt, E. (2007). Nuclear export of ribosomal 60S subunits by the general mRNA export receptor Mex67-Mtr2. Mol Cell *26*, 51-62.
Yoshihama, M., Uechi, T., Asakawa, S., Kawasaki, K., Kato, S., Higa, S., Maeda, N., Minoshima, S., Tanaka, T., Shimizu, N*., et al.* (2002). The human ribosomal protein genes: sequencing and comparative analysis of 73 genes. Genome Res *12*, 379-390.
Yusupova, G., and Yusupov, M. (2017). Crystal structure of eukaryotic ribosome and its complexes with inhibitors. Philos Trans R Soc Lond B Biol Sci *372*.
Zakrzewska-Placzek, M., Souret, F.F., Sobczyk, G.J., Green, P.J., and Kufel, J. (2010). Arabidopsis thaliana XRN2 is required for primary cleavage in the pre-ribosomal RNA. Nucleic Acids Research *38*, 4487-4502.
Zhang, J., Harnpicharnchai, P., Jakovljevic, J., Tang, L., Guo, Y., Oeffinger, M., Rout, M.P., Hiley, S.L., Hughes, T., and Woolford, J.L., Jr. (2007). Assembly factors Rpf2 and Rrs1 recruit 5S rRNA and ribosomal proteins rpL5 and rpL11 into nascent ribosomes. Genes Dev *21*, 2580-2592.
Zhang, L., Wu, C., Cai, G., Chen, S., and Ye, K. (2016). Stepwise and dynamic assembly of the earliest precursors of small ribosomal subunits in yeast. Genes Dev *30*, 718-732.
Zhu, J., Liu, X., Anjos, M., Correll, C.C., and Johnson, A.W. (2016). Utp14 Recruits and Activates the RNA Helicase Dhr1 To Undock U3 snoRNA from the Preribosome. Mol Cell Biol *36*, 965-978.
Zinder, J.C., and Lima, C.D. (2017). Targeting RNA for processing or destruction by the eukaryotic RNA exosome and its cofactors. Genes Dev *31*, 88-100.